MODELING, ANALYSIS AND OPTIMIZATION OF CYLINDRICAL STIFFENED PANELS FOR REUSABLE LAUNCH VEHICLE STRUCTURES

By

SATCHITHANANDAM VENKATARAMAN

A DISSERTATION PRESENTED TO THE GRADUATE SCHOOL OF THE UNIVERSITY OF FLORIDA IN PARTIAL FULFILLMENT OF THE REQUIREMENTS FOR THE DEGREE OF DOCTOR OF PHILOSOPHY

UNIVERSITY OF FLORIDA

1999

This dissertation is dedicated to my parents, S. Venkataraman and Gowri Venkataraman.

TABLE OF CONTENTS

ACKNOWLEDGEMENTS

I want to thank Dr. Raphael T. Haftka for providing me with the opportunity to complete my Ph.D. studies under his exceptional guidance. Without his untiring patience, constant encouragement, guidance and knowledge this work would not have been possible. Not only did Dr. Haftka direct my learning and research as a student, but he also played the very important role of mentor. I want to thank him for the financial support he has provided me and for all the opportunities he has created during the last five years for me to grow as a professional and as a person. My academic and general with discussions Professor Haftka have broadened my vision and given me new insight in to many areas of engineering design, philosophy and history.

I would also like to thank my Ph.D. supervisory committee members, and Dr. David Bushnell, Dr. Theodore F. Johnson, Dr. Bhavani Sankar, Dr. Andrew Rapoff, Dr. Gary Consolazio. I am grateful for their willingness to serve on my committee, providing me help whenever needed and for reviewing this dissertation. Special thanks to Dr. David Bushnell for his help with the PANDA2 program and for educating me on the various aspects of stiffened shell analysis and design. Special thanks to Dr. Bhavani Sankar for the many discussions I have had with him and for the knowledge he has imparted to me in the area of composite materials and fracture mechanics. I would like to mention my special thanks to Dr. Theodore F. Johnson, for sponsoring my studies, co-authoring and reviewing some of my publications, and for the weekly teleconferences, where his

practical experience and technical knowledge made this research more interesting and relevant.

I would like to thank my colleagues, Dr. Peter Harrison, Dr. Willem Roux and Luciano Lamberti with whom I have collaborated while working on my Ph.D. dissertation, for the interaction and many fruitful discussions. Special thanks to Luciano Lamberti, without his help this dissertation would not have been completed.

I would like to thank all my colleagues in the Structural and Multidisciplinary Design Optimization Research Group for their help and support. I am grateful for the friendship of Dr. Gerhard Venter, Roberto Vitali, Boyang Liu, Raluca Rosca, Melih Papila, and Steven Cox, which made my doctoral studies a pleasurable experience.

The financial support provided by NASA grants NAG-1-669 and NAG-1-1808 is gratefully acknowledged.

My parents deserve my deepest appreciation. I am especially grateful for the countless sacrifices they made to ensure that I can pursue my dreams and for always being there for me.

Lastly, I would like to thank my dear friend, confidante and true love Beth. Her love, support and encouragement has had made my life rich and complete. I thank her for helping me discover the meaning of companionship and sharing, and for teaching me to enjoy the simple things in life.

LIST OF TABLES

Table Page

LIST OF FIGURES

Abstract of Dissertation Presented to the Graduate School
of the University of Florida in Partial Fulfillment of the
Requirements for the Degree of Doctor of Philosophy

MODELING, ANALYSIS AND OPTIMIZATION OF STIFFENED CYLINDRICAL PANELS FOR REUSABLE LAUNCH VEHICLE STRUCTURES

By

Satchithanandam Venkataraman

December 1999

Chairman: Dr. Raphael T. Haftka
Major Department: Aerospace Engineering, Mechanics and Engineering Science

The design of reusable launch vehicles is driven by the need for minimum weight structures. Preliminary design of reusable launch vehicles requires many optimizations to select among competing structural concepts. Accurate models and analysis methods are required for such structural optimizations. Model, analysis, and optimization complexities have to be compromised to meet constraints on design cycle time and computational resources.

Stiffened panels used in reusable launch vehicle tanks exhibit complex buckling failure modes. Using detailed finite element models for buckling analysis is too expensive for optimization. Many approximate models and analysis methods have been developed for design of stiffened panels.

This dissertation investigates the use of approximate models and analysis methods implemented in PANDA2 software for preliminary design of stiffened panels. PANDA2 is also used for a trade study to compare weight efficiencies of stiffened panel concepts for a liquid hydrogen tank of a reusable launch vehicle. Optimum weights of stiffened panels are obtained for different materials, constructions and stiffener geometry. The study investigates the influence of modeling and analysis choices in PANDA2 on optimum designs.

Complex structures usually require finite element analysis models to capture the details of their response. Design of complex structures must account for failure modes that are both global and local in nature. Often, different analysis models or computer programs are employed to calculate global and local structural response. Integration of different analysis programs is cumbersome and computationally expensive.

Response surface approximation provides a global polynomial approximation that filters numerical noise present in discretized analysis models. The computational costs are transferred from optimization to development of approximate models. Using this process, the analyst can create structural response models that can be used by designers in optimization. It allows easy integration of analysis models in optimization.

The dissertation investigates use of response surface approximations for integrating structural response obtained from a global analysis in the local optimization of stiffened panels. In addition, response surfaces are used for correcting structural response predictions from a low fidelity model with a few expensive detailed finite element analyses.

CHAPTER 1
INTRODUCTION

Composite materials are desirable in lightweight structures due to their high specific stiffness and strength. Laminated composite materials provide the designer with freedom to tailor the properties and response of the structure for given loads to obtain the maximum weight efficiency. However, high modulus and strength characteristics of composites result in structures with very thin sections that are often prone to buckling. Stiffeners are required to increase the bending stiffness of such thin walled members (plates, shells). Consequently, stiffened panels are often used in aircraft and launch vehicles to obtain lightweight structures with high bending stiffness. Stiffened shells are also more tolerant to imperfections and resist catastrophic growth of cracks.

NASA is investigating the use of composite materials in the propellant tank design for next generation reusable launch vehicles. In the design of such large structures, many decisions have to be made regarding materials selection, fabrication techniques, and stiffener types. These decisions affect structural weight and operational costs. A large number of preliminary structure or substructure design optimizations need to be performed in order to understand the impact that different design constraints have on the optimum design. Often there are constraints on the available computational resources, time and design cycle time. Designers are faced with the task of choosing between model, analysis and optimization complexity. This introduction presents some issues in the areas

of stiffened panel modeling, analysis and optimization addressed in this dissertation, with a brief outline of each chapter. Detailed literature review of stiffened panel design methods is presented in *Chapter 2*.

Simple Models for Panel Design

Stiffened panels exhibit complex failure mechanisms and therefore require careful selection of the model, theory and numerical procedure used for analysis. A variety of analysis methods based on simple physical models, smeared models, finite strip models and finite element models have been implemented in software. For example, BOSOR4 [24] and FASOR [44] analyze shells of revolutions; PANDA2 [25] uses closed form solutions for individual failure modes and some 1-D discrete analysis models for design of stiffened panels; PASCO [6], VICONOPT [126], and PANOPT [16] are finite-strip-based design codes. A survey of these programs is presented in *Chapter* 2.

Finite element analysis provides the highest fidelity in modeling complex structures as it can incorporate many local details such as stiffener termination, cutouts, and local reinforcements. However, such analysis has several problems when directly used in an optimization environment. Using finite element analysis for design optimization of stiffened panels is often impractical due to high computational expense. When the geometry of the shell and stiffeners is optimized, remeshing is frequently required for acceptable accuracy. The numerical noise introduced by the discretization makes it difficult to use gradient based optimization methods.

Kaufman *et al.* [67] investigated the numerical noise and human errors that are present in results obtained using large and complex analysis codes. Numerical noise introduced by the discretization (meshing) and round off, in finite element analyses, was

discussed by Burden and Faires [21, p. 10]. Venter *et al.* [120] described the noise introduced by finite element discretization in a stepped plate optimization problem. Giunta *et al.* [57] and Dudley *et al.* [52] investigated such noise in aerodynamic analyses.

Significant time and effort are often required to interface analysis and optimization when using finite element analysis models. In particular, developing design constraints for use with general-purpose analysis codes in optimization is a time-consuming task. Furthermore, using general-purpose analysis software requires a good understanding of the physical problem and the limitations of the model or theory being used. Some panel design software implement a variety of design constraints that serve as an expert system and thereby significantly reduce the modeling effort and chances of obtaining unreasonable designs from the optimization.

Performing design optimization using finite element based non-linear analyses is often too expensive to be practical. Aside from computational cost, the complexity of analysis models presents a major challenge in design. Simpler analysis models such as those used by PANDA2, PASCO, or VICONOPT are therefore very useful for optimization purposes.

Panel Modeling Issues in Optimization

The choice of modeling details, analysis methods, and optimization techniques determines the computational cost of the design. To compensate for an expensive analysis (e.g., nonlinear response) or expensive optimization (e.g., global optimization), the designer may have to introduce approximations to the modeling of the designed structure.

Optimization of composite structures often involves a large number of design variables. Laminate stacking sequence optimization using discrete thickness and ply angles is a combinatorial design problem. Laminates optimized using a small number of load cases often are highly tailored to the loading and can perform very poorly in off design conditions. Furthermore, composite laminates exhibit a variety of failure modes that are difficult to model or analyze. Designers in such cases have to rely on data obtained from experiments.

In order to reduce model complexity, composite laminates are often approximated using homogenized models or other approximations. Such approximations are valid under certain assumptions and hence should be used with caution in optimization. In particular, it is known that optimization programs are very unforgiving in exploiting the weaknesses and limitations of the analysis models or theories used. They often find designs in regions where the assumed model is no longer valid. Knowledge of the validity and accuracy of such approximations is therefore required in order to develop appropriate constraints to be imposed in the optimization to avoid serious design errors.

Multi-Fidelity Approximations

The limitations of simple models often require the use of more complex and expensive analyses, which cannot be practically coupled with optimization programs. This has led to the development of approximation methods based on function evaluation at one or more points. These approximations may be accurate in a small region or in a larger region of design space based on the data used in their construction.

Response surface methods typically fit low order polynomials sense to function values over large regions of design space using least square fitting procedure. The fitted

approximation model is used to replaces the expensive analysis program in the optimization. An approximation can be developed independently for each failure mode from different analyses, so that the designer can readily integrate the various analysis models and codes into the optimization.

Venter and Haftka [119] demonstrated the usefulness of response surface approximations for expensive structural optimization in design for uncertainty. Ragon *et al.* [88] used response surface methods for a global–local design study of an aircraft wing.

Response surface approximations have their limitations. The cost of fitting the approximation increases rapidly with the number of design variables (the curse of dimensionality). Fitting a good global approximation that is valid over the entire design space is not possible with low order polynomials. To address these problems, correction response surfaces may be used to correct the less expensive analyses (lower fidelity models), rather than fit approximations directly to the response functions obtained from the more accurate analyses (higher fidelity models). The correction response surface model is fitted using a small number of higher fidelity analyses.

Recently, different methods of using correction response have been proposed and tested in the area of structural optimization. Mason *et al.* [78] used a 2-D finite element model as a lower fidelity model to predict failure stresses and applied corrections calculated using a full 3-D finite element analysis. Vitali *et al.* [123] used the approach for optimizing a blade stiffened composite panel with cracks. The lower fidelity model employed an infinite plate model to predict the stress intensity factor. The higher fidelity model used a detailed finite element model with a crack to calculate the stress intensity

factor at the crack tip. Knill *et al.* [69] demonstrated the use of correction response surfaces for the aerodynamic configuration design of a high-speed civil transport airplane. Toropov and Markine [109] demonstrated the approach for the design of a four-bar mechanism.

Objectives of the Dissertation

The first objective of the present research was to investigate the efficiency, accuracy and advantages of using design codes based on simple methods for stiffened panel design. The PANDA2 program was used as an example of such a design code. PANDA2 uses a variety of simple physical models (smeared, finite strip, and 1-D discretized) for capturing the failure of stiffened panels. The PANDA2 program was used for design studies on stiffened panels. The effects of modeling choice and analysis methods on optimum design of panels were investigated. The optimized designs were verified using detailed finite element analysis.

The second objective was to illustrate the effect of laminate model choice on design optimization. Stiffened composite panels often require a variety of global and local analysis models and approximations. Simplified modeling and approximation can affect the optimization results if used without proper constraints.

The third objective was to demonstrate the use of approximation techniques for integrating analysis models or codes. Stiffened panels are substructures that form a larger tank or vehicle structure. Interaction of the local (panel) design on the global (vehicle structure) design should be taken into account in the design optimization of panels. Use of approximations for integration of global and local analysis models is presented. In addition, designers are often faced with the situation where the currently

available analysis code or model has certain limitations and a more detailed analysis is required. Integrating the more complex analysis technique into the optimization can be costly and cumbersome. Correction response surface techniques allow the use of a simple model with a correction function fitted using a small number of "exact" (costly) analyses.

Outline of Dissertation

Panel analysis and design methods, which are key aspects of the present dissertation, are reviewed in *Chapter 2*. The review focuses on design and analysis of panels using specialized programs. A few examples of stiffened panel optimizations using finite element analysis that employ special techniques to reduce optimization costs such as sub-structuring or that use easily available analytic sensitivities are included. Also, panel design methods that address global-local design issues are discussed.

Chapter 3 presents design optimization of various metallic and composite stiffened panels using the PANDA2 program. The choice of models for analysis (closed form, 1-D discretization), choice of shell theories (Donnell, Sanders), and inclusion of details such as the effects of geometric imperfections and post-local buckling response are investigated for the designed panels. The designs obtained from PANDA2 are analyzed using more rigorous finite element analysis. The assistance of Mr. Luciano Lamberti [72] in performing the numerous structural optimizations required for this study is gratefully acknowledged.

Chapter 4 discusses the effects of using simplified laminate models in optimization. Examples of modeling composite laminates as an orthotropic material and a sandwich hexagonal core as a continuum foundation are presented. The tendency of optimization programs to exploit modeling weaknesses is demonstrated.

In *Chapter 5*, approximation methods are reviewed. Response surface approximation techniques are presented. These techniques are then used for a global-local design problem and analysis model integration problem in *Chapter 6.* Finally, *Chapter 7* presents some conclusions.

CHAPTER 2
PANEL ANALYSIS AND DESIGN METHODS

The use of composite materials in aircraft and space vehicles is becoming prevalent. The need to reduce weight makes composite materials a very attractive choice. Using composite materials with very high specific modulus and strength often results in structures with thin members. While the structures so designed may be sufficient to carry the in-plane tensile loads and satisfy strength requirements, they are often prone to buckling failures under compression or shear loads.

Stiffeners are used to increase the bending stiffness of thin-walled members (plates and shells). The stiffeners add an extra dimension of complexity to the model compared to unstiffened plates and shells. However, stiffened structures often employ a repeating stiffener pattern. The repeated (periodic) nature of the geometry allows the use of simplifying assumptions to obtain approximate analyses. The design of composite stiffened panels present even more challenges due the additional failure modes and anisotropy effects introduced by composite materials.

A variety of methods and programs are available for the analysis of stiffened panels, ranging from simple closed form solutions to complicated 3-D discretized solutions. The analysis costs typically increase with the level of detail modeled (e.g., branched shells vs. smeared representation of stiffeners) and the fidelity of the analysis procedure used (e.g., linear vs. nonlinear analysis).

Stiffened Panel Analysis Methods

A variety of simple analysis methods have been developed for the analysis of stiffened panels. These methods typically belong to one of the following classes: analysis based on smeared properties, simple plate analysis under simple supports, and accurate linked or segmented plate analysis or finite strip analysis. The more complicated or detailed modeling usually employs discretized models such as finite element and boundary element analysis. In the next section, some programs or software for design optimization of composite stiffened panels that use the simplified analysis methods will be reviewed. Examples of design optimization techniques and design for various performance factors such as structural instability, crashworthiness, damage tolerance, and postbuckling strength will be presented. The discussion will focus mainly on the design optimization of stiffened plates and stiffened cylindrical shells or panels.

Stiffened Panel Analysis using Closed Form Solutions and Smeared Models

Agarwal and Davis [1] optimized composite hat stiffened panels for buckling (local and Euler column buckling) and strength requirements. The buckling analysis was based on simplified assumptions. The local buckling load factor was calculated by assuming that panel segments were simply supported. The load distribution on the different segments of the panel (skin, stiffener segments) was obtained using the effective elastic modulus of the different segments. The Euler column buckling was obtained from a smeared model. The results were verified using the BUCLASP-2 [111, 121] linked plate analysis program that treats stiffeners as branched shells.

Agarwal and Sobel [2] presented weight comparisons for stiffened, unstiffened and sandwich cylinders under axial compression loading. The overall buckling load was

captured using a smeared representation. The stiffeners in this case were treated as one-dimensional beams with twisting taken into account. The resulting designs were also analyzed with the BUCLASP-2 program. It was shown that smeared models underestimate buckling loads by 30%.

Stroud and Agranoff [99] extended the approach of using simplified buckling equations to the design of more general hat and corrugated panels under axial compression and shear loads. The analyses treated individual segments as simply supported flat plates, calculating buckling loads of each individual element. The authors investigated the weight efficiencies of the different stiffeners and also calculated weight penalties that were due to the imposition of manufacturing constraints (discrete ply thickness, stiffener dimensions). The global buckling was analyzed using a smeared model similar to that used by Agarwal and Davis [1]. The failure margins obtained using simple analysis were found to be conservative for most cases due to the assumption of simple supports for the different members. The simplification also could not account for stiffener rolling modes that were critical for some of the designed panels.

Simple smeared representations of stiffened panels are used often for optimizing them with general instability constraints. Tomashevskii *et al.* [107, 108] used such a smeared model and simple expressions for stiffener buckling to optimize stiffened composite cylinders. Sun and Mao [104] optimized stiffened composite cylinders to investigate the effects of shell geometry, stiffener eccentricity and laminate stacking sequence under axial compression and hydrostatic pressure loads. A smeared representation taking into account the stiffener-introduced eccentricity was used. The initial postbuckling was investigated using Koiter's general theory of general instability

[62, 70]. The analysis method provided an efficient tool to investigate the effects of different design variables on general instability.

Analysis using Finite Strip Methods

Finite strip methods (FSM) represent a class of analysis that has an accuracy (and computational expense) that lies between closed form solution of the type seen in linked or segmented plate analysis models and the finite element method. Linked plate analysis solves the exact plate equation in the segmented-plate model and hence is considered as the "exact" finite strip method. Inexact finite strip analysis divides the panel segments into strips and approximates the displacement field in the strips. Within each strip, the displacement field is expressed using polynomials to describe the widthwise variation and trigonometric functions to describe the displacement field. Dawe and his coworkers [47-51] published several papers on such approximate finite strip methods for buckling and postbuckling analysis of prismatic composite structures.

Williams and his coworkers [130] developed a rigorous analysis procedure (VIPASA, Vibration and Instability Analysis of Plate Assemblies including Shear and Anisotropy), where the buckling loads of stiffened panels were calculated by treating them as plate assemblies. The procedure accounts for the physical connections between the adjacent members and permits a buckling pattern that is continuous along the connection. The buckling solutions are based on exact plate analysis equations. This procedure was implemented into the VIPASA analysis code. The analysis was restricted to uniform transverse or edge loading with simple supports at the panel ends.

Stroud and Anderson coupled the VIPASA analysis code with the CONMIN [115] optimization program for design optimization of hat and corrugated stiffened

panels [101]. CONMIN used the method of feasible directions for the optimization, and Taylor series approximation for its constraint approximation. The designs obtained were compared with those obtained from the simplified analysis described in Stroud and Agranoff [99]. It was shown that for hat stiffened panels loaded in axial compression, the simplified analysis was conservative (2% to 9% heavier). The simplified analysis was found to be inadequate when local buckling wavelengths coincided with the short buckling wavelengths of overall buckling due to anisotropy effects. It was found that under combined shear and axial loading, inclusion of anisotropy terms (D_{16} and D_{26}) was very important (i.e., replacing laminates with orthotropic representations can lead to incorrect buckling loads). The authors demonstrated that while the simplified models provided reasonably accurate predictions of response, using such models for optimization or sizing without proper design constraints resulted in very unconservative designs.

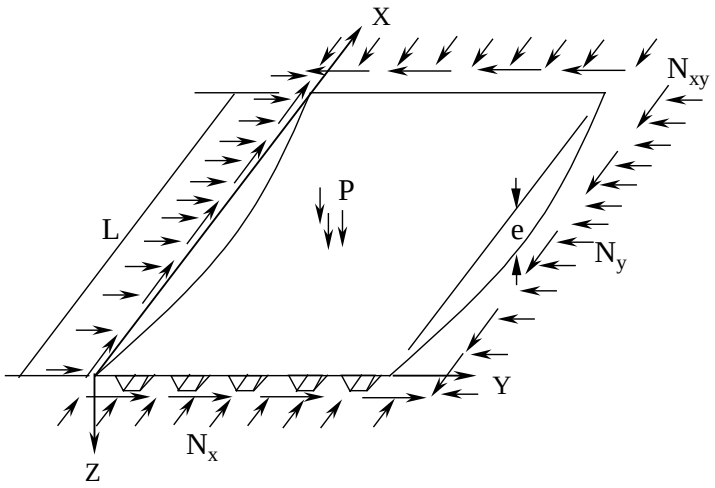

Figure 2.1: Panel showing global imperfection

Anderson and Stroud [6, 101] implemented the VIPASA analysis into an automated panel sizing code (PASCO). The VISPASA analysis was enhanced to include

global (overall bowing type) imperfection as shown in Figure 2.1. The maximum bending moment on the panel was calculated by using the classical beam formula

$$M = \frac{N_x e}{1-\gamma} + \frac{PL^2}{\pi^2}\frac{1}{\gamma}\left[\sec\left(\frac{\pi}{2}\sqrt{\gamma}\right) - 1\right] \tag{2.1}$$

where, $\gamma = \frac{N_x}{N_{xE}}$ (2.2)

in which N_x is the applied axial load per unit width, N_{xE} is the Euler buckling load for the panel, and P is the pressure acting on the panel. The maximum bending moment was then used to calculate stress resultants on the skin and stiffener segments to determine the buckling load factors. Weight efficiencies of hat and blade stiffened panels were compared at different values of global imperfection amplitude. Small geometric imperfections had a big influence on the optimal weight. Comparison with experimental results showed the importance of including imperfections. The PASCO code provided a rational method for including the effect of bow-type imperfections, unlike other simplified analysis methods decribed so far that required some empirical knockdown factors to account for imperfections.

A shortcoming of PASCO or VIPASA analysis [102] was the inexact matching of boundary conditions under shear load. The displacement field used under shear loads results in a skewed plate. The analysis model used in VIPASA and PASCO was found to be inaccurate for shear buckling with long wavelength. The VICON (VIPASA with Constraints) program developed by Williams and coworkers [126, 127] overcame the problem by using Lagrange multipliers to provide arbitrary supports or boundary conditions. Swanson *et al.* [105] incorporated this model into design optimization via an ad hoc correction. An iterative approach was used where the PASCO smeared

(approximate) model was used to size panels. A correction factor was obtained using a VICON analysis for the next PASCO optimization cycle. The approach illustrates the use of multi-fidelity models using corrections based on a small number of accurate and expensive function evaluations during the optimization. The procedure was used to perform weight comparisons of hat, blade stiffened, and trapezoidal corrugated panels.

The correction approach developed by Swanson *et al.* [105] was found to be quite inefficient. To overcome this deficiency and to implement the VICON directly into the sizing code and refine some analysis features [128] the VICONOPT program [42, 43] was developed.

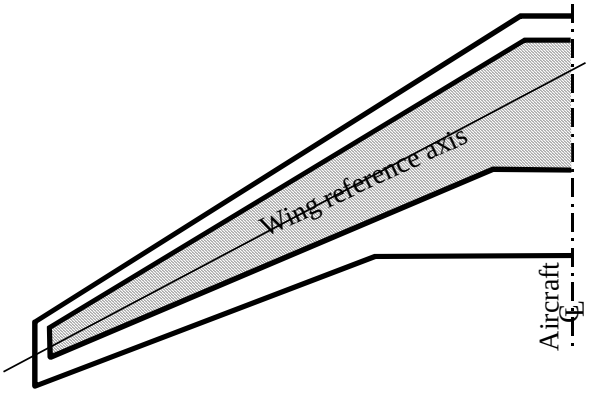

Figure 2.2: Schematic of wing showing skewed panels

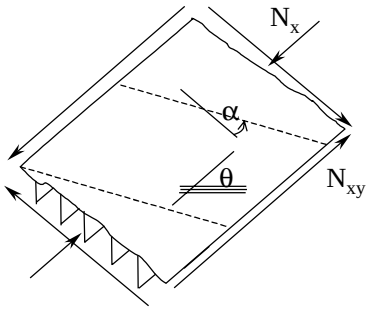

Figure 2.3: Stiffened panel analysis model of VICON

A similar problem in using approximate end conditions for stiffened panels is encountered in aircraft wing design. Stiffened panels used in aircraft wing structures have skewed (Figure 2.2) edges. However, they are often approximated as rectangular panels in the design process. York and Williams [131] showed that the approximation led to sub-optimal panels, because response of skew panels under shear load is very different from that of rectangular panels. An accurate method of analyzing skew panels was implemented in the VICON program by use of Lagrange multipliers [127]. The dotted lines in Figure 2.3 indicate support lines along which simple support boundary condition are enforced in VICON using the Lagrange multipliers. This provided a more accurate representation of the boundary conditions for skew panels and rectangular panels under shear loads.

Analysis costs typically increase with increase in the fidelity and accuracy of the analysis model. York and Williams [132] demonstrated the use of infinite width model for analysis of the skewed panels and compared the results to those obtained using exact models. It was shown that the infinite width model provides conservative estimates for buckling loads of skewed plates. The optimizations were performed for two metallic panels (blade and J-stiffened) and for two composite panels (blade and hat stiffened). The analyses were performed for different skew angles and aspect ratios and the buckling loads were compared. The errors in buckling loads were typically in the range of 5-7% with the worst case being 15%. However, the CPU run times for the infinite width analysis were typically 7% to 30% of those required by the exact analysis. The efficiency of such approximations is of great value in performing structural optimizations.

The PANOPT program developed at the National Aerospace labs, Netherlands, by Arendsen and coworkers [16] is capable of design optimization of stiffened composite panels for buckling and postbuckling. The PANOPT program is an extension of the finite strip analysis method proposed by Riks [94] enhanced by Arendsen [15] to include higher order energy terms.

Several other programs that use similar analysis approaches have been developed for design optimization of stiffened composite panels. The analysis and sizing program STIPSY developed by Baburaj and Kalyanaraman [17] uses approximate finite strip models similar to those presented by Agarwal and Davis [1] and by Stroud and Agranoff [99]. The authors included a more rigorous model for the torsional buckling of the stringers. Postbuckling strength is considered by using the effective width of elements undergoing local buckling. The effective width calculations of composite panels implemented in STIPSY were originally developed by Rhodes and Marshall [92]. The analysis code was coupled with an optimizer based on Rosen's gradient projection method and an indirect method based on Sequential Unconstrained Minimization Technique (SUMT). Optimal designs were obtained for various combinations of in-plane compression and shear loads. The effect of allowing local postbuckling on the optimal design weight was also investigated.

Zabinsky, Graesser, Kim and Tuttle [59, 68, 112, 133, 134] at the University of Washington collaborated with researchers at Boeing [76] in the development of the program COSTADE (Composite Optimization Software for Transport Aircraft Design Evaluation) program. The structural analysis and optimization module of COSTADE was based on the UWCODA code (University of Washington Composite Optimization and

Design Algorithm) [59]. The UWCODA program was developed for global optimization [133] of composite stiffened panel structures with continuous and discrete variables. COSTADE used a smeared stiffness approach for calculation of critical buckling and stress margins. A stochastic algorithm denoted “Improving Hit-and-Run” [134] was employed for the design optimization of the composite laminates. The program can perform preliminary design optimization of stiffened composite panels with strength constraints. COSTADE is capable of point design where a single panel type spans the whole structure or can perform optimization of a blended design. In the latter, compatibility constraints need to be imposed for continuity of plies and structural members from one panel to the other. The buckling analysis of COSTADE as based on a finite strip analysis method developed by Kim and Tuttle [68]. Three different strength criteria are used. A pristine strength criterion calculated first ply failure load using maximum strain failure. The ultimate damage tolerance criterion obtained strain constraints using the ultimate loads. The failsafe damage tolerance criteria were based on proof load conditions. COSTADE was further augmented using more detailed finite element models for other damage scenarios (transverse crack) [58].

More recently researchers have started investigating methods for designing stiffened shell structures with nonlinear analysis. Stoll and Gürdal [96] developed an approximate semi-analytical approach for non-linear analysis of stiffened plates. The NonLinear Panel ANalysis code (NLPAN) can predict postbuckling stresses and deformations, elastic limit points, and imperfection sensitivities of linked plate assemblies subject to inplane axial and pressure loads with temperature effects. The program was developed as an extension of VIPASA so that it could be used in an

automated fashion with the VIPASA. The non-linear plate theory applied to each component plate-strip accounts for the large in-plane rotations that occur in the postbuckling response. Buckling eigensolutions with the second order contributions from VIPASA were used to describe the displacements. NLPAN uses a stationary potential energy condition to obtain a set of nonlinear algebraic equations governing equilibrium. These equations are load independent with a relatively small number of variable modal amplitudes, allowing a rapid exploration of the nonlinear regime. Stoll [97] extended the capabilities of NLPAN to include various end support boundary conditions. The load deflection and load vs. end shortening are compared with experimental test results. Comparisons of the analysis results obtained using NLPAN with the STAGS [4, 90] analysis code was presented by Stoll *et al.* [98]. The NLPAN program was shown to provide nonlinear analysis capability at a small fraction of the cost of performing a nonlinear finite element analysis.

Analysis of Cylindrical Stiffened Panels

Cylindrical stiffened panels are as important as stiffened plates. Stiffened cylindrical panels or cylinders are used in aircraft fuselage, rocket and missile structural components, and launch vehicle tank structures. The curvature of circular cylindrical shells increases their load carrying capacity. However, the nonlinearities introduced by the curvature result in unstable postbuckling behavior and make the shell structures more sensitive to geometric imperfections. Therefore, much research has been done in the area of stability of unstiffened and stiffened cylinders made of isotropic and anisotropic materials. Examples discussed here only include analysis methods and programs that have been used for obtaining optimum designs of curved stiffened panels.

The VICONOPT program was discussed in detail for analysis of stiffened plates. Until recently, stiffened curved panels were modeled only approximately in VICONOPT by discretizing it into a series of flat plates. While this approach gave quite accurate results, it required a large number of plate elements to approximate the curved surface. Since this was not very efficient, a curved plate element was developed [79] for inclusion in VICONOPT. The curved plate element was developed using the non-linear equilibrium equations that include transverse shear deformation effects. The plate element can be used for obtaining linear bifurcation buckling and postbuckling responses.

Analysis of Shell of Revolution

Complex analysis methods and programs that can analyze shells of revolution have been used extensively for shell analysis and design. The BOSOR4 program [24] is an energy based discrete analysis method where the model is discretized along the meridian of a shell of revolution. BOSOR4 can perform linear and nonlinear static and buckling analysis of shells. For axisymmetric geometry and loads BOSOR4 can obtain very accurate estimates of displacements, stress and buckling loads. BOSOR4 can also be used for analysis of prismatic structures such as stiffened panels. The FASOR program [44] provides similar capabilities using direct integration of the governing ordinary differential equations for a shell of revolution.

Analysis using Multiple Models

Cylindrical stiffened shells exhibit complex failure modes and hence often require multiple models for efficient analysis. An important and significant contribution to the area of preliminary design of stiffened cylinders by Bushnell [25-33] at Lockheed Palo

Alto Research Laboratory has led to the development of PANDA2. The PANDA2 program finds the minimum weight designs for laminated composite plates, cylindrical panels or cylinders with and without stiffeners that can run along one or two orthogonal directions. The philosophy of PANDA2 is to provide optimum preliminary design of stiffened panels that experience complex and nonlinear behavior without resorting to the use of general purpose (finite element) analysis codes that require elaborate database management systems. Instead, PANDA2 uses several separate relatively simple models, each designed to capture specific failure modes or mechanisms (often with the same accuracy as general-purpose FE codes). PANDA2 uses a combination of approximate physical models, exact closed form (finite strip analysis) models and a 1-D discretized branched shell analysis models to calculate prebuckling, buckling and postbuckling responses.

The most challenging task in stiffened shell optimization is the selection of appropriate modeling, analysis theories, and design constraints. PANDA2 has automated this task and therefore can be regarded as an expert system for stiffened shell design. The capabilities of PANDA2 and its efficiency allow it to perform global optimization of stiffened panels. A more detailed overview of PANDA2 theory, analysis models, procedure and optimization capabilities is presented in *Chapter 3*.

Arbocz and Hol [11, 12] at the Technical University of Delft, have developed an expert system (DISDECO, Delft Interactive Shell Design Code) for design of anisotropic stiffened panels and shells. The program uses a hierarchial analysis approach for accurate prediction of buckling load and a reliable estimation of imperfection sensitivity. With this tool, the designer can access a series of analysis programs of increasing complexity. The

analysis modules of DISDECO can calculate the critical buckling loads of stiffened anisotropic shells subject to combined loads, investigate the effects of various types of boundary conditions on critical buckling load, and obtain perspective of degrading effects of possible initial imperfections on buckling loads.

Three hierarchical analysis models were implemented in the DISDECO code. The Level-1 analysis uses the GANBIF [12] analysis routine. The analyses in level-1 are the most approximate and are to be used for investigating overall or general buckling characteristics of the shell. The solutions are based on membrane prebuckling solutions and linearized stability equations reduced to algebraic eigenvalue problems by the use of a truncated double Fourier series. The program can also be used to determine the coefficients in Koiter's asymptotic expansion for initial postbuckling response.

The level-2 analysis accounts for the primary nonlinear effects such as edge restraints and can satisfy the prescribed boundary conditions exactly. The level-2 analysis, based on the ANLISA code [10, 11], uses a rigorous prebuckling solution and reduces the stability problem to the solution of a set of ordinary differential equations. ANILISA solves the Donnell type anisotropic shell equations. The buckling analysis can include geometric imperfections that are of the form of a double periodic trigonometric ($\sin(mx)\sin(ny)$) function or axisymmetric imperfections that are similar to the critical buckling mode of the perfect shell. The solutions from this level are very accurate for axisymmetric geometry and loading. Also present in level-2 are other computational modules such as COLLAPSE [13] that can handle axisymmetric initial imperfections, and ANSOVI [91] that solves Novozhilov type anisotropic shell equations.

The level-3 analyses are the most accurate and use two-dimensional finite element analysis codes with advanced analysis capabilities that include geometric and material nonlinearities. At present different members of the STAGS family [3, 5] are used in this level.

When fully implemented DISDECO will provide a comprehensive interactive analysis and design tool that will allow the designer to explore the effects of choice of shell theory, analysis models, and edge conditions. Also, the database of imperfections and other stochastic methods for determining effects of imperfections will enable the designer to obtain reliable designs for stiffened composite shells.

Optimization of Stiffened Panels

Stiffened Panel Optimization Using Approximate Analyses

In this section, design optimization techniques and designs obtained using the analysis methods or programs described in the previous section are reviewed. Even with the availability of fast computers, simple analysis methods continue to be used. The simplicity of the analysis makes it possible to do more complicated optimization, such as reliability-based design, local-global design, and multi-criteria (cost-weight minimization) optimization.

A number of papers have been published on design optimization of panels using PASCO and VICONOPT, but only a sample of those are reviewed here. Butler and his coworkers [40, 41, 42, 43] have published several papers on the use of VICONOPT [42, 43] for stiffened panel optimizations in aircraft wing design. Butler performed design optimizations for stiffened panels [40] using different loads as encountered in practical wing design. The results obtained were then verified using a finite element analysis

program and the PANDA2 program. Integrally stiffened and built up panels were optimized using VICONOPT. The integrally stiffened (machined) stiffeners provided a significant weight saving (20%) compared with the conventional built-up stiffeners (with a bottom flange) when designed for buckling. The weight difference was smaller (3%) for designs optimized for postbuckling strength. In addition, comparison with finite element analysis showed very good agreement except for cases with substantial shear loading. The optimal weights obtained were compared with designs obtained using PANDA2 for a T-stringer stiffened panel and were almost identical.

Butler [41] demonstrated the use of VICONOPT [42, 43] for an aircraft wing design. The wing structure was divided into six different panels. The skew panels were approximated by treating them as infinitely long. Initial minimum weight optimizations of panels were performed, for a range of loads and panel lengths, to generate design charts. The design charts were used for selection of stiffener spacing and cross-sections for panels used in the wing structure. In order to provide compatibility between panels, the stiffener spacing and cross-section were fixed and the thicknesses optimized in the wing structure design. Four different panel concepts were considered: metallic blade stiffener, composite blade stiffener, composite hat stiffener, and composite foam sandwich with blade stiffener. VICONOPT uses a gradient-based optimizer and can get trapped in local optima. Butler further showed that design charts obtained for minimum weight designs by varying loads or panel size helped to identify panels in the wing design that were trapped in local optima.

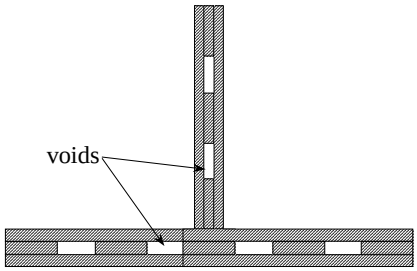

Figure 2.4: Blade stiffened panel with voids

Williams and his coworkers presented further demonstrations of the VICONOPT capabilities for stiffened panel optimization. Williams and Jianqiao [129] used VICONOPT to optimize blade-stiffened panels with centrally located voids. Figure 2.4 shows a stiffener cross-section with a series of equally spaced voids in its central core layer, which run for the full length of the plate and have a constant cross-section. The longitudinal voids were used, in a manner analogous to a core material in sandwich composite laminates, to increase in the bending stiffness of the laminates used for the panel skin and blade stiffeners. In addition to optimizing the blade spacing, stiffener segment width and thickness the optimization can also size the length of voids in the skin and stiffener segments. This work demonstrated the design features of VICONOPT and the use of voids for weight savings in composite panels.

Structural optimization of panels can often result in designs that are either impractical or too expensive to manufacture. There is an increased interest in combining cost constraints with structural constraints during the optimization. Edwards *et al.* [53] replaced the minimum mass objective with minimum cost or a combination of cost and mass and obtained optimal designs. The VICONOPT program was used for optimization with new cost functions (material, manufacturing, and operational costs) incorporated. Panels can be optimized for different combinations of cost and weight. This example

demonstrates the advantage of having inexpensive analysis models for use in expensive (multiobjective) optimizations.

Kassapoglou [66] performed simultaneous cost and weight optimization of composite panels under compression and shear loading using a simple analysis. The panels were analyzed for global and local buckling. The simple analysis used smeared stiffness for global buckling and simply supported plate models for local buckling. Analysis results were compared with more detailed finite strip based solution procedures developed by Peshkam and Dawe [87] and were shown to be reasonably accurate. The simple analysis procedure enabled the author to perform several design optimizations for different stiffener geometries at various fixed spacings. The panels were optimized separately for cost and weight. Cost functions were developed that accounted for material, manufacturing and operational costs. It was found that the blade stiffener design was the best minimum cost concept, whereas the J-stiffener design was the best minimum weight concept. A multiobjective optimization was performed to minimize weight and cost objectives that were combined using a penalty function. A Pareto-optimal curve was obtained for the panels that represented a compromise solution between minimum weight and cost. Also information about dominating failure mode along the Pareto curve was obtained. Such qualitative information is often useful to the designer in concept selection.

Panel Optimization for Global Optimum and/or Discrete Variables

A distinctive feature of using composite materials is the ability to tailor the material properties. Typically, this is achieved by optimizing the ply stacking sequence in the laminate. The programs discussed thus far have all used gradient based optimization routines. In all cases, the ply thicknesses for a pre-chosen stacking sequence are used as

optimization variables. Composite laminates that are manufactured from pre-pregs (tape lay-ups) have plies of discrete thickness. Hence, the ply optimization must use discrete variables. Since, continuous optimization problems are easier to solve often continuous values are used for ply thicknesses and orientations. This can lead to several problems. Using ply angles and thicknesses as optimization variables result in non-convex design space and also lead to multiple local optima. It has also been found that rounding the ply thickness to thickness of discrete number of plies can lead to sub-optimal designs.

Genetic algorithms (GAs) have been developed for the stacking sequence optimization of laminates with discrete ply angles and thicknesses [73, 75, 83]. In addition to having capability to use discrete variables, GAs also provide global optimization capabilities. The optimization results in a family of optimum designs, with comparable performance, rather than a single optimum as in the case of gradient based methods.

Nagendra *et al.* [81, 82] applied a simple genetic algorithm with crossover, mutation and permutation operators for blade stiffened composite panel design. The ply thicknesses, orientations, and blade height were also coded using an integer representation. The stiffened panel was optimized for minimum weight under inplane axial compression and shear loads. The panel was required to satisfy buckling, strain, and contiguity (no more than four plies of the same orientation are stacked together, to prevent matrix cracking) constraints. The PASCO program was used for analysis of the stiffened panel. An eccentricity (axial bowing) of 3% was used for the initial geometric imperfection. To avoid mode interaction effects, penalty parameters were introduced in the optimization to obtain buckling mode separation. Besides optimizing for discrete

variables, the genetic optimization searches for the global optimum in the design space. Furthermore, it can provide a family of near optimal solutions (unlike a single optimum obtained from gradient based optimization). The design obtained using the simple GA was lighter (25.19 lb) compared to the rounded design (26.08 lb) obtained using a continuous optimizer. The advantages of global optima and family of near optimal designs come at a very expensive computational cost because the simple GA requires tens of thousands of analyses.

Nagendra *et al.* later presented an improved genetic algorithm [83] that introduced new genetic operators. In addition to the basic crossover, mutation, and permutation operators, the following new operators were added: sub-string crossover, stack deletion, stack addition, orientation mutation, inter-laminate swap and intra-laminate swap operators. The new features of the improved GA were found to improve the convergence and reliability of the algorithm. The optimal design weight (24.2 lb) obtained using the improved GA was lower than the optimal design weight (25.2 lb) obtained using the simple GA. However GA's are still expensive to use for practical design applications. Even with the improved efficiency of the genetic algorithm and the efficient analysis methods (such as in PASCO or PANDA2), performing discrete optimization of stiffened panels remains a challenging task.

Harrison *et al.* [61] investigated the use of response surface (RS) approximations to replace the analyses program in the genetic optimization. A hat stiffened cylindrical panel under axial compression load was optimized. The stacking sequence of the wall and stringer segments and the stiffener geometry parameters were used as optimization variables. In order to fit a response surface, the buckling load and stress failure margins

of panels were obtained using the PANDA2 program. A weighted least square procedure was used to fit a polynomial approximation. Each laminate stacking sequence was represented using five lamination parameters. The lamination parameters of the three laminates and four hat stiffener geometry variables resulted in a total of 19 variables that were required to describe the response of the panel. A set of 450 points obtained from the first 15 generations of the genetic optimization were used as fitting points. Once the response surface was obtained, it replaced the PANDA2 analysis for a number of generations and then the process was repeated. The polynomial (response surface) captured the failure envelope of the design space for a large number of designs. Convergence histories averaged over six trials showed that the RS approximation reduced the number of generations required for convergence to about 30, from about 95 required for optimization with exact analysis.

Crossley and Laananen [45] used genetic optimization for design of stiffened panels for maximum energy absorption. Constraints were imposed on local buckling and stiffener buckling. Simple closed form solutions were used to obtain buckling loads. Energy absorption was estimated by a semi-empirical method based on an analogy to the crippling of metal cross sections [19] with empirical corrections obtained from experiments. The novel feature of this genetic optimization was that the stiffener type was also encoded as a design variable. In past work, the geometry was chosen *a priori* and then optimized for size. Here, stiffener types such as blade, channel, I-section, hat section, J-section and angle-section were represented by a binary string along with the stacking sequence for the different segments. The emphasis was on crashworthiness design rather than design for instability under inplane flight loads.

Programs such as PANDA2 treat stiffener spacing as continuous design variables. This can often lead to non-integral number of stiffeners in a cylinder. Jaunky *et al.* [63, 64] used genetic algorithms for grid stiffened cylinders to optimize the number of stiffeners, stiffener cross-section geometry, and laminate stacking sequence. A global smeared model was used to calculate general instability loads. Local buckling was calculated using a Rayleigh-Ritz analysis of individual skin and stiffener segments.

Panel Optimization for Imperfections, Postbuckling and Damage Tolerance

Buckling loads of thin walled composite stiffened panels are highly sensitive to geometric imperfections. It has been shown that optimization can heighten imperfection sensitivity by driving multiple modes to have similar buckling modes, thus increasing mode interactions. Researchers have investigated extensively the effect of geometric imperfections on buckling loads and have developed a variety of analysis methods and tools to incorporate imperfections into the analysis. However, there is still no good way to incorporate imperfections into design because the imperfection amplitudes and shapes of panels being designed are not known. Designers often assume worst case scenarios for the design optimization.

Elseifi, Gürdal, and Nikolaidis [54] developed an elliptical convex model to represent worst-case geometric imperfections. The convex model provides the imperfection corresponding to the weakest panel profile and the minimum elastic limit load. The nonlinear analysis for the panels with imperfections was performed using NLPAN. Response surfaces were used to approximate the elastic loads. This was done so as to smooth out the noise from the analysis. Two response surfaces were required (one each for positive and negative imperfection amplitudes). The results from the convex

model were compared to those obtained using a Monte Carlo simulation. It was shown that the convex models provide significant computational cost savings over traditional probabilistic analysis methods.

Elseifi, Gürdal, and Nikolaidis [55] further developed a manufacturing model for predicting imperfection profiles of composite laminate panels. The manufacturing model was successfully implemented into the optimization for postbuckling design. It was demonstrated that the laminate design influences the manufacturing imperfections in the panel. Therefore, if an arbitrary imperfection is used for designing a panel, the designed panel will have a very different imperfection when manufactured. The panel so designed will fail because the imperfection that results from manufacturing was not taken into account during the design. A closed loop design procedure, where the manufacturing model is used to obtain the imperfection mode of the designed panel, was implemented. The resulting designs were compared to those obtained using an empirical imperfection with non-linear analysis using NLPAN. The designs obtained using arbitrary or empirical imperfection could still fail at loads smaller than the design loads.

Perry and Gürdal [85, 86] coupled the nonlinear stiffened panel analysis program NLPAN developed by Stoll and Gürdal [96] with the ADS [116] optimization routine and used it to design panels for postbuckling response. Weight minimization of stiffened panels was performed with limit point stress and strain constraints for panels with and without initial geometric imperfections. The maximum strain failure criterion was used for limiting strains in the panel segments. Results were compared with designs obtained using PASCO for buckling constraints. The weight savings were 28% for panels optimized without initial imperfection and 34% for panels optimized assuming a bowing

imperfection of 1% of panel length. Panels designed for buckling were more sensitive to imperfections and did not carry the design load even for small values of imperfection. Panels designed for buckling loads often have poor load carrying capabilities in the postbuckling regime due to mode interactions. Consideration of the postbuckling response in the optimization of stiffened shell structures can be greatly beneficial, and the availability of an efficient code such as NLPAN is very valuable to designers.

Damage tolerance of optimized stiffened panel designs is of practical importance. Stiffened panels have been optimized for different damage scenarios such as through the thickness crack, delamination, stiffener failure and other problems. The vast majority of this work on damage tolerance has been accomplished using finite element analysis programs. Wiggenraad and Arendsen [125] have demonstrated the modeling of damage scenarios using finite strip analysis methods. The PANOPT program was used to analyze panels with damage models. Stress, buckling and postbuckling responses were obtained to enforce the damage constraints. Optimizations were performed with a single model and with multiple models that included the damage. The accuracy and effectiveness of the approach was demonstrated by validating the results from optimization with experiments.

Stiffened Panel Optimization with Finite Element Analysis Models

Finite element analysis programs that use 2-D discretization (plate and shell elements) are commonly used for analysis purposes. However, fewer examples are available for finite element analysis based optimization of stiffened panels. Using finite element analysis for design optimization of stiffened panels expensive. Stiffened panel design often involves optimizing for the geometry of the shell and stiffeners, which

frequently requires remeshing for acceptable accuracy. The numerical noise introduced from the discretization makes it difficult to use gradient based optimization methods. Often significant time and effort are required to create analysis models and even more effort is required to implement design constraints for optimization when using FE models. However, with the availability of modern computers and advances in modeling and approximation techniques, more papers are beginning to appear that discuss optimization of stiffened panels coupled with general purpose finite element analysis software. A few examples are mentioned here. Tripathy and Rao [110] used finite element model for optimization of stiffened panels for maximum buckling strength obtained using a linear bifurcation buckling analysis. Eschenauer *et al.* [56] have developed new modeling techniques that minimize the effort required for adaptive mesh generation required in shape optimization of stiffened panels. More recently Vitali *et al.* [122, 123] have used finite element analysis for optimization, with correction response surface techniques. The methodology employs detailed finite element analysis models in tandem with the approximate low cost analysis models. A correction function is fitted to the ratio of the accurate result from the expensive analysis and less accurate analysis at a small number of points using a least square regression. The obtained correction function is used to correct the less approximate analysis. The corrected model was then used in the design optimization of stiffened panels for buckling strength [122] and crack resistance [123].

CHAPTER 3
PANEL DESIGN STUDIES USING PANDA2

Preliminary design optimizations of stiffened panels for propellant tanks or launch vehicles are often performed to obtain accurate weight estimates in the concept selection phase. A large variety of analysis and design codes are available for stiffened panel optimization. Chapter 2 presents an overview of available programs and methods for stiffened shell design and analysis. The present section is focuses on PANDA2, one of the premier programs for analysis and optimization of cylindrical composite stiffened panels under buckling, out-of-plane displacement and stress constraints. The program uses a combination of closed form solutions and discrete models for buckling load prediction, and it accounts for a large number of failure modes. A significant feature of PANDA2 is the large number of design constraints it has implemented that are based on the developer's expertise in the design of shell structures.

Many papers describing PANDA2 have been published by its developer, David Bushnell. However, much less literature is available on its use by others. Here, the present capabilities, modeling, and theories of PANDA2 are summarized with references to original publications for additional details. The objective is to report on the usefulness of the PANDA2 program for the large number of stiffened panel optimizations required at the preliminary design stage.

Computational resources, cost, and design cycle time are often limited. Compromises are required in the model, analysis and optimization complexities to meet such restrictions. The present work presents issues of the modeling and analysis complexity involved in stiffened panel design. Modeling choices and features in PANDA2 are explored. In particular, the difference in the use of closed form and discretized stiffener models in PANDA2 and the different options to account for geometric imperfections are investigated. This chapter also presents the results from optimization of metallic and composite stiffened panel concepts considered for a liquid hydrogen RLV tank. Weight efficiencies and sensitivity to geometric imperfections are compared for the different concepts.

The PANDA2 Program

PANDA2, developed by Bushnell [25-33] at Lockheed Palo Alto Research Laboratory, is a program for preliminary design of cylindrical composite stiffened or unstiffened panels for minimum weight or distortion. Panels can have stiffeners along one or two orthogonal directions with blade-, hat-, T-, J- or Z-shaped cross-sections. PANDA2 is also capable of analyzing panels with Z-shaped stiffeners that are attached by riveting. The riveted attachment significantly affects the buckling response of the panels. PANDA2 can also be used to analyze and optimize sandwich panels with either hexagonal core or foam core, truss core sandwich panels, and isogrid panels.

The philosophy of PANDA2 is to provide at low cost optimum preliminary design of stiffened panels that experience complex and nonlinear behavior. PANDA2 uses several relatively simple models each designed to capture a specific failure mode or mechanism. PANDA2 uses a combination of approximate physical models, exact closed

form (finite strip type analysis) models and 1-D discrete branched shell analysis models (based on one dimensional discretization) to calculate prebuckling, buckling and postbuckling response. For details of the models see Bushnell [26], [27], and Bushnell and Bushnell [35] and [37].

PANDA2 Capabilities

Analysis Models

There are five model types. The first model is based on closed form models (PANDA type, [26]) for general, local and panel buckling, bifurcation buckling of stiffener parts and rolling of stiffeners with and without participation of the skin. This model represents the buckling mode displacement components u, v, w as one-term Rayleigh-Ritz expansions. Buckling load factors are computed for each combination of modal wave number and slope of buckling nodal lines, (m,n,s), from Eq. (57) in Bushnell [26].

The second model type obtains buckling load factors and local postbuckling response from a skin-stringer “panel module” or “repeating module” model [25]. A module (Figure 3.1) includes a length of panel between rings and a cross-section of a stringer plus a portion of the panel skin of width equal to the spacing between stringers. The segments of the skin-stringer module cross-section are discretized. Buckling load factors and mode shapes are obtained via a finite difference energy formulation analogous to that used in BOSOR4 [23, 24].

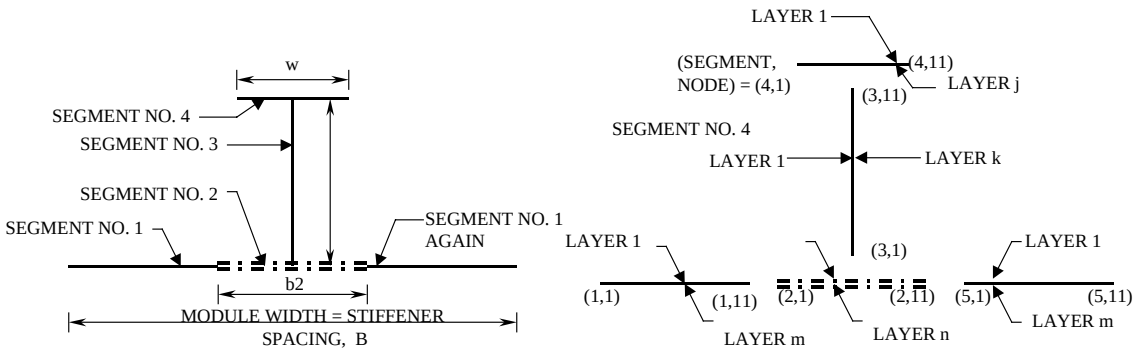

Figure 3.1: View of single module of panel with T-shaped stringer, showing layer numbering convention and discretization used.

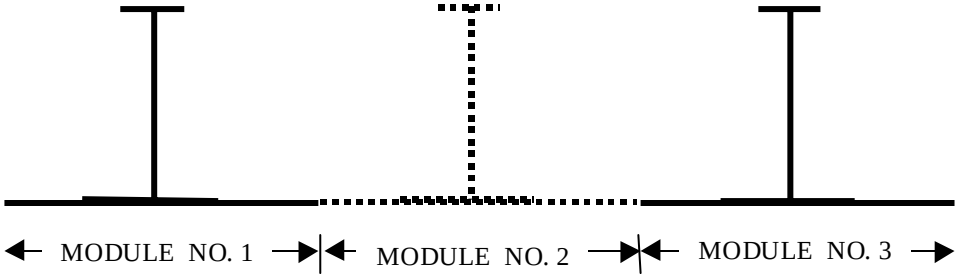

Figure 3.2: PANDA2 repeating module for a panel with T-shaped stiffeners.

A repeating module of a T-shaped stiffener is shown in Figure 3.1. The panel module treats the stiffener as a branched shell assembly. Each segment of the panel module can have a different laminate. The exploded view of the panel module in Figure 3.1 shows the node numbering used in the discretized analysis as well as the convention of layer numbering (stacking sequence specification). The numbers in parentheses in the exploded view indicate the segment and node numbers. Symmetry boundary conditions are used at Segment 1, Node 1 and Segment 5, Node 11. The variation of deflections in the direction transverse to the discretization plane (normal to the plane of the paper) is assumed to be harmonic. This discretized model is similar to that used in BOSOR4 for analysis of shells of revolution [24]. The PANDA2 model for stiffened panels is valid

only when there are more than two repeating elements as shown in Figure 3.2. Panels with a single stiffener cannot be handled using PANDA2. The single module gives good approximations for local skin buckling, wide column buckling, and buckling of stiffener parts.

In the third model, the entire width of the panel is discretized. The stiffeners are smeared out. This model is used to capture the effect of loads that vary along the width of the panel or to capture the prebuckling behavior of flat panels if normal pressure is present. Stresses and displacements calculated from this model are used for buckling analyses.

The fourth model [33] is analogous to the discretized skin-stringer module of the second model. In the fourth model, the ring cross-section is discretized and a segment of panel skin with smeared stringers equal to the spacing between rings is also discretized. Buckling load factors and mode shapes are obtained via the finite difference energy formulation that is used in BOSOR4 [24]. The model is useful in obtaining inter-ring buckling loads, ring segment buckling loads, and prebuckling displacement along the meridional length.

The fifth model [33] is analogous to the first model. This model is based on a double trigonometric series expansion of the buckling modal displacement components, u, v, w. This model is especially useful for panels in which in-plane shear loading plays a significant role or the panel has significant anisotropic terms, that is, terms that govern coupling between normal and shear stress and moment resultants.

PANDA2 performs the buckling analysis using closed form solutions [26] or 1-D discrete models (e.g., Figure 3.1) [25, 33]. The type of analysis used in optimizations is

chosen by setting the value of the IQUICK flag in the “mainsetup” processor execution. When IQUICK=1, closed form solutions (Models 1 and 5) are used for the buckling analysis. The discretized BOSOR4 type model of the repeating skin-stringer module (Model 2) is included in the buckling analysis when IQUICK=0. The 1-D skin-ring discrete module (Model 4) in the length direction is used to calculate inter-ring buckling analysis with both IQUICK= 0 and IQUICK=1. The analysis performed with the 1-D skin-stringer discrete module is computationally more expensive and is not available for all types of stiffeners.

Analysis Procedure

Bushnell describes the analysis features of PANDA2 in detail in references [26-33]. However, for the sake of convenience some of the essential features of the analysis are summarized here. The analysis summary includes calculation of constitutive relations, equilibrium behavior, and buckling analysis.

The constitutive relations are developed in stages and account for general laminated components of each segment of a module. The constitutive matrix [C] is a 6x6 matrix that relates the reference surface strains and changes in curvature and twist to the force and moment stress resultants. PANDA2 computes the integrated constitutive law for each segment of a panel module. In addition, thermal resultants and strains from curing and from applied thermal loading are calculated for each segment. For stiffened panels, a smeared stiffener theory is used and an integrated equivalent constitutive matrix C_s is computed for the smeared approximation. The tangent stiffness of the locally buckled skin C_{tan} is also computed in PANDA2. In case of stiffened panels with locally

buckled skin, the reduced stiffness for the smeared model due to local buckling C_{stan} is computed using C_{tan} for the panel skin between the stiffeners.

The prebuckling analysis of PANDA2 includes the membrane and, if the panel is cylindrical, axisymmetric bending effects, using nonlinear or linear analysis for response to pressure loads. The prebuckling analysis uses a smeared model of the global model and a discrete model for the response of a single panel module. In a ring-stiffened shell, the models used for prebuckling analysis calculate stresses at the mid-bay and at ring-web intersection in order to obtain buckling loads. The overall static response of the global model (smeared) and the local static response of the panel module are combined together to get the total state due to applied pressure. Strain and stress resultant distributions in all panel modules are determined using (i) all loads except normal pressure and (ii) only normal pressure load. The effect of bowing of the panel due to curing, applied thermal loads, normal pressure and edge moments is included along with initial geometric imperfections in the form of general, inter-ring and local buckling loads. An out-of-roundness (ovalization) type imperfection is also included.

Stresses are calculated for all layers of each segment in the material direction. The stress states of the panel module are calculated either for an unbuckled or postbuckled state, whichever is applicable. Tensile forces in parts of the stiffener web that tend to pull the web from the panel are calculated to provide safety against stiffener-skin separation. Von Mises stress criterion or maximum stress criterion can be chosen for isotropic materials. For composite materials, maximum stress criterion is used for ply failure. PANDA2 also models transverse ply cracking. The transverse stiffness of plies that have exceeded the allowable stress is reduced to zero to account for transverse ply cracking.

PANDA2 computes buckling load factors using closed form solutions (called "PANDA type" [26]) for general instability, local buckling of the panel skin, local buckling of stiffener segments, rolling of stiffeners with and without stiffener participation. General instability is predicted using a model in which the stiffeners are smeared out as prescribed by Baruch and Singer [18]. The local instability load is also obtained using a discrete model (Figure 3.1) of a single module along either the circumferential or axial direction. The discretized model is also used for calculating wide column bucking. The discretized model accounts for local bending of the skin and deformation of the stiffener parts in the wide column buckling mode. These details cannot be captured using the smeared model. PANDA2 also allows design optimization of panels with local postbuckling. The theory used in PANDA2 for postbuckling is similar to that formulated by Koiter for panels loaded into the far postbuckling regime [71]. Local skin postbuckling is captured in PANDA2 [29] by the second model, the discretized skin-stringer repeating module.

PANDA2 subroutines, PANEL and STAGSMODEL, can generate input files for more detailed BOSOR4 [26, 33] and STAGS [34, 90] analysis. This provides the user with an easy way to check the final optimum using more rigorous analysis models.

Analysis and Design with Effects of Initial Imperfections

Shape imperfections greatly affect the load carrying capacity of cylindrical shells under axial compression. However, it is often difficult or impossible to choose *a priori* an imperfection shape for design optimization of the shell structure. A considerable amount of research has been done in the area of imperfections. Stochastic approaches to account for the effect of imperfections on panel instability have been developed [46, 54, 74].

These methods are expensive to use and require a database of imperfections based on the manufacturing process. More recently, manufacturing models have been proposed to predict manufacturing induced geometric imperfections [55].

PANDA2 considers a variety of modal imperfections, such as global, local, inter-ring, and out-of-roundness imperfection [35, 37]. A user supplied imperfection amplitude is applied to the corresponding critical buckling mode shape of the panel. For cylindrical panels, the imperfections affect the buckling load factors calculated by closed form solutions directly by changing the effective radius of the shell. Additionally, global or bowing imperfections affect the distributions of the prebuckling stress resultants over the various segments of the panel, which in turn affects the buckling loads.

PANDA2 calculates knockdown factors to reduce buckling loads due to imperfections. The buckling loads are calculated for general instability (skin, stringers, rings all buckle together, smeared), inter-ring buckling (skin and stringers buckle between rings), and local buckling (skin buckles between adjacent stringers and rings). The knockdown factors are calculated using closed form solutions of both perfect and imperfect cylindrical panels, in which the imperfections (global, inter-ring, local and out-of-roundness) are used to reduce the radius of curvature of the portion of the panel used, thereby reducing the buckling loads. Imperfections also cause stress redistribution due to prebuckling bending caused by the load eccentricity in initially imperfect panels. More details of the implementation can be obtained from Bushnell and Bushnell [35, 37]. The knockdown factors are reduced further by the ratio Arbocz/PANDA for the perfect panel if the ratio is less than unity. Arbocz theory [9] accounts for the induced prebuckling membrane hoop compression generated in a cylindrical shell with axisymmetric

imperfections subjected to uniform axial compression. More details of the Arbocz theory implementation in PANDA2 can be found in Bushnell [30].

In practice, since the shapes of the initial imperfections are unknown (buckling modes), it is difficult for the user to judge whether or not the chosen imperfection amplitude is reasonable. Use of a fixed value for the imperfection amplitude can lead to non-conservative or over-conservative designs. To overcome this, PANDA2 provides an option to automatically adjust the value of the buckling modal imperfection amplitude supplied to the program. PANDA2 reduces the value of the imperfection amplitude that it judges to be larger than that which would be easily detectable by the most casual inspection. For a given value of imperfection amplitude, imperfection shapes with shorter (axial and circumferential) wavelength are more easily detectable than imperfection shapes with long wavelengths because the high curvatures are easily detected. PANDA2 reduces the imperfection amplitude to a value that will give no more than 0.1 radians wall rotation if the user selects the option to adjust imperfection amplitudes. This option is used in the present design optimizations of panels with imperfections.

PANDA2 applies the given amplitudes to the shape of the critical buckling modes for general, inter-ring, and local buckling models. The shapes of the imperfections change during optimization as the critical buckling mode changes. The out-of-roundness does not have wavelength and therefore stays the same. The buckling mode and the corresponding number of half-waves is determined from closed form solution [26]. For discrete models, the local buckling mode is predicted from the single skin-stringer module; the inter-ring buckling mode is predicted from the single “skin”-ring module, where “skin” denotes skin with smeared stringers.

The buckling mode is introduced in the imperfection sensitivity analysis as a harmonic function of the *x* and *y* coordinates and the unknown number of half-waves *m* (axial) and *n* (circumferential) [26]. The amplitude of the harmonic function is set to the modal imperfection amplitude (provided by the user and possibly adjusted by PANDA2). The strains are then calculated as the sum of two distinct contributions: the strain induced by the applied loads acting on the perfect shell and the strains induced by amplification of the modal imperfection shape during loading. Then the stresses and the resultant re-distributed stress resultants are calculated using the stress-strain relation. The buckling analysis is carried out for the imperfect structure with closed form solutions [26] or 1-D discrete models [25, 33].

Designing shell structures without considering the effects of initial imperfections can lead to critical designs. Initial imperfections have two effects. First, they reduce the effective radius of curvature of cylindrical panels leading to lower buckling loads. Second, they give rise to prebuckling bending which leads to local increases in destabilizing stress resultants in parts of the segmented structure. The wide column buckling model ignores curvature and calculates the column buckling failure load. The wide column buckling model compensates for the first effect and can be used as an alternative to designing without imperfections. However, there are significant modal interaction effects in flat panels that are not captured by the wide column buckling model (see Van der Neut [113]). A comparison of designs obtained without imperfections to those obtained with wide column buckling and with imperfections is presented in the Modeling Issues section in this chapter.

Optimization Capabilities

PANDA2 can analyze and optimize panels with up to five different load sets that are combinations of in-plane loads, edge moments, normal pressure and temperature gradients. Design constraints include general, local, and stiffener buckling; lateral displacement under pressure; and stress failure (in plies). PANDA2 can optimize stiffener spacing, cross-sectional dimensions, ply thicknesses and orientation angles of the laminates. The PANDA2 optimization is performed using the gradient based ADS optimization subroutine developed by Vanderplaats [116].

PANDA2 performs gradient based optimization and therefore can use continuous design variables. Optimum designs obtained with continuous values for ply thicknesses are not practical as they have to be integer multiples of the commercially available tape or pre-preg ply thicknesses. . Rounding ply thicknesses often results in sub-optimal designs. Hence, ply thickness of the preliminary optimum designs were rounded to the nearest integer ply thickness value and re-optimized again for the other design variables (excluding ply thickness variables).

PANDA2 uses the method of feasible directions [116] for constrained optimization. The line search (gradient based) is controlled by the PANDAOPT processor of PANDA2. PANDAOPT performs successive line searches with a new search direction vector calculated at the new design points. The gradient vector required to obtain the search direction is calculated from a forward finite difference calculation. In order to ensure convergence, the move limit is reduced by 50% after each successive iteration. The iterations are stopped when the line search converges to an optimum or when the number of iterations has reached the user-specified maximum. Bushnell [25] recommends that a small number of iterations be used in each PANDAOPT execution

and that many PANDAOPT executions be performed to obtain an optimum. However, for cases where the constraints are highly oscillatory, the user should specify a large number of iterations in PANDAOPT to ensure convergence.

PANDA2 also has the capability to perform global optimization [30] with the use of the SUPEROPT processor. The global optimization strategy of PANDA2 is based on automated random multiple restarts of gradient based (line) searches to locate the global optimum. SUPEROPT performs a user specified number of PANDAOPT executions with an intermittent restart (AUTOCHANGE process). A total of 275 iterations (line searches) are performed for each SUPEROPT execution.

The AUTOCHANGE process of PANDA2 randomly changes the vector of design variables (Item 51 of "panda2.news" [25]). The AUTOCHANGE processor changes the design variables as follows:

$$y_i = x_i(1+\delta x_i), \qquad i = 1,2,3,\ldots,\text{number of design variables} \tag{3.1}$$

in which x_i is the old value of the i^{th} design variable, y_i is the new value and δx_i is the relative change in the value of the variable, and takes a random value between -0.5 and 1.5 (except for stiffener spacing, where a range between –1.0 and 1.0 is used). The perturbed design then provides a new initial point for the optimization.

Bushnell recommends that initial panel optimization in PANDA2 be performed with closed form solutions (IQUICK=1) to locate a near optimal design with small computational effort. The obtained results must be analyzed using discrete models (of stringer-skin module in IQUICK=0 option), and if they are not satisfactory, optimized again using the IQUICK=0 option. The recommended practice is useful because the discretized solutions can result in discontinuous behavior at the critical loads because the

failure mechanisms change significantly when small perturbations are made to the design. Such changes in failure mechanisms cause problems for gradient based optimization.

Another advantage of using the IQUICK=1 option is that when geometric imperfections (in the shape of critical modes) are included in the design, the analysis estimates stresses and buckling loads for different combinations of positive and negative imperfection amplitudes. The IQUICK=0 option requires the designer to add new load cases that have different combinations of the positive and negative imperfection amplitudes. Modeling general and inter-ring imperfection with both positive and negative signs therefore results in four different load cases. Optimum designs obtained using IQUICK=0 and IQUICK=1 are compared in the Modeling Issues section. The required computation (CPU) time is also presented for the optimizations. Computers have become faster and cheaper than they were at the time when PANDA2 was initially developed. It appears that with the availability of faster computers, the user should use the IQUICK=0 option whenever possible

Papers comparing PANDA2 analysis and design optimization results using either the STAGS program [34] or experiments have been published. Bushnell and Bushnell [36] optimized composite stiffened panels under combined loads and verified the optimized designs using STAGS. Bushnell *et al.* [38] also validated PANDA2 designs with experiments. The Modeling Issues section presents finite element analysis verification of panels optimized using PANDA2.

The most challenging task in stiffened shell optimization is the selection of appropriate modeling, theories and design constraints. Programs such as PANDA2

partially automate this task and thereby serve as an expert system for stiffened shell design.

Reusable Launch Vehicle Propellant Tank Design

Unlike expendable launch vehicles, reusable launch vehicles (RLV) have tanks that are an integral part of the vehicle structure. RLVs require extra fuel to carry the tank structures through the entire mission. It is hence of paramount importance to reduce the structural weight of the tanks. Selection of structural concepts for RLV tanks is therefore driven primarily by minimum weight design. In the present work, different stiffened cylindrical panels were optimized for use in the liquid hydrogen tank of RLVs. The minimum weight structure is obtained for given loads and is designed with buckling, strength (stress failure), and strain constraints.

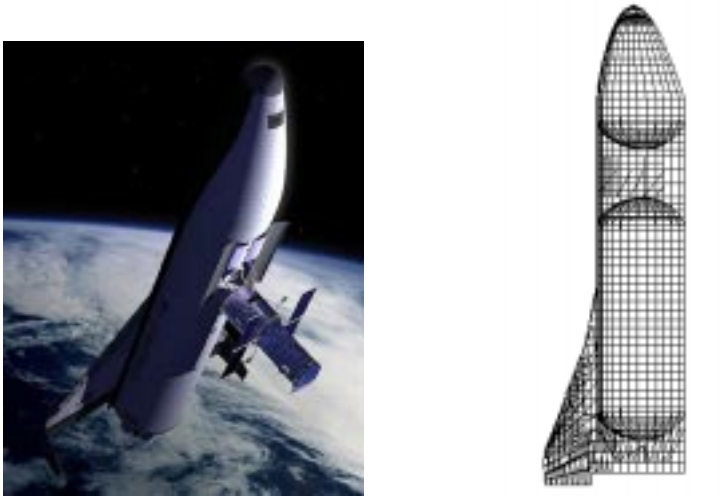

Figure 3.3: Schematic of a Reusable Launch Vehicle

The RLV considered here is a lifting body (see Figure 3.3) which has a circular tank structure with wings attached. The radius of the tank is 160 inches. The cylindrical portion of the tank is manufactured in short barrel sections and assembled to form the

entire tank. The attachment line between the barrel sections has a substantial ring frame. For the preliminary design trade studies, a barrel length of 300 inches was used. The cylinder geometry is modeled with different longitudinal (stringers) and circumferential (ring) stiffeners.

Table 3.1: Panel concepts, stiffener locations, and materials considered for the RLV liquid hydrogen tank design

Panel Type	Stringers	Rings	Material
Aluminum T-Stringer and J-rings	Internal	External	Al-2219 T87
Aluminum isogrid stiffened panel	Internal blade isogrid	External J-rings	Al-2219 T87
Aluminum orthogrid stiffened panel	Internal blade stiffeners		Al-2219 T87
Titanium symmetric sandwich - T rings	N/A	Internal	Ti-6Al-4V
Titanium asymmetric sandwich - T rings	N/A	Internal	Ti-6Al-4V
Titanium truss core sandwich	Hat-shaped corrugation	N/A	Ti-6Al-4V
Composite T stringer and T rings	External	External	IM7/977-2
Composite symmetric sandwich – T rings	N/A	Internal	IM7/977-2
Composite asymmetric sandwich – T rings	N/A	Internal	IM7/977-2
Composite truss core sandwich	External corrugated skin	N/A	IM7/977-2

The design concepts, stiffener location, and materials used in the design of RLV liquid hydrogen (cylindrical) tanks are shown in Table 3.1. The selection of stiffener types and their positioning (external vs. internal) is based on manufacturing consideration, type of thermal protection system (TPS), and the TPS attachment method used for the vehicle. Both metallic and composite panels were designed. Material properties are given in Appendix A. The aluminum and titanium alloys used for metallic

concepts had the same specific stiffness, but the titanium alloy had 45% higher specific strength. The composite material used was the IM7/977-2 graphite epoxy system.

Composite panels were optimized with fixed lay-ups, or with some ply thicknesses included as design variables. Table 3.2 shows the laminates used in the optimization and the ply thicknesses that were used as variables. The laminate thickness bounds are also shown. Skin laminate thickness of stiffened panels (thickness of inner facesheets in the case of sandwich) was required to be at least 12 plies (0.06 inch thick) in order to avoid the liquid hydrogen permeation.

Table 3.2: Different laminate lay-up used for composite panel design

Concept	Shell segment	Lay-up design	Laminate thickness (inch)
Panel with	Wall	$[(+65/-65)_3]_S$	0.06
T-stringers and T-rings	Wall	$[+45/90_3/-45/0_3/-45/90_3/45]_T$	0.065
	Stiffeners	$[+45/-45/0_n/-45/+45/0_m]_S$	0.055 to 0.100
Sandwich Panel	Stiffeners	$[+45/-45/0_n/-45/+45/0_m]_S$	0.055 to 0.100
with T-rings	Stiffeners	$[+45/90_n/-45/0_m]_S$	0.035 to 0.080
	Inner facesheet	$[+45_{n1}/90_{n2}/-45_{n3}/0_m]_S$	0.06 to 0.14
	Outer facesheet	$[+45_{n1}/90_{n2}/-45_{n3}/0_m]_S$	0.035 to 0.14
	Wall	$[(+65/-65)_3]_S$	0.06
Truss core Panel	Stiffeners	$[+45/-45/0_n/-45/+45/0_m]_S$	0.055 to 0.100
	Stiffeners	$[+45/90_n/-45/0_m]_S$	0.035 to 0.080
	Skin	$[(+65/-65)_3]_S$	0.06

In the design, 0.005 in thick plies were used and lay-ups were chosen so that no more than four contiguous plies have the same orientation (n, n_1, n_2 and n_3 in Table 3.2 can be up to 4 while m is limited to 2 due to symmetry). Continuous optimization of ply thicknesses was performed first. A new optimization was performed after rounding the

ply thicknesses to an integer multiple of 0.005 inch (thickness of pre-preg plies used). This strategy was applied to all the composite panel concepts studied in this work.

Stiffening Concepts, Geometry and Design Variables

PANDA2 analysis uses a single repeating element module along the longitudinal and circumferential directions. Figure 3.4 shows the stiffeners that were used in the optimizations. The isogrid and the stringer-stiffened panels have external J-rings in order to provide attachments for the TPS. Internal rings were used for the sandwich case because the foam type insulation used requires a smooth outer surface.

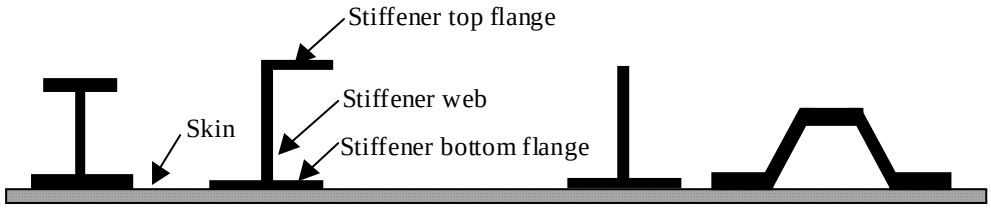

Figure 3.4: Schematic of a T, J, blade, and Hat stiffener geometry.

Table 3.3 lists the design variables for stringer-ring stiffened panels. The upper and lower bounds are also provided. Design variable bounds for composite panels are shown in parentheses only when they differ from the corresponding bounds used for metallic panels. This notation will be used in the rest of the paper.

Aluminum isogrid panel (see Figure 3.5) has blade stiffeners that delimit equilateral triangles. In this study, the isogrid has stiffeners running along the circumferential direction because the load cases considered produce substantial hoop stresses. In addition to the internal isogrid stiffeners, the panel also has external J-ring

stiffeners for attaching the TPS. The design variables and their bounds are described in Table 3.4.

Aluminum orthogrid panels have blade stiffeners that run along the longitudinal and circumferential directions, as shown in Figure 3.6. Design variable linking is used to maintain identical stiffener cross-section along the longitudinal and circumferential directions. However, stiffener spacings are not linked. The design variables and their bounds are listed in Table 3.5.

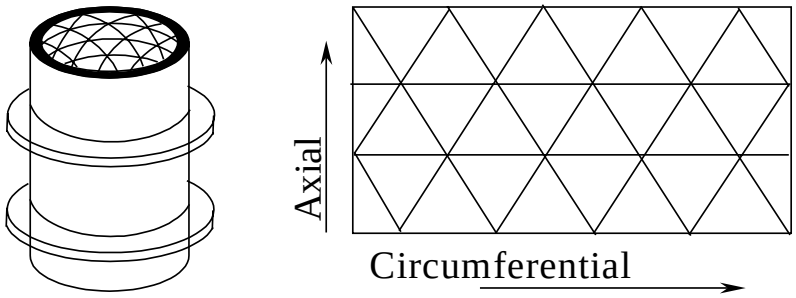

Figure 3.5: Cylinder with internal isogrid and external rings, circumferential Isogrid pattern

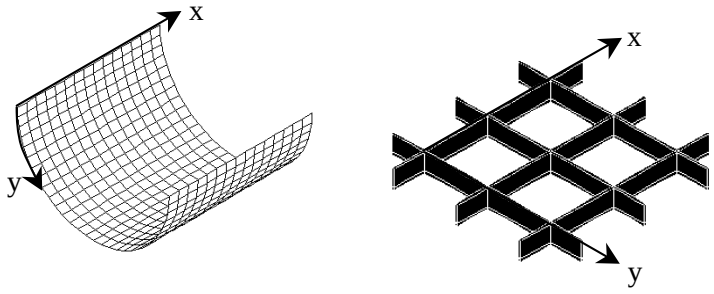

Figure 3.6: Schematic of orthogrid stiffening concept

Table 3.3: Design variables and bounds (in inches) used in the optimization of stringer-ring stiffened panels (Values shown in parantheses correspond to composite panels when different from metallic designs)

T-stiffener stringer geometry variables			J-stiffener ring geometry variables		
Description	Lower bound	Upper bound	Description	Lower bound	Upper bound
stringer spacing	5.0	30.0	ring spacing	10 (12)	30 (36)
width of stringer bottom flange	0.4 (1.0)	3.0	width of ring bottom flange	0.4 (1.5)	3.0 (2.5)
height of stringer	1.0	2.0	height of ring	2	4
width of stringer top flange	0.4 (1.0)	3.0	width of ring top flange	0.4 1.5	(3.0) 2.5
skin thickness	0.08 (0.06)	0.25 (0.06)	skin thickness	0.08 (0.06)	0.25 (0.06)
stringer bottom flange thickness	0.05	0.25	ring bottom flange thickness	0.05	0.25
stringer web thickness	(0.055)	(0.10)	ring web thickness	(0.055)	(0.10)
stringer top flange thickness			ring top flange thickness		

Table 3.4: Design variables and bounds (in inches) used in the optimization of aluminum isogrid stiffened panels

Description	Lower bound	Upper bound
Skin thickness	0.08	0.25
Isogrid module size (spacing)	10	25
Isogrid web height	1	5
Isogrid web thickness	0.03	0.25
ring spacing	30	120
Width of ring bottom flange	0.4	4
Height of ring	2	5
Width of ring top flange	0.3	3
Thickness of ring bottom flange	0.03	0.25
Thickness of ring web	0.03	0.25
Thickness of ring top flange	0.03	0.25

Table 3.5: Design variables and bounds (in inches) used in the optimization of aluminum orthogrid stiffened panels

Description	Lower bound	Upper bound
Stringer spacing	5.0	20.0
Ring spacing	5.0	60.0
Height of stringer	1.0	2.0
Skin thickness	0.08	0.25
Thickness of stiffener bottom flange	0.05	0.25
Thickness of stiffener web	0.05	0.25

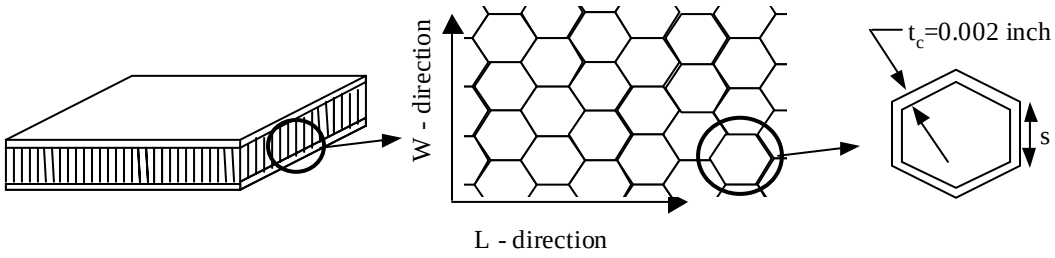

Figure 3.7: Honeycomb sandwich laminate

Table 3.6: Design variables and bounds (in inches) used in the optimization of honeycomb core sandwich panels

Description	Lower bound	Upper bound
Facesheet thickness	0.001 (0.06 internal; 0.035 external)	0.1 (0.14)
Core thickness	0.25	2
Ring spacing	30 (10)	120
Ring bottom flange width	1.5	2.5
Ring height	2	4
Ring top flange width	1.5	2.5
Ring bottom flange thickness	0.01 (0.035)	0.25 (0.1)
Ring web thickness	0.01 (0.035)	0.25 (0.1)
Ring top flange thickness	0.01 (0.035)	0.25 (0.1)
Honeycomb core cell diameter	0.125	0.375
Thickness of hex-cell wall	0.002	0.002

Ring stiffened sandwich panels with titanium or composite facesheets having an (expanded ribbon) honeycomb hexagonal core made of Titanium (Ti-6Al-4V) and brazed to the facesheets were also studied. Manufacturing imposes a constraint that the core cell wall (t_c) has to be at least 0.002 inch. PANDA2 can size the core diameter and cell wall thickness. A typical sandwich laminate and a transverse section of its hexagonal honeycomb core are shown in Figure 3.7. The design variables and their bounds are listed in Table 3.6. Panels were optimized using a value of 10^{-3} for the ratio of initial facesheet waviness to facesheet wrinkling half-wavelength, as recommended for panels of good quality [31].

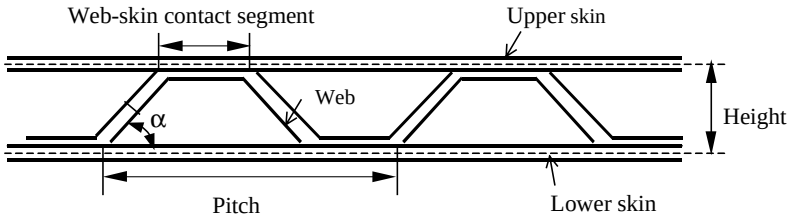

Figure 3.8: Schematic of the truss core sandwich module

Sandwich panels were designed with both fixed and varying core thickness. The sandwich core for fixed thickness may add to the weight of the panel. However, the increased thickness gives higher insulation capacity for the wall construction and can result in total weight savings from the reduced external insulation required for the hydrogen tank. Therefore, for RLV tank designs, core weight is not considered as structural weight but as insulation weight. In this study, for structural design comparisons, this weight is part of the panel weight.

Asymmetric sandwich wall constructions were also investigated. To minimize hydrogen permeation internal facesheets were required to have a minimum thickness of

12 plies. Since the outer facesheet was not required to have the 12-ply thickness, optimizations were performed for asymmetric sandwich constructions. In order to provide comparisons to the composite designs, similar optimizations were also performed for the titanium honeycomb core panels.

The metallic truss core panel is a corrugated panel with smooth face sheets and is designed using the titanium alloy to keep it consistent with metallic sandwich concepts. The schematic of the truss core concept as treated in PANDA2 is shown in Figure 3.8. The design variables and their bounds are listed in Table 3.7.

Table 3.7: Design variables and bounds (in inches) used in the optimization of truss core sandwich panels

Description	Lower bound	Upper bound
Pitch	1.0	5.0
Length of the contact segment skin-web	0.2	1
Height	0.5	1.5
Thickness of lower skin	0.01 (0.06)	0.1 (0.06)
Thickness of web	0.01 (0.035)	0.1 (0.1)
Thickness of upper skin	0.01	0.1
Web or corrugation angle α	45°	45°

Design Loads and Safety Margins

Only a small number of load cases are used for preliminary design optimizations. In the present study two loading conditions were selected: (i) Internal proof pressure of 35 psi; (ii) Axial compressive load N_x = 1000 lb/in, with an internal (stabilizing) pressure of 5 psi. The selected load cases were the most critical for stress failure and bucking failure, respectively.

The following safety margins were used in the optimization: general buckling safety factor of 1.4; all other buckling and stress safety factors equal to 1.2. Stress margins are calculated using the Von Mises stress criterion for metallic alloys and maximum stress failure for composite materials. In case of metals, stress margins are calculated taking the yield stress as stress limit. See Appendix A for stress limits.

For the present design study, the general buckling load factor is higher than the local buckling load factor. This implies that the panel can undergo local buckling before it fails in general buckling mode. Local buckling results in softening of the skin, increase in stresses, and amplification of initial imperfections, thereby reducing the general buckling load.

PANDA2 is capable of capturing the effects of local buckling on general instability for panels with stringers or both stringers and rings. Local postbuckling analysis is performed with the use of a discretized stringer-skin module (IQUICK=0) in PANDA2. This model ignores the curvature of the stiffened shell. Therefore, PANDA2 local postbuckling analysis cannot be used for deeply curved shells. In addition, the discretized analysis (IQUICK=0) is not available for shells without stringers. In the present study, stringer-ring stiffened panels optimized with effects of local buckling on general instability were compared with panels designed with safety factors applied to buckling loads from linear analyses. These results are presented in the next section. However, local postbuckling was not permitted in panels that were optimized for comparing the different stiffened panel concepts.

Modeling Issues

With PANDA2 employing a variety of approximate models, one may ask what are the effects of the approximations. In addition, PANDA2 offers the user the choice between more approximate and faster analyses (IQUICK=1) and accurate and slower analyses (IQUICK=0). The choice could depend on the required accuracy and computational effort. The PANDA2 accuracy issues have been addressed by Bushnell [34] and his coworkers [38]. Here, the effect of the different approximations and modeling choices available in PANDA2 on optimum stiffened panel designs are investigated. PANDA2 analysis results are also compared with results from detailed finite element analysis models.

Comparison of PANDA2, BOSOR4 and STAGS Analysis Models

PANDA2, BOSOR4, and STAGS represent programs in increasing order of modeling fidelity, model time preparation, and computational expense. The PANDA2 1-D discretized models [20, 34] are similar to those developed for the BOSOR4 program. However, unlike the BOSOR4 program in which the entire shell along one direction can be modeled, PANDA2 assumes a repeating pattern for the stiffeners and therefore uses only a single repeating (skin and stiffener) module with appropriate boundary conditions.

BOSOR4 is an energy-based discrete analysis method where the model is discretized along the meridian of a shell of revolution. BOSOR4 can also be used for prismatic structures such as stiffened panels [25]. For axisymmetric geometry and loads, BOSOR4 can obtain very accurate solutions. The 1-D discrete models in PANDA2 are based on BOSOR4 analysis models.

Using non-linear 2-D finite element models provides a more detailed analysis of stiffened shells. Finite element analysis allows the designer to model the shell structure and support conditions more accurately. However, the cost of analysis and modeling increases sharply with addition of such details. A variety of commercial finite element programs are available to users. In the present study the STAGS program [4, 90] was used. STAGS is a finite element code for general-purpose nonlinear static and dynamic analysis of shell structures of arbitrary shape and complexity. Its capabilities include stress, stability, vibration and transient analysis using both material and geometric nonlinearities. The element independent fully co-rotational procedure [89] implemented in STAGS allows large rotations required for nonlinear analysis. In addition, incorporation of the Riks arc-following algorithm [93] permits STAGS to analyze stiffened panels in the nonlinear regime.

Three examples are used here to illustrate the accuracy and computational effort of PANDA2 analysis. The examples chosen to investigate PANDA2 analysis are a stringer stiffened plate, a cylindrical stringer-ring stiffened panel, and a cylindrical honeycomb core sandwich panel with ring stiffeners. The second and third examples are panels designed for the reusable launch vehicle liquid hydrogen tank. Optimized stiffened panel designs are chosen, as it is known that optimizers often exploit model/analysis weaknesses and obtain poor designs.

The first example is the analysis of a T-stiffened flat panel with three stringers optimized for minimum weight and designed to resist buckling under a compressive axial load of 1000 lb/in. The predicted buckling loads and corresponding computational times required by PANDA2, BOSOR4, and STAGS are compared in Table 3.8. The results

demonstrate the accuracy of PANDA2 for regularly stiffened panel structures under uniform loads and gives evidence of its high computational efficiency. Figure 3.9 shows the buckling mode shapes from BOSOR4 and STAGS. A more significant difference that cannot be quantified is the effort required to generate the analysis models. PANDA2 has implemented in its library a variety of routines for the different stiffened panel models with the design constraints necessary to prevent generation of poor designs. The implementations of such constraints for use with general-purpose finite element programs would require substantial investment of time by the designer.

Table 3.8: Buckling loads and analysis time for PANDA2, BOSOR4 and STAG models for an optimized stringer stiffened plate.

	PANDA2	BOSOR4	STAGS
Buckling load factor	0.7781 (*closed form*)	0.7821	0.7848
	0.7751 (*1-D discrete module*)		
CPU time per analysis (s)	2.49	7.30	970.1

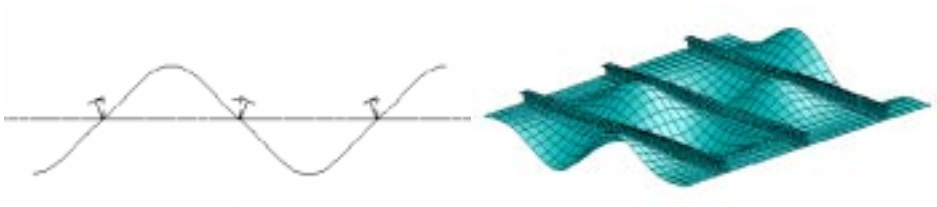

Figure 3.9: Comparison of the buckling mode shapes obtained with BOSOR4 and STAGS

The second example is an aluminum stringer-ring stiffened panel optimized using PANDA2 with imperfections (Column 3, Table B.1 in Appendix-B). The stringer-ring stiffened panel was modeled in detail, with stringers and rings modeled using branched shell assembly. A one-quarter finite element model (MSC/NASTRAN [8]) of the cylinder with symmetry boundary conditions applied to the structure was used for the linear

bifurcation buckling analysis. The NASTRAN finite element analysis program was chosen for the stringer-ring-stiffened panel, as it had a more user-friendly preprocessor than STAGS. Linear bifurcation buckling loads were obtained for a uniform axial compression load of 600 lb/inch.

The third example chosen for verification with STAGS, is the symmetric titanium sandwich panel (symmetric thick core) optimized using PANDA2 with imperfections (Column 5, Table B.6 in Appendix-B). The sandwich walls were modeled using the first order shear deformable shell elements (480 elements) in STAGS. To reduce the computations, symmetry was used, and only one half of the cylinder was modeled. The ring stiffeners were modeled as branched shell elements (as opposed to approximating them with beam elements). An axial compression load case with N_x = -1000 lb/in and 5 psi internal pressure was used for the analysis. A linear bifurcation buckling analysis was performed. The critical mode shape obtained from linear analysis was used as an initial imperfection with amplitude of 0.8 inch (0.5% of cylinder radius) to obtain the limit buckling load from a non-linear analysis.

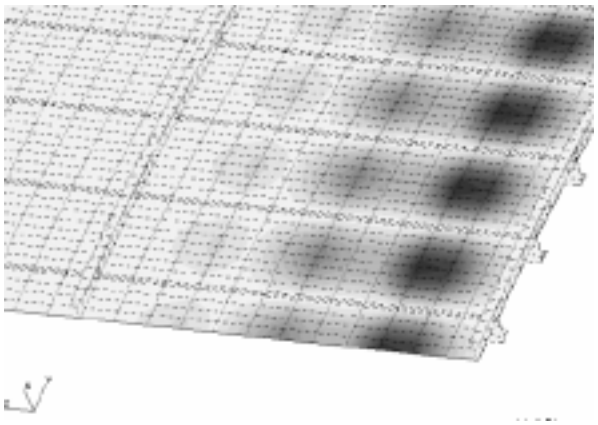

Figure 3.10: Critical buckling mode for the cylindrical stringer-ring stiffened panel

Figure 3.11: Mode shape for limit buckling of composite sandwich cylinder

Table 3.9: Comparison of buckling load factors obatined from PANDA2 and Finite element analysis for cylindrical panels optimized using PANDA2

Concept	PANDA2	Finite Element Analysis
Cylindrical stringer-ring stiffened panel (analyzed without imperfections)	1.2 (+10%)	1.07 (NASTRAN)
Cylindrical sandwich panel with T-rings (analyzed without imperfections)	4.224 (-8%)	4.576 (STAGS)
Cylindrical sandwich panel with T-rings (analyzed with global imperfections)	1.251 (-20%)	1.562 (STAGS)

Table 3.9 shows the results of the finite element analysis (NASTRAN or STAGS) and compares it to the PANDA2 analysis results. For stringer-ring stiffened panels PANDA2 results were about 10% higher from the finite element analysis results. The lower value of finite element analysis results was due to buckling at the supports. For stringer-ring stiffened panels PANDA2 optimizes using conditions at the ring and midbay between rings. Panels exhibit localized bending at end supports where they will need

extra stiffening. Figure 3.10 shows the critical buckling mode shape of the stiffened panel. The buckling failure mode is local.

For sandwich panels the buckling load predicted using PANDA2 analysis is lower than that obtained from STAGS finite element analysis. Results are compared for linear buckling analysis of a perfect structure and nonlinear analysis of the shell with a global imperfection amplitude of 0.8 inch. The imperfection shape used in STAGS analysis was the first critical buckling mode shape obtained from the linear analysis with amplitude of 0.8. The difference is 8% for linear analysis and 20% for nonlinear analysis with imperfections. The reasons for the larger difference for the second case is be partly due to the difference in the imperfections used for the buckling analysis and the conservative approach PANDA2 takes in dealing with imperfections. The buckling mode shape predicted by PANDA2 (general buckling with 11 axial halfwaves) was in good agreement with the mode shapes obtained from the STAGS linear and nonlinear (Figure 3.11) analyses.

To summarize, three examples were presented. The first example, a flat stringer stiffened panel that can be modeled almost identically in PANDA2 and STAGS, showed excellent agreement in buckling loads calculated using the two programs. The PANDA2 model cannot capture the details at the end supports for the second example, a composite stringer-ring stiffened panel, and therefore resulted in small differences in the predicted buckling loads. The difference in buckling loads of the sandwich ring-stiffened panel (example three) is attributed to three factors: the conservative knockdown factors applied for transverse shear correction, the conservative approach PANDA2 takes to account for

effect of imperfections, and the differences in the initial imperfections used in the analysis models in the two programs.

Comparison of Designs Obtained Using PANDA2 Analysis for IQUICK=0 and 1

Table 3.10 presents the optimized weights of aluminum and composite stringer-ring stiffened cylindrical panels designed for the RLV tank.

Table 3.10: Optimum weight of panel designed using IQUICK=0 and IQUICK=1 analyses

Panel concept	IQUICK FLAG	Without imperfections			With imperfections		
		Panel weight (lb/ft^2)	Stiffener weight fraction %		Panel Weight (lb/ft^2)	Stiffener weight fraction %	
			Stringers	Rings		Stringers	Rings
Aluminum stringer and ring stiffened	1	1.588	6.84	5.91	1.852	19.73	4.81
	1-0	1.602	5.43	7.78	1.842	19.31	4.95
	0	1.600	7.59	5.70	1.840	19.32	4.76
Composite stringer and ring stiffened	1	0.826	23.30	17.10	0.910	28.40	17.50
	1-0	0.822	23.64	16.46	0.909	28.24	17.57
	0	0.821	23.43	16.61	0.911	32.29	13.63

Table 3.11: Critical margins of design obtained optimized using IQUICK=1 and analyzed using IQUICK=0

Concept	Without imperfections		With imperfections	
	Critical margin %	Failure mode	Critical margin %	Failure mode
Aluminum stringer and ring stiffened	-3.3	Local buckling	-0.1	Stringer web and top flange buckling
	-11.1	Wide column buckling		
Composite stringer-ring stiffened	-0.8	Stress (pressure)	2.0	Local buckling
			3.5	General buckling

Optimum designs are obtained with and without initial imperfections. Stringer-ring stiffened panels resulted in almost equal weights for the optimum designs obtained using IQUICK=1 and IQUICK=0 analyses. The aluminum stringer-ring stiffened panel without imperfections that resulted in lower weight also violated the buckling constraints in IQUICK=0 analysis. For composite panels, there were no constraint violations (Table 3.11). The weights were almost identical.

Optimum designs obtained using IQUICK=1 analysis exhibited small violations of buckling and stress constraints. The designs obtained from global optimization (SUPEROPT) with IQUICK=1 analysis were re-optimized locally (PANDAOPT) with IQUICK=0 analysis. The final designs obtained are shown in Table 3.10 on rows indicated with IQUICK flag value of 1-0. The re-optimized designs satisfied all constraints and had weights very similar to those obtained using IQUICK-0 analysis. The small differences in the case of composite designs arise from the re-optimizations performed after rounding ply thicknesses to discrete values.

It appears that the IQUICK=1 analysis is sufficiently accurate to use for preliminary optimizations. Designs should, however, be analyzed and reoptimized using IQUICK=0 models whenever possible to ensure that there are no small violations or optimization failures.

Optimization of Panels with Local Postbuckling Effects

Safety factors were used in the design of panels for the RLV tank design for the stability and stress constraints. Factors of safety equal to 1.2 and 1.4 were applied to the local and general buckling load factors, respectively. In design of stiffened shell structures, it is typical to have a lower safety factor for local buckling compared to

general buckling failure. This is because local buckling of the skin or wall often does not significantly affect the structural integrity of the aircraft wing or launch vehicle structure.

However, using safety factors for buckling constraints can lead to critical designs. The design constraints are calculated from the buckling load factors obtained using service loads and the specified safety factors. PANDA2 has separate models to capture local and general buckling failure modes. The buckling loads are obtained independently and used as design constraints with different safety factors.

Table 3.12: Analysis of stiffened panels with use of PANDA2 local postbuckling analysis

Concept	Optimum weight (lb/ft^2)	Buckling loads (lb) and maximum stress (Kpsi)		
		Mechanism	Without local postbuckling	With local postbuckling
Aluminum stringer-ring stiffened panel	1.840	Bending stress (Kpsi)	48.34	80.67
		Local Buckling	1197	944
		Stringer buckling	1682	1158
		General Buckling	1666	1599
Aluminum orthogrid stiffened panel	2.147	Bending stress (Kpsi)	48.07	201.4
		Local Buckling	1225	602
		Stringer buckling	1199	735
		General Buckling	1410	1408
Composite stinger and ring stiffened panel	0.911	Bending stress (Kpsi)	73.86	249.7
		Local Buckling	1500	875
		Stringer buckling	1671	1029
		General Buckling	1509	1565

The rationale of linear behavior of the structure, on which safety factors are based, does not hold true in the case of buckling of stiffened shell structures in which local buckling is allowed. Local buckling of the shell wall reduces the effective stiffness

of the structure. The reduced stiffness of the structure will result in general buckling failure at a load somewhat lower than the design load factor applied to it. Furthermore, the local buckling also generates additional stresses near local buckling creases that can lead to stress failure and other local instabilities such as buckling of stringer segments at load factors possibly well below those used in the design. It is therefore recommended that the shell be designed for the ultimate load it will need to withstand and correctly account for postbuckling response if the local buckling load is lower than the general buckling failure load.

PANDA2 is capable of capturing the effects of local buckling on general instability for panels with stringers and panels with both stringers and rings. The IQUICK=0 (discrete) analysis model is used. However, the loads applied in the PANDA2 analysis must be set equal to the desired value of the general buckling load. The local buckling load factor will then have a value of less than one, (e.g., 1.2/1.4 in the case of RLV tank design).

Three panels (namely metallic stringer-ring stiffened panel [Table B.1]), orthogrid stiffened panel [Table B.3] and composite stringer-ring stiffened panel [Table C.1] that were optimized without permitting local postbuckling) are chosen for analysis with postbuckling. The panels were designed with initial imperfections included in the analysis model. Table 3.12 shows the maximum stress and buckling load of the designs analyzed with an ultimate load of N_x=-1400 lb/inch and internal pressure of 5 psi, with local postbuckling permitted. In the present study a stress safety factor of 1.0 is used for analysis with ultimate loads.

Table 3.13: Comparison of aluminum stringer-ring stiffened panel designs optimized with and without local postbuckling effects

Variable	Design obtained without local postbuckling	Design obtained with local postbuckling	Design obtained with local factor=1.4
Stringer spacing	7.764	7.287	6.545
Stringer height	1.927	2.000	1.936
Stringer top flange width (and thickness)	1.065 (0.071)	1.107 (0.078)	1.037 (0.071)
Stringer bottom flange width (and thickness)	0.400 (0.050)	0.400 (0.050)	0.400 (0.050)
Ring spacing	30.00	30.00	30.00
Ring height	2.000	2.141	2.3718
Ring bottom flange width (and thickness)	0.584 (0.104)	0.686 (0.122)	0.814 (0.137)
Ring top flange width (and thickness)	0.436 (0.050)	0.474 (0.054)	0.400 (0.05)
Wall thickness	0.097	0.096	0.096
Stringer web thickness	0.050	0.053	0.05
Ring web thickness	0.050	0.050	0.056
Panel weight	1.840	1.915 (4.1%)	1.924 (4.6%)
Stringer weight fraction %	19.32	22.02	21.92
Ring weight fraction %	5.30	5.42	6.57

Analysis of panels with postbuckling results in large increases in stress, and significant decreases in local buckling and stringer buckling loads. The reduction in general buckling loads is insignificant. The designs from Table 3.12 were re-optimized with local postbuckling allowed. The axial compression load case was modified such that the applied load was 1272.73 lb/inch, with safety factors of 0.9429, 1.1, and 1.1, respectively, for local buckling, general buckling, and stress failure. The value of the applied axial compression load (1272.73 lb/inch) is 10% lower than the required 1400 lb/inch load. This is because a load factor of 1.0 is changed by PANDA2 to 1.1 to avoid numerical difficulty.

Table 3.14: Comparison of aluminum orthogrid stiffened panel designs optimized with and without local postbuckling effects

Variable	Design obtained without local postbuckling	Design obtained with local postbuckling	Design obtained with local buckling factor =1.4
Stringer spacing	6.544	6.851	6.266
Stringer height	1.791	2.000	2.000
Ring spacing	19.70	29.71	24.33
Wall thickness	0.092	0.093	0.093
Stringer web thickness	0.156	0.205	0.166
Panel weight	2.147	2.400 (11.8%)	2.295 (6.9%)
Stringer Weight fraction %	28.69	35.92	33.15
Ring weight fraction %	9.53	8.28	8.54

Table 3.15 Comparison of composite stringer-ring stiffened panel designs optimized with and without local postbuckling effects

Variable	Design without local postbuckling	Design obtained with local postbuckling	Design obtained with local buckling factor=1.4
Stringer spacing	8.545	7.598	10.51
Stringer height	1.656	2.000	2.000
Stringer bottom flange width	1.000	1.000	1.073
Stringer top flange width	1.170	1.488	1.046
Ring spacing	34.49	36.00	36.00
Ring height	3.221	2.121	3.141
Ring bottom flange width	1.500	1.500	1.500
Ring top flange width	1.799	1.500	1.500
Panel weight	0.911	1.035 (13.6%)	0.954 (4.7%)
Stringer Weight fraction	32.3	42.2	33.7
Ring weight fraction	13.6	10.2	14.7

Table 3.13 compares an aluminum stringer-ring stiffened panel design obtained using linear bifurcation buckling analysis with the design obtained where local postbuckling was permitted. Tables 3.14 and 3.15 present similar results for an aluminum orthogrid stiffened panel and composite stringer-ring stiffened panel. The composite stringer-ring stiffened panels were designed with a $[(+65/-65)_3]_s$ laminate for the skin and a $[45/-45/0_3/45/-45/0]_s$ laminate for the stiffeners.

Optimized designs are also obtained for the case where the local buckling load is increased to the value of the general buckling load factor (1.4). In the present case, the applied load for axial compression is set at 1272.73 (1.4x1000/1.1) with general buckling and stress safety factor set equal to 1.1.

The aluminum stringer-ring stiffened panels showed a smaller increase in weight for metallic designs (4.1%) compared to their composite counterparts (13.6%) The weight increase is primarily due to the increase in weight of the stringers and rings. The reduced wall stiffness due to local buckling is compensated by the increased stiffness of the stringers and rings.. The increase in weight is small for the present case, as the driving factor for the designs was the hoop stress from the (35 psi) internal proof pressure load case. The weight increase for the orthogrid panel was higher (11.8%) than for metallic stringer-ring stiffened panel (4.1%).

Designs obtained using local buckling load factor set equal to the general buckling load factor (1.4) were found to be lighter that those obtained with local postbuckling permitted (except for aluminum stringer-ring stiffened panel for which the weight increase was approximately equal). The higher weight of panels designed for local postbuckling is due to the conservative approach used in PANDA2 analysis for the non-

linear response of panels after local buckling has occurred (when local buckling load factor is less than 0.95). The analysis models reduce the effective stiffness of the skins, which in turn result in higher amplification of the initial imperfections leading to lower buckling loads.

The weight increase in panels optimized with a higher local buckling load factor of 1.4 (also used for general buckling) was, 4.6%, 4.7%, and 6.9%, (see the third column of Tables 3.13, 3.14 and 3.15) respectively, for aluminum stringer-ring stiffened panel, aluminum orthogrid stiffened panel and composite stringer-ring stiffened panel. The weight increase of panels designed with a higher load factor for local buckling) is smaller than the weight increase for corresponding panels optimized with local postbuckling effects.

It appears that higher weight increase in panels optimized with local postbuckling permitted is due to the conservative models used for estimating the nonlinear effects in the PANDA2 analysis. The optimizer does not have the freedom to choose a lighter design that can be obtained by raising the local buckling load factor. The designer using PANDA2 for stiffened panel design should therefore perform two optimizations, one with local postbuckling included and another with a local buckling load factor raised to the value of general buckling load, to select a design with lower weight.

Nevertheless, the model used in PANDA2 to design panels with both stringers and rings for local postbuckling is a useful tool because the nonlinear analysis of PANDA2 requires several orders of magnitude lower computational effort compared to performing a full non-linear finite element analysis. The RLV panels designed showed weight increases (5 to 14%) due to the more critical proof pressure load cases. For panels

designed without such a load case, local buckling could result in larger reductions in general buckling load margins.

Modeling Geometric Imperfections vs. Using Wide Column Buckling

This section presents optimum designs of perfect and imperfect stringer-ring stiffened panels. The perfect panels were optimized with and without the wide column buckling constraint. The optimum weights and failure margins of the optimum designs are compared.

PANDA2 permits use of wide column buckling constraint for curved panels. The wide column model treats the cylindrical panel between rings as a flat panel and obtains the inter-ring buckling load. Two models are available in PANDA2 [25] to capture the wide column buckling failure. A 1-D discrete model (IQUICK=0) of the skin-stringer module and a closed form solution (IQUICK=1) for inter-ring buckling where a large shell radius replaces the actual radius. The inter-ring buckling load factor is also computed with a 1-D skin-ring discrete model that accounts for the shell curvature [34]. PANDA2 optimizations use the lower bounds from the different analyses to ensure conservative designs.

Optimizations were performed for panels with and without imperfections. Panels designed without imperfections were optimized with and without wide column buckling constraint. Imperfect panels were optimized with global and out-of-roundness imperfection amplitudes of 0.8 inch (0.5% of the cylinder radius), inter-ring and local imperfection amplitudes of 0.1 inch and 0.01 inch, respectively. PANDA2 was allowed to adjust these values if the rotation of the wall exceeded 0.1 radian for the critical mode shape used for imperfections.

Table 3.16: Optimum weight of panels optimized with and without imperfections and/or wide column buckling constraint

Ring spacing (inch)	Optimum panel weight (lb/ft^2)		
	Perfect panel without wide column buckling constraint	Perfect panel with wide column buckling constraint	Panels designed with initial imperfections
30	1.5908	1.6157	1.8411
60	1.5840	1.6825	1.8640
90	1.5736	1.8640	1.9032
120	1.5688	2.1602	2.0890

Table 3.17: Comparison of margins of perfect composite stringer-ring stiffened panels analyzed with imperfections

Ring spacing	Constraint margins (in percentage) of perfect panels obtained from an optimization without wide column buckling constraint				obtained from an optimization with wide column buckling constraint			
(inch)	Bending stress	Local Buckling	General Buckling	Stringer (Ring) buckling	Bending stress	Local Buckling	General Buckling	Stringer (Ring) buckling
30	-98.8	-99.0	-48.9	-98.0 (-97.3)	-95.2	-96.0	-40.5	-91.4 (-85.1)
60	-98.6	-98.6	-49.2	-97.6 (-98.3)	-67.3	-76.5	-23.6	-73.3 (-25.2)
90	-98.9	-98.5	-54.6	-97.2 (-98.3)	-17.8	-38.0	-0.75	12.6 (-36.9)
120	-98.5	-98.5	-49.2	-97.4 (-98.5)	6.96	-36.3	17.1	58.5 (-39.8)

Table 3.16 presents the optimized weight of panels at different ring spacings obtained from optimization with the discretized analysis model (IQUICK=0). Table 3.17 compares the critical constraints for perfect panels designed without and with wide column buckling constraint enforced, and analyzed with imperfections. Table 3.16 shows

that perfect panels are insensitive to ring spacing if wide column buckling constraint is not included. The resulting designs are critical in hoop stress due to proof pressure and local buckling.

The perfect panels optimized with wide-column buckling constraint imposed were critical in wide column buckling failure for all values of the ring spacing. However, for larger ring spacing, the effect was more pronounced and resulted in optimum designs with taller stringers to provide increased bending stiffness. The optimized weight is more sensitive to ring spacing when the wide column model is used. This is expected because the wide-column buckling uses the inter-ring portion of the stiffened shell and column buckling is a function of the length.

Panels designed without imperfections are less sensitive to imperfections if designed with the wide column buckling constraint. Introduction of imperfections in the analysis of these panels (perfect panels optimized with wide column buckling constraint) results in critical buckling and stress constraints. This is because in addition to reducing the curvature, imperfections induce bending in the prebuckling phase that result in redistribution of the stress resultants and increase stresses in the stiffener segments. Using wide column constraint cannot simulate these conditions and hence cannot entirely protect against the detrimental effects of imperfections.

Panels optimized without imperfections and without wide column constraint can be extremely unconservative and can fail at loads much smaller than design loads in actual use. Wide column constraint alleviates this problem but does not eliminate it. However, at smaller ring spacing it appears that the wide column buckling constraint

alone is not enough to design the panels. Even if unknown, small values of imperfections that are reasonable should be used in the optimization of panels with PANDA2.

Modeling Issues in Truss Core Panel Design

In preliminary comparisons of optimum weight of stiffened panel designs, it was discovered that truss core panel weights were very different from weights of the remaining concepts. The present section presents the results of the investigation performed to explain the reason for heavier weights for truss core sandwich panels. In particular, the effect of not including rings as clamped supports and the effect of having different corrugation angles are investigated.

Optimization of panels without rings

The PANDA2 program has a limitation in the modeling of truss core panels: it does not allow inclusion of ring frames in the analysis model. Figure 3.12 shows optimum weight of panels designed with rings replaced by clamped supports for different lengths. The optimizations were performed with the IQUICK=1 analysis.

Figure 3.12 shows that the optimum designs are lighter for panels of short lengths (10 inches). For short panels, the bending boundary layer length (BLL) at supports is comparable to the panel length (see Items 175, 242 and 378 of …/panda2/doc/panda2.news file [25]). The bending effects help counteract hoop tensile stresses that arise due to the clamped edge supports, resulting in a low weight for the optimized panels. Local buckling failure and stiffener buckling drive the design at short lengths.

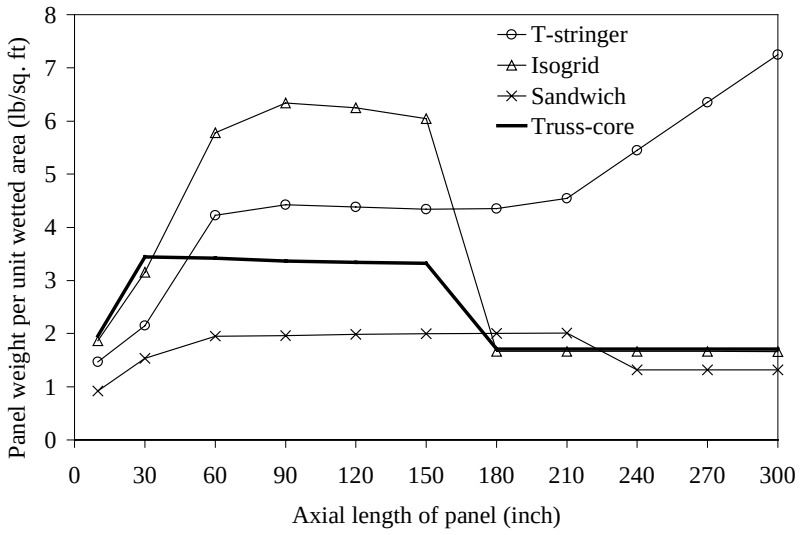

Figure 3.12: Effect of axial length on optimized weight for panels without rings

The sharp increase in weight observed when the panel length changes from 30 to 60 inches (or from 10 to 30 inches for sandwich and truss core panels) is due to the stress field produced by local bending near the clamped edges. The clamped edges counteract the radial expansion induced by the internal pressure and produce large compressive and bending stresses at the supports. For panel lengths from 30 to 150 inches, the optimum weight of panels remains approximately constant. The active constraints are those corresponding to the internal proof pressure load case. Stress is the only critical margin for the T stringer and isogrid concepts; upper skin buckling and core shear failure modes are active for truss core and honeycomb-core sandwich panels, respectively.

Beyond this length (150 inches), the weight increases for stringer stiffened panels. The weight increase for panels longer than 180 inches is attributed to column buckling modes becoming active at large lengths. The weight of sandwich panels decreases because PANDA2 neglects conditions at the support for long panels. When there are no rings in the model, PANDA2 designs for conditions at the midsection of the panel and the

conditions at the supports. However, if the BLL is very small compared to the panel axial length PANDA2 ignores the local bending at supports and the resulting stress field. The panel designed thus will need to be stiffened locally at supports to carry the high local stresses.

PANDA2 cannot design panels with varying cross-sections along the length. PANDA2 works well for panels with many repeating stiffeners in the cylinder, where the inter-ring buckling behavior of the shell can be characterized by extracting a segment between two adjacent rings. The design is performed using the stress state at rings and at mid section between rings. In the absence of ring stiffeners, PANDA2 uses the conditions at mid panel and at end supports for the design. For long panels, large bending stresses are present at the end supports. Using the local stresses to design the entire panel produces overly heavy designs.

However, the designer can obtain designs for mid-bay conditions and end support conditions by performing two sequential optimizations in PANDA2. The first optimization uses a “complete” analysis, in which the margins are computed including conditions at both mid-length and ring locations. The results of the first optimization are used as input for a new optimization that neglects the conditions at the shell edges. The optimum values of stiffener spacing, thicknesses, and cross-section dimensions obtained from the initial optimization with complete analysis (using stress state at mid-bay and at rings) are chosen as new lower bounds for the stiffener sizing in the optimization that uses only the stress state at mid-bay (between rings). Stiffener spacing and cross-section can no longer be optimization variables. A new optimization is performed and a lighter design is obtained. The panel skin and stringer dimensions from the first optimum design

would be used for a certain axial length of panel near the rings; the panel skin and stringer dimensions and ring dimensions from the second optimum design would be used for the panel mid-length region and for the rings. The length of the "edge" design, i.e. the length at which the cross-section changes, is chosen based on engineering judgment or based on value of the boundary layer length. The "hybrid" design then must be verified by finite element analysis of the detailed model.

For truss core panels this approach was not used because too few design variables were used in the optimization, and there was not enough design freedom. It was felt that the weight obtained for the 300 inch long panel was a reasonably accurate representation of truss core panel, even though weight of local stiffening is ignored.

Effect of corrugation angles on optimum weight

Truss core stiffened panels behave differently from honeycomb or foam core sandwich panels. In the case of truss core sandwich panels, the thickness and orientation of the corrugation web affect the out-of-plane shear stiffnesses. The G_{13} shear deformation of the sandwich is carried by inplane shear deformation of the corrugation webs, whereas the bending and inplane (compression/tension) loading of the web provide the G_{23} shear stiffness. In the case of truss core sandwich, internal pressure in the cylinder causes transverse compression of the sandwich laminate. Since the webs of the sandwich core are inclined, the compressive forces in the web induce compressive stresses in the facesheets at the crown portion of the truss core corrugation. Optimized panels must choose a corrugation angle that will minimize the compressive stresses induced in the facesheets while maximizing the transverse shear stiffness.

Table 3.18: Effect of corrugation angle on optimum weight of truss core panel (Internal pressure load case and axial compression load case are indicated by the numbers 1 and 2 in parenthesis)

Web angle α	Optimum panel weight (lb/ft^2)	Critical constraints
15°	5.098	Corrugation (1) and Upper skin bucking (2)
30°	2.926	Corrugation (1) and Upper skin bucking (2)
45°	2.126	Corrugation (2) and Upper skin bucking (2)
60°	1.735	Stress (1) and Corrugation buckling (2)
Optimized (62.312°)	1.705	Stress (1); Corrugation (2), Upper skin (2), and General buckling (2)
75°	1.744	Stress (1); Corrugation (2) and General buckling (2)
85°	1.781	Stress (1), Corrugation (2) and General buckling (2)

Table 3.18 presents optimum weight and critical failure constraints obtained for truss core panels with different corrugation angles for a 300 inch long panel clamped at the supports. Heavier panels are designed for web angles that are smaller than 60°. The fixed value of corrugation angle (45°) prescribed from manufacturing constraints is not optimal for structural efficiency. The weight obtained for the very small web orientation angle (15°) is very high. The analysis of constraint margins indicates that small corrugation angles result in critical margins for corrugation web buckling and upper skin buckling, leading to thicker corrugation webs. For larger corrugation angles, general buckling becomes more critical. This is due to the reduction in transverse shear stiffness of the core when the corrugation angle becomes large. The optimum corrugation angle is 53° for panels optimized without imperfections and 62° for panel optimized with imperfections.

Optimization and Cost Issues

This section presents some optimization issues and the computational effort required for such optimizations. The discussion will focus on the global optimization capability of PANDA2 and the computational effort (CPU time) required for the optimization.

Structural optimization of stiffened panels often involves large numbers of design variables that are somewhat redundant. The redundancy creates different optimum designs that have almost identical weights, that is, multiple local optima. Expensive global optimization techniques are often required to obtain the best design. Introducing optimization complexity such as global optimization requires an increased amount of computational effort. However, global optimization algorithms often provide multiple solutions with similar performance. The designer can use such information, if the weight difference is small, to choose a design that satisfies other considerations (such as manufacturing cost and damage tolerance) that were not included in the analysis.

The efficiency of PANDA2 analysis methods and models allows it to perform global optimization of stiffened panels. Global optimization typically requires a computational effort of magnitude one or more orders higher than that required for locating local optima. Table 3.19 shows the computation (CPU) time required for one SUPEROPT execution for global optimization of a stringer-ring stiffened panel. The computations were performed on a 233 MHz Digital Alphastation-200 4/233. The weight of the optimum design obtained using IQUICK=1 analysis is same as that obtained using IQUICK=0 analysis at a fraction of the computation cost. The CPU time for a global optimization is still much lower than that required for a single nonlinear finite element analysis (Table 3.8).

Table 3.19: Comparison of CPU times required for one SUPEROPT execution for global optimization of an aluminum stringer-ring stiffened panel using IQUICK=0 and IQUICK=1 analysis options

	IQUICK=1	IQUICK=0
CPU time (seconds)	134.2	394.2
Optimum weight of panel (lb/ft^2)	1.852	1.840
Constraint violation of optimum (IQUICK=0 analysis).	0.10% (stringer web and top flange buckling)	0.24% (local buckling)
Constraint violation of optimum (IQUICK=1 analysis).	0.04% (stringer web and flange buckling)	2% (local buckling) 10% (stringer rolling)

Table 3.20: Number of optimization iterations and optimized weight of isogrid stiffened panels with different initial designs (design vectors of the optimum designs are presented in Table 3.21)

Initial design	Number of SUPEROPT executions	Number of optimization iterations to obtain:		Panel weight (lb/ft^2)	
		Local optimum	Best optimum	Local optimum	Best optimum
Optimum design of perfect panel	2	47	284	2.627	2.409
All variables at lower bound	1	267	267	2.409	2.409
All variables at median value	3	33	593	2.761	2.472
All variables at upper bound	2	259	292	3.128	2.474

In the present study of stiffened panel designs, it was discovered that even with the SUPEROPT procedure of PANDA2 it was not possible to obtain a global optimum. Several examples of such failures in locating global optimum are presented and methods were used to identify the failure is discussed.

Among stiffened panel concepts, optimization failure was encountered for isogrid stiffened panels (with blade stiffeners) with imperfections. The inspection of the iteration history file (*.OPP file) revealed that constraints were oscillatory near the optimum and

the design shifted from feasible to infeasible domains. This was because some constraints had very large gradients at the optimum. One way to deal with such oscillations is to allow smaller move limits. This is achieved in PANDA2 by increasing the number of iterations in each PANDAOPT execution. This has a disadvantage because with smaller move limits, gradient based optimizations are likely to get trapped at a local optimum.

Table 3.21: Isogrid stiffened panel designs obtained from different initial designs.

Design variable	Design 1	Design 2	Design 3	Design 4
Skin thickness	0.107	0.107	0.113	0.098
Isogrid module size (spacing)	10.0	10.0	11.4	10.71
Isogrid web height	1.509	1.510	1.662	2.049
Isogrid web thickness	0.125	0.125	0.129	0.126
Ring spacing	30.00	30.00	42.01	113.9
Height of ring	2.160	2.160	2.084	2.000
Thickness of ring web	0.030	0.030	0.030	0.076
Panel weight (lb/ft^2)	2.409	2.409	2.472	2.474
Isogrid weight (%)	33.9	33.9	32.8	42.1
Ring weight (%)	2.2	2.3	1.3	1.1

Table 3.22: Constraint margins (%) for optimized designs of isogrid panels

Design	Optimized weight (lb/ft^2)	Stress in the skin	Triangular skin buckling	Isogrid web buckling
1	2.409	27.0	-1.26	-0.483
2	2.409	27.0	-1.09	-0.596
3	2.472	31.9	-0.815	-0.432
4	2.474	21.1	0.578	8.84

Table 3.20 summarizes the number of iterations required to converge to a practical optimum for optimizations with four different initial starting points. Tables 3.21

and 3.22, respectively, present the optimized designs and active failure mechanisms of designs obtained from optimizations using the different starting points.

The optimum designs obtained for different starting points (Table 3.20) are marginally different. There is also a wide scatter in the number of iterations required to converge to a local optimum and locate a practical global optimum. The designs obtained from the four optimizations are compared in Table 3.21. It can be seen that even though the final weights of the optimum designs are almost equal, the design variables are quite different. The final designs obtained for optimization from initial designs 1 and 2 (Table 3.20) were identical. Optimizations with initial Designs 3 and 4 were trapped in local optima due to large gradients of some critical constraints. However, the optimum weight obtained for initial designs 3 and 4 are only marginally higher (2.7%) than those obtained for designs 1 and 2. For practical purposes all four designs are equally acceptable. The results indicate that it often requires multiple SUPEROPT executions to find the global optimum.

Similar results were also found in the design of titanium honeycomb core sandwich panels (Table 3.23). Titanium honeycomb core sandwich panels were optimized with different options of fixed or optimized core and with symmetric and asymmetric facesheets. The optimum designs obtained from a single SUPEROPT execution are shown in the second column of Table 3.23. Optimization failure was detected when the sandwich panel optimized with increased design freedom (asymmetric fixed core) resulted in a higher weight. Re-optimizing the designs with more executions of the SUPEROPT process resulted in improved designs as shown in column 5 of Table 3.23.

Table 3.23: Titanium honeycomb core sandwich panel optimization: optimum weights and iterations for global optimum

Panel type	Best design from one SUPEROPT execution		Best design from two SUPEROPT executions	
	Optimum weight (lb/ft^2)	Optimization iterations	Optimum weight (lb/ft^2)	Optimization Iterations
Symmetric, fixed core	1.337	275	1.358	399
Asymmetric fixed core	1.383	275	1.354	361
Symmetric optimized core	1.323	275	1.323	275
Asymmetric optimized core	1.327	275	1.320	365

In the use of PANDA2 it is common to encounter small differences as shown in Table 3.23. Such small differences could be due to small difference in the analysis models, modeling philosophy, or occasionally failure of the optimization process. Designers should pay attention to small differences to ensure that they are indeed acceptable differences that reflect the analysis and optimization accuracy. The low cost analysis of PANDA2 permits the designer to re-optimize or re-analyze the panel designs at very little additional cost.

The designer does not have information on the actual global optimum and has to rely on other methods to determine if the design obtained is a practical global optimum. Often, multiple optimizations are performed either with different degrees of design freedom or in different areas of the design space (using fixed ranges for a selected design variable). In addition to helping identify convergence to local optima, such exercises also provide the designer with multiple designs from which a selection can be made based on considerations that were not included in the analysis. More accurate finite element analysis models should be used to verify the designs. Replacing the PANDA2 analysis

with such detailed finite element analysis models for optimization, however, is neither a feasible nor a justifiable option.

Table 3.24: Estimated number of panel analyses for stiffened panel trade study

Number of stiffened panel concepts (n_c)	14
Variations of each concept (n_v)	2
Average number of design variables (n_d)	10
Number of line searches performed in PANDA2 global optimization (n_g)	275
Number of analyses per search (n_s)	11
Total number of analyses performed (n_c x n_v x n_g x n_s)	84700

In the next section, different stiffened panel concepts are optimized to compare their weight efficiency and sensitivity to imperfections. Table 3.24 gives an estimate for the minimum number of analyses required for the trade study. The numbers in parentheses indicate the results when local searches make use of approximations. Using detailed finite element models for such large number of analyses would be extremely expensive and time consuming.

Comparison of Weight Efficiency of Stiffened Panel concepts

This section presents the results of the optimization performed for the various stiffened panel concepts introduced earlier for the RLV tank design. The library of analysis tools implemented in PANDA2 depends on the type of stiffeners. Optimizations were performed with the IQUICK=0 option for stringer-ring stiffened panels and orthogrid panels. Isogrid stiffened panels, truss core and honeycomb-core sandwich panels were optimized with IQUICK=1. The choice reflects the best analysis choice available in PANDA2 for each concept.

Weight Efficiencies of Metallic Panels

PANDA2 optimizations were perfomed for metallic stringer-ring, isogrid, orthogrid and sandwich stiffened panels with variable and fixed (30, 60, 90, and 120 inches) ring spacing.

Table 3.25: Comparisons of weight efficiencies of metallic stiffened panel concepts (Sandwich panel weights shown in parenthesis do not include core weight)

Concept	Total weight (lb/ft^2)	% weight of rings (stringers)	Active failure modes
Stringer and Ring	1.840	4.756 (19.32)	Stress (pressure), Stress, Local buckling, Stringer web , top flange buckling
Isogrid	2.409	2.273 (33.94)	Local buckling, Stiffener web buckling
Orthogrid	2.147	9.530 (28.69)	Stress (pressure), Stress in stringer and ring webs, Local buckling, General buckling, Stringer web buckling
Symmetric sandwich fixed core (1.0 inch)	1.358 (1.030)	2.175	Stress (pressure), Ring sidesway, Ring top flange buckling
Symmetric Sandwich optimized core (0.881 inch)	1.323 (1.034)	2.501	Stress (pressure), General buckling, Local buckling , Ring web buckling, Ring top flange buckling
Asymmetric Sandwich fixed core (1.0 inch)	1.354 (1.026)	2.315	Stress (pressure), Interring buckling, Ring sidesway, Ring top flange buckling
Asymmetric Sandwich optimized core (0.887 inch)	1.320 (1.029)	2.440	Stress (pressure), General buckling, Ring sidesway and top flange buckling
Truss core (weight with optimized corrugation angle)	2.126 (1.705)		Corrugation web buckling, upper skin buckling

Sandwich wall constructions with symmetric and asymmetric facesheets were optimized. A fixed core thickness of 1.0 inch was used for one set of optimizations; for

the thin core sandwich, the thickness of the core was used as a design variable. The higher core thickness was desirable as it increases the insulation capacity of the liquid hydrogen tank wall, thereby reducing weight of additional exterior insulation. Small levels of initial imperfections were used for the cylinders. Global and out-of-roundness imperfections were set to 0.5% of the cylinder radius (160 inch), while the inter-ring and local imperfections were set equal to 100% and 10% of the skin or cylinder wall thicknesses, respectively. PANDA2 adjusts this value if it detects that the wall rotation exceeds 0.1 radian.

Optimization of T-stringer J-ring stiffened panels at different ring spacings showed that the weight increased for ring spacings over 30 inches. The other concepts were insensitive to ring spacing. Details of optimal values of the design variables and failure margins are shown in Appendix B. Table 3.25 shows the optimal weights, ring spacing, and active failure modes of the metallic panels optimized with ring spacing as a design variable.

Comparison of designs indicate that for the given load cases, the sandwich panel with ring stiffeners is the most weight efficient concept. The weight savings of sandwich panels can be attributed to the imperfection insensitivity that is provided by the high bending stiffness of sandwich constructions, the reduced local failure modes (such as stiffener buckling) exhibited by sandwich panels, and the increased specific strength of the Titanium alloy material used. The weight of the sandwich panels shown in the parenthesis (Table 3.25) is the panel weight excluding the weight of the core. For RLV tank design, the sandwich core plays a dual role as structural member and as insulation. This indicates further advantage to the sandwich concept.

There were no panel failure modes active for symmetric sandwich panels with fixed core (1.0 inch) indicating sub-optimal weight. The sandwich core does not carry the hoop load and it can be much thinner than 1.0 inch but must be thick enough to satisfy the buckling constraints. Sandwich panels were hence optimized including core thickness as a variable. The sandwich panels with optimized core thickness are marginally more efficient than panels designed for a fixed core thickness of 1.0 inch. For sandwich panels with fixed core (1.0 inch thickness), the honeycomb core accounts for 24 % of the total panel weight (0.33 lb/ft^2). For optimized core, the core weight fraction reduces to 22% of the total panel weight, resulting in an optimum design that is 2.6% lighter than the design with fixed core thickness. The weight savings from optimized core are greater (20%) for panels designed without including imperfections (Table 3.29). Asymmetric sandwich construction did not yield substantial weight savings, when imperfections were included in the design. On the contrary, asymmetry resulted in lowering the bending stiffness causing buckling failures to become more critical. Asymmetric honeycomb core sandwich panel optimized with fixed core (1.0 inch thick) was critical in interring buckling failure mode.

The stringer-ring stiffened panel is more efficient than the isogrid and orthogrid stiffened concepts. The weights of isogrid and orthogrid concepts are heavier because the blade stiffeners used for these concepts are more susceptible to buckling failure modes.

The truss core panel was the heaviest design (2.026 lb/ft^2). Investigation into the cause of the very high weight of the truss core sandwich was presented earlier in section on Modeling issues. The high weight was due to two reasons. PANDA2 does not allow analysis of truss core panels with rings; instead of rings, clamped boundary conditions

were used. In addition, the optimum weight was sensitive to the corrugation angle. Further weight reduction was possible when corrugation angles were allowed to vary. The optimum design obtained had a corrugation angle of 62.3° and an optimum weight of 1.705 lb/ft^2. PANDA2 designs for truss core need to be evaluated carefully using more accurate models with ring stiffeners included.

The list of active failure modes in Table 3.25 shows that stress constraints that arose from the proof pressure load case were active for all designs except for isogrid and truss core sandwich panels. The buckling constraints were also active, indicating the importance of including the axial compression load case.

Weight Efficiencies of Composite Panels

PANDA2 optimizations were also performed for composite stringer-ring, honeycomb core sandwich and truss core sandwich stiffened panel concepts. Ring spacing was included as a design variable in all optimizations. Sandwich panels were optimized with symmetric face sheet and asymettric facesheet constructions. Fixed thickness (1.0 inch) and optimized thickness of sandwich core were considered. Composite truss core panels were also optimized for a 300 inch barrel length. Panels were optimized with the same initial imperfection values as those used for metallic panels.

In the present study, laminate stacking sequences were chosen *a priori* for most cases and in some cases plies of the laminate were optimized for thickness with constraints to ensure symmetry, balance and contiguity (no more than four contiguous plies of same orientation) requirements. Ply thicknesses of the preliminary optimum

designs were rounded to the nearest integer ply thickness value and reoptimized again for the other design variables.

Table 3. 26: Comparisons of weight efficiencies of composite stiffened panel concepts

Concept	Panel weight (lb/ft^2)	% weight of rings (and stringers)	Active failure mechanisms
Stringer - Ring stiffened	0.911	13.6 (32.3)	Fiber tensile stress (pressure), Stringer top flange buckling, Rolling of stringers
Symmetric sandwich fixed core (1.0 inch)	1.433 (1.105)	2.667	Local buckling and ring rolling
Symmetric sandwich optimized core (0.726 inch)	1.358 (1.120)	3.858	Local buckling, Global buckling
Asymmetric sandwich fixed core (1.0 inch)	1.167 (0.839)	1.612	Fiber tensile stress (pressure), Local buckling
Asymmetric sandwich optimized core (0.862 inch)	1.169 (0.887)	2.097	Fiber tensile stress (pressure), Local buckling , Global buckling
Truss core	1.324	-	Fiber tensile stress (pressure), Upper skin buckling, Global buckling

Table 3.26 shows the optimum weights, stiffener weight fractions, and active failure modes for the composite concepts. The optimum weights indicate that the stringer-ring stiffened panel is the most efficient concept. The extra design freedom available (compared to metallic panel optimization) for tailoring the laminate lay-up in the wall and stringers was helpful in distributing material more optimally. The effects of design freedom in tailoring composites on optimum weight and imperfection sensitivity are presented in the next section. The angle ply laminate used for the tank wall with ±65° plies was efficient in carrying the hoop stress, while the stringers with laminates of

$[45/-45/0_3/-45/45/0]_S$ were optimal to carry axial compression loads. The optimum design had a stringer weight fraction of 32.3%.

In the case of sandwich, the lower bound imposed on the inner facesheet thickness (0.06 inch, or 12 plies) is higher than that required for structural purposes. The 12 ply thickness constraint is imposed to ensure that the tank built for the liquid hydrogen tank will have low permeation rates. The asymmetric sandwich panel has a lower weight, as the outer face sheets had only 7 plies (0.035 inch thickness). The reduced bending due to the bending extension coupling introduced by the asymmetry did not prove to be critical. It was also noticed that the core thickness increased when asymmetry was introduced in the sandwich laminate. However, asymmetry may have other implications such as warping after cooling and causing more severe initial imperfections in panels. Without additional consideration of such issues, asymmetric sandwich panel constructions cannot be recommended for use. Small differences in results are found in the case of composites. For example, the weight an asymmetric sandwich panel with optimized core (1.169 lb/ft^2) is marginally higher than the weight of a symmetric sandwich panel with optimized core (1.167 lb/ft^2). Theoretically, the weight of the asymmetric panel should be the same as or lower than that of the symmetric panel. The small differences are attributed to the optimization noise and effects of rounding ply thickness.

When the core weight is not included, sandwich panel weight, shown in parenthesis (Table 3.26), is closer to the weight of the stringer-ring stiffened concept. Truss core panel has optimum weight comparable to sandwich panels with fixed core thickness.

Comparison of Metallic and Composite Panels

An interesting aspect of the design trade study is the comparison of weight efficiencies of metallic and composite stiffened panel concepts. Optimized weight, stiffener percentages in weight are shown in Table 3.27 and the corresponding active failure modes are presented in Table 3.28.

Table 3.27: Optimal weights (lbs/ft^2), stiffener percentages in weight for the optimized designs

Concept	Metallic		Composite	
	Panel weight (lb/ft^2)	% weight of rings (and stringers)	Panel weight (lb/ft^2)	% weight of rings (and stringers)
Stringer-Ring stiffened	1.840	4.76 (19.32)	0.911	13.6 (32.3)
Symmetric sandwich fixed core	1.358	2.18	1.433	2.667
Symmetric sandwich optimized core	1.323	2.50	1.358	3.86
Asymmetric sandwich optimized core	1.320	2.44	1.169	2.10
Truss core	2.126 (1.705)	n/a	1.324	n/a

Comparison of the optimal weights shows that honeycomb sandwich constructions (symmetric and asymmetric) are the least sensitive to material choice. The difference in material (titanium versus composite) used for facesheets is not significant; e.g., in the case of symmetric sandwich with fixed core of 1.0 inch, the weight of the facesheets are identical for titanium and composite constructions. More evidence can be gathered from the active failure modes for sandwich panels. There are no critical local buckling failure modes for the sandwich laminate that depend on the overall bending stiffness. The sandwich laminates optimized (0.9 inch thick core) have a core to facesheet

thickness ratio of 15, and so the facesheets are in a virtually pure membrane stress state. The composite material, therefore, does not have a significant advantage for the global failure mechanisms of a sandwich panel.

Table 3.28: Active failure mechanisms for the optimized designs

Concept	Metallic	Composite
Stringer-ring stiffened	Stress (pressure), Stress, Local buckling, Stringer web and top flange buckling	Fiber tensile stress (pressure), Stringer top flange buckling, Rolling of stringers
Symmetric Sandwich fixed core (1.0 inch)	Stress (pressure)	Local buckling, Ring rolling
Symmetric Sandwich optimized core	Stress (pressure), General buckling, Local buckling, Ring web buckling, Ring top flange buckling	Local buckling, Global buckling
Asymmetric Sandwich optimized core	Stress (pressure), General buckling, Ring sidesway, Ring top flange buckling	Fiber tensile stress (pressure), Local buckling, Global buckling
Truss core	Corrugation web buckling, Upper skin bucking	Fiber tensile stress (hoop pressure), Upper skin buckling, Global buckling

The optimum weight comparison of metallic and composite stringer-ring stiffened panel and truss core sandwich panel constructions illustrates the advantage of composite materials. The composite materials permit design freedom to provide higher bending stiffness that can resist the local buckling failure modes that these panels exhibit. In addition, the highly tailored skin laminate (angle ply with 65° plies) is designed to carry the hoop loads more efficiently.

For all the stiffening concepts, PANDA2 designs shells with flimsy rings (always less than 10% of total weight) because the loading condition that can cause buckling is pure axial compression. Rings do not offer much help in reducing buckling loads under

axial compression nor do they carry the hoop tension loads. Other load cases such as overall bending of the cylinder or non-symmetric external pressure from flight loads have to be used to size the ring stiffeners.

Sensitivity of Optimal Weights to Geometric Imperfections

This section presents optimum weights of stiffened panels designed with and without imperfections. The objective was to compare the sensitivity of optimum weights of the different concepts to geometric imperfections. The imperfection amplitudes that were used were in proportion to the stiffness (or governing dimensions). The global and out-of-roundness imperfections were set to 0.5% of the cylinder radius (0.8 inch); while the inter-ring and local imperfections were set equal to 100% and 10% of the skin or cylinder wall thickness (obtained from a preliminary optimization of a perfect cylinder), respectively.

Effect of imperfections on optimum design of metallic panels

Table 3.29 summarizes the optimum weight and stiffener weight fraction for metallic panels designed with and without geometric imperfections. Table 3.30 summarizes the dominant failure mechanisms for the corresponding designs in Table 3.29. Details such as optimum value of the design variables and critical failure margins for the different stiffened panel designs are presented in Appendix B.

Substantial increase in weight is observed for all panels optimized with imperfections except for the titanium honeycomb core sandwich panels optimized with fixed core thickness. The weight penalty for the stringer-ring stiffened, isogrid, and orthogrid concepts are 15.4%, 56.7%, and 39.6 %, respectively. The eccentricity introduced by imperfection results in increased loads acting on the stiffeners. This is

confirmed by the critical margins of panels designed with imperfections: some stiffener buckling failure modes become active. The optimized designs, therefore, have a larger stiffener weight fraction. The stringer weight fraction increases by a factor of 3.0, 4.6, and 5.8 for the stringer-ring, isogrid and orthogrid stiffened panels, respectively.

The high penalty in weight for grid stiffened panels is partly due to the stiffener profile chosen. T-shaped stiffeners make the panel weight less sensitive to imperfections because the outstanding flange provides additional stiffness and carries a fraction of the load, making the stiffener web failure modes less critical.

Table 3.29: Sensitivity of optimum weight of metallic panels to geometric imperfections

Concept	Without Imperfections		With Imperfections	
	Total Weight (lb/ft^2)	% Weight of rings (and stringers)	Total Weight (lb/ft^2)	% Weight of rings (and stringers)
Stringer-ring stiffened	1.600	5.91 (6.83)	1.840	4.76 (19.32)
Isogrid	1.537	1.13 (7.34)	2.409	2.27 (33.9)
Orthogrid	1.538	5.12 4.92)	2.147	9.53 (28.69)
Symmetric Sandwich - fixed core	1.347	3.27	1.358	2.18
Symmetric Sandwich - optimized core	1.110	2.09	1.323	2.50
Asymmetric Sandwich-fixed core	1.341	1.65	1.354	2.32
Asymmetric Sandwich -optimized core	1.095	1.54	1.320	2.44
Truss core	1.752	n/a	2.126	n/a

Sandwich panels optimized with a fixed core thickness of 1.0 inch have negligible (< 1%) weight penalty due to imperfections. Optimum weight of sandwich panels with

thin core increases by 20% when optimized with imperfections. The sandwich panels with fixed thickness core (1.0 inch) do not exhibit the same amount of weight increase as other panels because of high bending stiffness. A global imperfection of 0.8 inch for the sandwich panel is about the same order of magnitude as the wall thickness and therefore does not affect the buckling loads much. The high bending stiffness of thick core sandwich panels also results in very large buckling wavelengths thereby resulting in small increases in bending stresses.

Table 3.30: Active constraints of metallic panels designed with and without imperfections

Concept	Without Imperfections	With Imperfections
Stringer & Ring	Stress (hoop pressure), Local buckling , Wide column buckling	Stress (pressure), Stress , Local buckling, Stringer web and top flange buckling
Isogrid	Stress (hoop pressure), Local buckling, Stiffener web buckling	Local buckling, Stiffener web buckling
Orthogrid	Stress (hoop pressure), Local buckling, Stringer web buckling	Stress (pressure), Stress in stringer and ring webs, Local, General and Stringer web buckling
Symmetric Sandwich fixed core	Stress (pressure)	Stress (pressure)
Symmetric Sandwich optimized core	Stress (hoop pressure)	Stress (pressure), General buckling, Local buckling, Ring web buckling, Ring top flange buckling
Asymmetric Sandwich fixed core	Stress (hoop pressure)	Stress (pressure), Ring web buckling
Asymmetric Sandwich optimized core	Stress (hoop pressure), Global buckling	Stress (pressure), General buckling, Local buckling, Ring web and top flange buckling
Truss core	Corrugation web buckling, Upper skin buckling	Corrugation web buckling, Upper skin bucking

The optimum designs for fixed core sandwich panels (with and without imperfections) were governed primarily by the stress constraint arising from hoop stress induced by internal pressure and does not depend on buckling constraints. Sandwich panels with thin cores have a lower bending stiffness and global buckling modes are more critical. This leads to a higher weight for optimum design when imperfections are introduced. The increased freedom allowed in asymmetric panels with optimized core result in lower weight design.

Effect of imperfections on optimum design of composite panels

Table 3.31 shows the optimum weights and stiffener weight fractions, and Table 3.32 shows the active failure modes for the optimum designs.

Table 3.31: Sensitivity of optimum weight of composite panels to geometric imperfections

Concept	Without Imperfections			With Imperfections		
	Panel weight (lb/ft^2)	% weight of		Panel weight (lb/ft^2)	% weight of	
		Stringers	Rings		Stringers	Rings
Stringer - Ring	0.822	23.4	16.6	0.911	32.3	13.6
Symmetric Sandwich optimized core	1.250	-	1.505	1.358	-	3.858
Asymmetric Sandwich optimized core	0.975	-	4.139	1.169	-	2.097
Truss core	1.297	-	-	1.324	-	-

Table 3.31 shows that the optimum weight of truss core sandwich panel is least sensitive to imperfections (2.1% weight penalty). However, this is the heaviest composite panel design. The asymmetric sandwich is the most sensitive to imperfections, because

the bending–extension coupling introduced by asymmetry reduces the effective bending stiffness making the panel critical in local and global buckling modes. Symmetric sandwich is marginally sensitive to imperfections (9% weight penalty) but the perfect panel has all design variables at their lower or upper bounds and has no active constraints so that the design has margins to spare (72% for local buckling, 159% for general buckling and 54% for stress failure).

The stringer-ring stiffened panel concept is less sensitive to imperfections (10% weight penalty), than the analogous metallic concept (15.4 % weight penalty, Table 3.23). Stringer weight fraction of stringer-ring stiffened panel increases only by a factor 1.5 and does not triple as it does for the metallic panel (Table 3.29) when imperfections are introduced into the design.

Table 3.32: Active failure margins of composite panels designed with and without imperefections

Concept	Without Imperfections	With Imperfections
Stringer - Ring	Fiber tensile stress (hoop pressure)	Fiber tensile stress (hoop pressure), Stringer buckling, Rolling of stringers
Symmetric Sandwich optimized core	None	Local buckling, Global buckling
Asymmetric Sandwich optmized core	Fiber tensile stress	Fiber tensile stress (hoop pressure), Local buckling, Global buckling
Truss core	Fiber tensile stress (hoop pressure), Upper skin buckling	Fiber tensile stress (hoop pressure), Upper skin buckling, Global buckling

Stiffened panels tailor the material distribution between the skin and the stiffeners to achieve required stiffness. In the absence of imperfections, stiffened cylinders designed for axial compression loads have a higher weight fraction of material in the

skin. However, if the skin thickness is fixed and not allowed to change, then the stiffener weight fraction must increase to achieve the required stiffness. Imperfections introduce eccentricity in the loading and lead to redistribution of the load from skin to stiffeners. In the present example, the composite panel optimized without imperfections has a thinner skin (0.06 inch; 12 plies) than the metallic panel (0.1 inch). The wall laminate thickness of the $[(+65/-65)_3]_s$ was kept fixed in the optimization. This meant that more material was added to the stiffeners (23.4% for composite panels, 6.8% for metallic panels) in order to carry the axial load. The weight penalty incurred by forcing more material into stiffeners for designs without imperfections helped when imperfections were introduced. The composite panels with imperfections could therefore carry required loads without much increase in weight.

Table 3. 33: Imperfection sensitivity of composite stringer-ring stiffened panels optimized with varying levels of design freedom

Wall laminate	Stiffener laminate	Panel weight (lb/ft^2)		Weight
		Without Imperfection	With imperfection	penalty %
$[(+65/-65)_3]_S$	$[\pm 45/0/\mp 45/0]_S$	0.839	1.019	21.45
$[(+65/-65)_3]_S$	$[\pm 45/0_n/\mp 45/0_m]_S$	0.826	0.910	10.04
$[+45_{n1}/90_{n2}/-45_{n3}/0_{n4}]_S$	$[+45/0/-45/90]_S$	0.826	1.333	61.38
$[+45_{n1}/90_{n2}/-45_{n3}/0_{n4}]_S$	$[+45_{m1}/0_{m2}/-45_{m3}/90_{m4}]_S$	0.802	1.206	50.38

Table 3.33 shows the optimized weights of both perfect and imperfect composite stringer-ring stiffened panels as a function of design freedom where different ply thicknesses were included as design variables. The optimized ply thicknesses for the design in Table 3.33 are shown in Table 3.34. Optimizations were performed with IQUICK=1 analysis.

Table 3. 34: Optimized lay-ups obtained for composite stringer-ring stiffened panels optimized with varying levels of design freedom

Without Imperfection		With Imperfection	
Wall laminate	Stiffener laminate	Wall laminate	Stiffener laminate
$[(+65/-65)_3]_S$	$[\pm 45/0_2/\mp 45/0]_S$	$[(+65/-65)_3]_S$	$[\pm 45/0/\mp 45/0]_S$
$[(+65/-65)_3]_S$	$[\pm 45/0_2/\mp 45/0_1]_S$	$[(+65/-65)_3]_S$	$[\pm 45/0_4/\mp 45/0_2]_S$
$[+45/90_4/-45/0_{½}]_S$	$[+45/0/-45/90]_S$	$[+45_2/90_2/-45_2/0_2]_S$	$[+45/0/-45/90]_S$
$[+45/90_4/-45/0_{½}]_S$	$[+45/0/-45/90_{½}]_S$	$[+45_2/90_3/-45_2/0_{½}]_S$	$[+45/0_4/-45/90_{½}]_S$

Table 3.33 shows that the weight penalty of the imperfect panel depends on the number of ply thicknesses that are optimized as design variables. This is very evident for composite panels with $[(+65/-65)_3]_S$ wall laminate and $[45/-45/0_n/-45/45/0_m]_S$ stiffener laminate. The weight penalty due to imperfections doubles if the stiffener lay-up is fixed. It is important to note that allowing more freedom to change laminate designs helps to obatin lower weight optimum designs. However, the designs beome more sensitive to uncertainties in loads and imperfections because the optimized laminates are highly tailored to the load cases used for the design.

CHAPTER 4
HOMOGENIZATION APPROXIMATIONS IN COMPOSITE LAMINATES

The design of stiffened composite cylinders introduces many approximate modeling issues. Two examples of modeling issues faced in the design optimization of the RLV tank are discussed in this chapter. The first is the approximation of composite sublaminates using equivalent orthotropic properties (engineering constants) in buckling analysis. The second example is the use of smeared continuum models for approximating a hexagonal sandwich core material for calculating facesheet wrinkling loads.

Errors from Use of Equivalent Properties for Sublaminates

Optimization of composite laminates may lead to designs that are tailored to the loading conditions used and sensitive to uncertainties in loads and material properties. Modeling and analysis of the different failure modes such as micro-cracking and fatigue failure are also problematic. Many failure modes are not well characterized or are difficult to model. In practice, laminates are usually tested before they are used in structural applications.

In order to reduce failure risks and design costs, industry usually employs sublaminates that have been well characterized through testing and detailed analysis. Sublaminates are chosen with fixed ratios of various ply orientations to tailor the stiffness and strength in different directions and provide safety against off-design conditions.

Sublaminates are also used in optimization models to reduce the number of design variables [77].

Since the inplane stiffness of a laminate with fixed ratios of ply thicknesses in different orientations is determined only by the thickness, designers often further simplify modeling by replacing the composite laminate with an equivalent homogenized orthotropic material [95, 122]. Using equivalent orthotropic material properties for sublaminates can lead to errors in bending stiffness (D-matrix) terms. These errors are small when the number of sublaminates is large [103]. Since detailed analyses of the optimized designs are usually performed using the exact stacking sequence, the use of equivalent properties does not normally constitute a safety risk. However, using equivalent properties for optimization can result in sub-optimal designs when the errors are large. The objective of this section is to identify conditions that can lead to large errors (greater than 20%) due to use of equivalent properties.

This chapter investigates the errors in bending stiffness terms and buckling loads that are due to use of equivalent properties for composite sublaminates are investigated. Analytical expressions are obtained for the maximal errors in bending stiffness terms of a four-layer sublaminate. The effects of ratio of inplane stiffnesses of the plies and ratio of ply thicknesses on errors are demonstrated. The maximal errors are also calculated for multiple repetitions of the sublaminate using two different stacking schemes used. Maximal errors in buckling loads of plates are also obtained for various aspect and load ratios.

Motivation Problem

Equivalent properties are obtained by equating the actual in-plane stiffness matrix terms (A_{ij}) to the in-plane stiffness constants for a single layered equivalent material. The effective elastic properties for a sublaminate of thickness h are then obtained as,

$$E_x = \frac{1}{h}\left[\frac{A_{11}A_{22} - A_{12}^2}{A_{22}}\right] \quad , \quad E_y = \frac{1}{h}\left[\frac{A_{11}A_{22} - A_{12}^2}{A_{11}}\right]$$

$$\upsilon_{xy} = \frac{A_{12}}{A_{22}} \quad \text{and} \quad G_{xy} = \frac{1}{h}A_{66} \tag{4.1}$$

Our interest in the effect of using equivalent or effective stiffness of laminates arose during preliminary design optimization of J-stiffened panels for reusable launch vehicle liquid hydrogen tank developed by Rockwell, Inc.

The panel optimized was a cylindrical stringer ring stiffened panel with a length of 300 inches and a radius of 192 inches. One half of the cylinder (180°) with symmetry boundary conditions was used for the optimization. The axial stiffeners or stringers were J-type stiffeners (Figure 4.1) attached internally to the cylinder walls. The ring stiffeners were T-type stiffeners. The panel was designed to resist buckling failure under an axial compression load of 1741 lb/in with a safety factor of 1.4. Details of the material properties and stacking sequence of the panel used for the analysis and design are shown in Tables 4.1 and 4.2. The optimization of the panels did not include any parameters associated with the ring frames such as ring frame spacing, cross-section, or segment ply lay-ups. However, ring frames were included in the model to account for their stiffening effect. Tables 4.2 and 4.3 provide details of the initial and optimized designs of the J-stiffened panel.

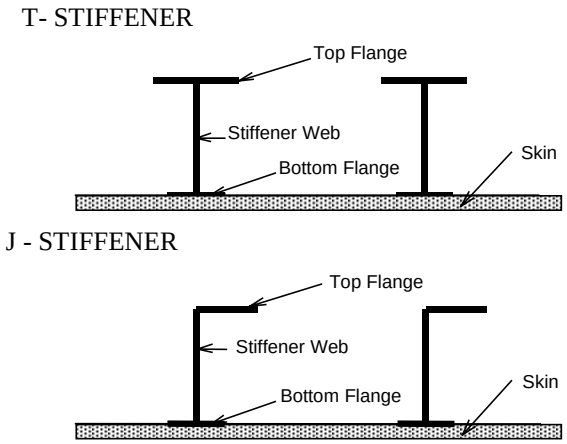

Figure 4.1. Stiffener geometry and associated terminology

Table 4.1: Initial design of panel (Subscript T and F denote pre-impregnated Tape and woven Fabric lamina, respectively)

Description	Cross-section or width (inch)	Laminate lay-up
Skin		$[\pm 65_{3T}]_S$
Stringer spacing	5.0266	
String bottom flange width	1.500	$[0_{2F}]_S$
Stringer top flange width	0.600	$[0_{1F}/0_{4T}/45_{1F}/0_{4T}/45_{1F}/0_{4T}/0_{1F}]_S$
Stringer web height	1.500	$[0_{1F}/0_{4T}/45_{1F}/0_{4T}/45_{1F}/0_{4T}/0_{1F}]_S$
Ring spacing	31.447 in	
Ring bottom flange	1.0 in	$[45_{1F}/0_{4T}/0_{1F}/0_{2T}]_S$
Ring top flange	2.0 in	$[45_{1F}/0_{4T}/45_{1F}/0_{2T}]_S$
Ring web height	9.0 in	$[45_{1F}/0_{2F}/45_{1F}]_T$
Weight (lb.)	1496 lb	

Table 4.2: Material properties of tape and fabric plies used for panel design

Parameter	Lamina type	
	Tape	Fabric
Thickness of single ply (inch)	0.005	0.0143
Elastic modulus in fiber direction, E_1 (Mpsi)	21.5	11.6
Elastic modulus in transverse direction, E_2 (Mpsi)	1.08	10.9
Poisson ratio ν_{12}	0.3	0.06
Shear modulus G_{12} (Mpsi)	0.6	1.12
Max. allowable tensile stress in fiber dir. (Kpsi)	222.3	113.7
Max. allowable tensile stress in transverse direction (Kpsi)	176.3	74.8
Max. allowable comp. Stress in fiber direction (Kpsi)	7.2	103.9
Max. allowable comp. stress in transverse direction (Kpsi)	36.0	75.6
Max. allowable shear stress (Kpsi)	10.9	16.32

Table 4.3: Optimized panel designs obtained from models using equivalent properties and ply layup

Geometry variable	Optimum using with exact laminate lay-up	Optimum using equivalent properties
Stiffener spacing (inch)	4.557	4.823
Stiffener height (inch)	1.326	2.035
Bottom flange width (inch)	1.165	1.324
Top flange width (inch)	0.5806	0.683
Panel weight (lb)	1484	1665

A problem was discovered when attempts were made to reconcile the differences in results obtained from two different models [118]. Table 4.3 provides details of the initial design and optimum designs of the stiffened panel. In one model, the stiffened panel included the laminate stacking sequence details while in the other, segments of the stiffened panels were modeled as orthotropic materials using equivalent properties. Table 4.4 presents the buckling loads of the initial and optimized designs of the J-stiffened panels.

Table 4.4: Buckling load factors for stiffened panel designs (from Table 4.3) obtained using exact and equivalent properties (values in paranthesis indicate errors)

Analysis Method	Initial Design		Optimum design obtained using	
	Buckling load	Critical mode	Exact properties	Equivalent properties
Exact	1.2528	Torsional buckling of stiffener	1.4	0.93 (-33.6%)
Equivalent Stiffness	0.994 (-21.1%)	local buckling	2.38	1.4 (41.2%)

The first three columns in Table 4.4 show the buckling load factor and buckling mode obtained for the initial and optimum designs (Table 4.3) using the two approaches. The panel modeled using ply lay-up details was critical in torsional buckling of the skin stringer segment, while the model with equivalent stiffness was critical in local buckling.

The two panel models were also optimized with stringer spacing, height and flange widths as design variables. The optimum based on effective material properties was 11% heavier with larger stringers. The optimum designs obtained using the two approaches were then analyzed using the opposite approach; the buckling loads are compared in Table 4.4. The optimization amplified the modeling errors: errors for the buckling load increased from 20% for the initial design to 34% and 41% for the optimized panels.

Bending and Inplane Stiffness Ratio for a Two-Ply Symmetric Sublaminate

While it may be evident that using equivalent properties introduces some errors, the magnitude of such errors is not universally appreciated. In this section, a four-layer symmetric sublaminate is used to illustrate the errors in bending stiffness due to use of equivalent properties. A symmetric sublaminate with layup $[t_1/t_2]_s$ is chosen where t_1 and t_2 are the thicknesses of layers 1 and 2, respectively. The sublaminate is a special case of laminates $[t_1/t_2]_{sn}$ and $[(t_1/t_2)_n]_S$, discussed later, for $n=1$. The bending stiffness of the laminate is calculated using exact and equivalent properties, and the effects of the stiffness ratio of the two plies and of the volume fractions of plies on the error are investigated.

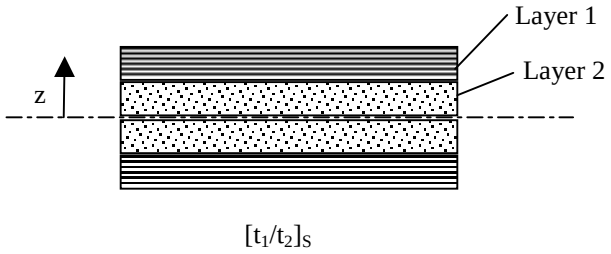

Figure 4.2: Sublaminate with layers t_1 and t_2.

Let $(\overline{Q}_{ij})_k$ be the inplane stiffness of the k_{th} layer, t_k the thickness of the k^{th} layer, z^{k+1} and z^k the coordinates of the top and bottom faces of the k^{th} layer, n_l the total number of layers in the laminate, and h the total thickness of the laminate. The laminate inplane stiffness (A_{ij}) and bending stiffness (D_{ij}) are then expressed as follows.

$$A_{ij} = \sum_{k=1}^{n_l} (Q_{ij})_k t_k \tag{4.2}$$

$$D_{ij} = \sum_{k=1}^{n_l} (\overline{Q}_{ij})_k \frac{(z_{k+1}^3 - z_k^3)}{3} \tag{4.3}$$

It is convenient to work with normalized stiffnesses obtained by dividing Eq. 4.2 and Eq. (4.3) by h and $h^3/12$, respectively, to give A_{ij}^* and D_{ij}^*. For the four-layer symmetric laminate $[t_1/t_2]_s$, the normalized inplane stiffness is

$$A_{ij}^* = \overline{Q}_{ij_1} v_1 + \overline{Q}_{ij_2} v_2 \tag{4.4}$$

where $v_1 = 2t_1/h$, $v_2 = 2t_2/h$, are the volume fractions associated with the two orientations. The bending stiffness calculated from equivalent properties is

$$D_{ij_{eq}}^* = \frac{12 D_{ij_{eq}}}{(h)^3} = A_{ij}^* \tag{4.5}$$

The exact bending stiffness is

$$D_{ij} = \frac{2}{3}\overline{Q}_{ij_2} t_2^3 + \frac{2}{3}\overline{Q}_{ij_1}((t_1 + t_2)^3 - t_2^3) \tag{4.6}$$

The normalized bending stiffness expressed in terms of volume fraction of the second layer is

$$D_{ij}^* = \overline{Q}_{ij_2} v_2^3 + \overline{Q}_{ij_1}(1 - v_2^3) \tag{4.7}$$

The ratio of the bending stiffness from equivalent properties and exact calculation is

$$\frac{D^*_{ij_{eq}}}{D^*_{ij}} = \frac{A^*_{ij}}{D^*_{ij}} = \frac{\overline{Q}_{ij_2} v_2 + \overline{Q}_{ij_1}(1-v_2)}{\overline{Q}_{ij_2} v_2^3 + \overline{Q}_{ij_1}(1-v_2^3)} = \frac{kv_2 + (1-v_2)}{kv_2^3 + (1-v_2^3)} \tag{4.8}$$

where k is the ratio of an inplane stiffness component of the two layers.

$$k = \frac{\overline{Q}_{ij_2}}{\overline{Q}_{ij_1}} \tag{4.9}$$

The ratio of bending stiffness from equivalent properties and exact calculation is calculated for different values of the inplane stiffness ratio (k=10, 4, 0.25 and 0.1). A value of k=10, is typical of the ratio of A_{11} for 0° and 90° plies of graphite-epoxy composites. A value of k=4 corresponds to the ratio of A_{11} for 0° and 45° plies. Values of k=0.25 and 0.1 are reciprocals of k=4 and 10, indicating that the outer layer is the stiffer material. Figure 4.3 shows the ratio of bending stiffness terms calculated using Eq. (4.8) for values of the volume fraction v_2 ranging between 0 and 1.

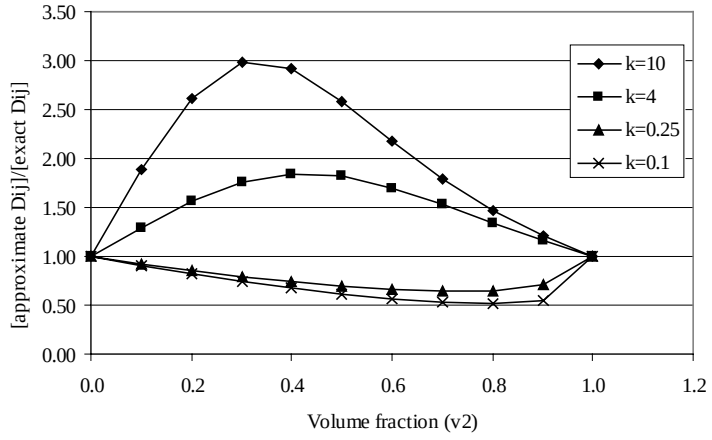

Figure 4.3: Ratio of bending stiffness from equivalent and exact properties

Table 4.5 lists the maximal values of the errors arising from using equivalent properties for a single sublaminate. The volume fractions corresponding to the maximal errors are also provided. The example laminates shown in the last column have volume

fractions at or close to the maximal error value, and they will exhibit errors in D_{11} similar to those shown in Column 2.

Table 4.5: Maximal errors in bending stiffness of a laminate calculated using equivalent properties

Stiffness ratio, k	Maximal error in bending stiffness (%)	Volume fraction (v_2) at max. error	Laminate layup that exhibits similar errors in D_{11} stiffness.
10	198.0	0.3	$[90_2/0]_s$
4	84.6	0.4	$[\pm 45_3/0_4]_s$
0.25	-36.0	0.7	$[0_2/\pm 45_2]_S$
0.1	-49.1	0.8	$[0/90_4]_S$.

As expected, larger maximal errors were found for k=10 and k=0.1, indicating that errors are large when the difference in stiffness of plies is large. The error is more severe when the ply with higher stiffness is closer to the symmetry plane. Bending stiffness calculated using equivalent properties overestimates the contribution of the layer that is closer to the plane of symmetry. When the stiffer ply is away from the plane of symmetry ($k<1$), the opposite happens, and equivalent properties underestimate the bending stiffness.

Table 4.6: Error in bending curvatures due to using equivalent property for graphite-epoxy (E_1=18.5 Mpsi, E_2=1.89 Mpsi, G_{12}=0.93 Mpsi and ν_{12}=0.3)

Laminate	Error in bending curvature (K_x) for pure cylindrical bending (%)	Error in twist curvature (K_{xy}) for pure twist loading (%)
$[90_2/0]_s$	-66.3	0
$[[45_2/0_2]_s$	-34.9	+32.8
$[0_2/45_2]_s$	43.6	-41.0
$[45_2/0_2/90_2]_s$	-8.3	50.9

Large errors are encountered in calculating bending strains when bending stiffnesses are calculated using equivalent properties. Table 4.6 shows the errors in curvatures calculated for pure cylindrical bending (K_x) and pure twist conditions for sample laminates. For most practical applications, the curvatures will depend on several bending stiffness (D_{ij}) terms that have compensating errors. The cylindrical bending and pure twist are examples of possible worst-case scenarios.

The $[90_2/0]_s$ laminate shown in Table 4.5 is an example of a laminate that can give 200% error in D_{11} (that is the exact D_{11} is three times the approximate one). The K_x curvature is proportional to the inverse of D_{11} term. Hence, the error is 66% (that is, the exact curvature is only one third of the value obtained using equivalent properties). The negative sign indicates that bending stiffness calculated from equivalent properties underestimates the curvature (and hence bending stresses). The second and third examples in Table 4.6 show that the error in a strain component in a given direction depends on the position of the ply with orientation corresponding to that strain component. The bending strain K_x is underestimated when the 0˚ fiber is located at the center (near symmetry plane), while the twist curvature is underestimated when the 45˚ layer is located close to the center. The bending curvature error is small for the last example because the 0˚ ply is located farther from the center, and the 90˚ ply that has the least stiffness in the *x* direction is located at the center.

Errors in Bending Stiffness of Laminates with Repeating Sublaminates

The large errors shown in Tables 4.5 and 4.6 are obtained from approximating the entire laminate with equivalent properties. In practice, equivalent properties are used for

sublaminates that are repeated in thicker laminates. With many repeating sublaminates, the use of equivalent material properties will lead to smaller errors. This section investigates how fast the errors decay as the number of sublaminates increases.

The designer has two choices in the arrangement of the symmetric sublaminates (Figure 4.4). One choice is to stack the *n* symmetric sublaminates on top of one another. For example, if the sublaminate has a layup of $[90/0]_s$ then the laminate layup will be $([90/0]_s)_n$ or $[90/0_2/90]_n$. An alternative choice is to repeat the symmetric part of the sublaminate. In other words, use *n* stacks of the bottom and top half of the sublaminate on two sides of the symmetry plane of the resulting laminate. For example, three repetitions of a sublaminate with layup of $[90/0]_s$ will result in a laminate with layup $[(90/0)_3]_s$ or $[(90/0/90/0/90/0]_s$. In the rest of the discussion, the first arrangement will be referred to as *full-sublaminate repetition*, while the second will be referred to as *half-sublaminate repetition*. The half-sublaminate repetition is often used because it permits more freedom to tailor thickness by dropping or adding more half-sublaminates [77].

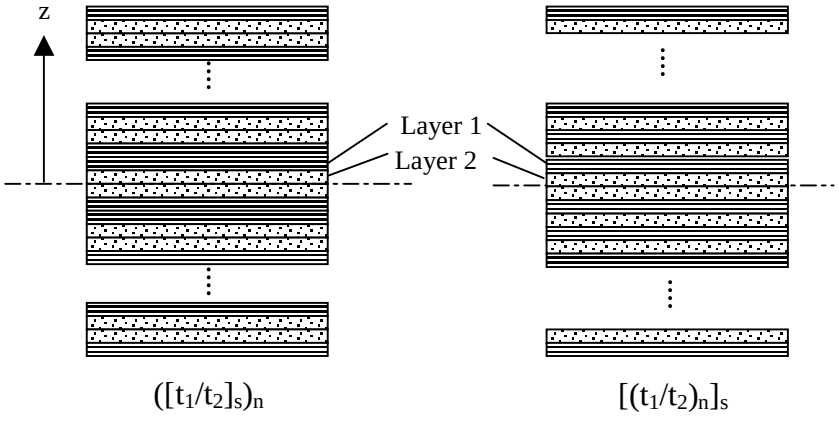

Figure 4.4: Schemes for stacking sublaminates: full-sublaminate and half-sublaminate repetitions

Analytical expressions for ratio of the bending stiffness obtained from equivalent properties and an exact approach are derived for symmetric laminates with *n* sublaminate repetitions for the two different arrangements of the sublaminate, namely full-sublaminate repetition and half-sublaminate repetition.

Laminate with Full-Sublaminate Repetitions

The case where a laminate with *n* symmetric sublaminates stacked on top of one another, as in $[t_1/t_2]_{sn}$ laminate is considered here. Let $(\overline{Q}_{ij})$ be the inplane stiffness of the material. The laminate inplane stiffness (A_{ij}) and bending stiffness (D_{ij}) obtained from lamination theory are expressed as

$$A_{ij} = \int_{-nh/2}^{nh/2} (\overline{Q}_{ij}) dz = \sum_{k=1}^{n_l} (Q_{ij})_k t_k \tag{4.10}$$

$$D_{ij} = \int_{-nh/2}^{nh/2} (\overline{Q}_{ij}) z^2 dz = \sum_{k=1}^{n_l} (\overline{Q}_{ij})_k \frac{(z_{k+1}^3 - z_k^3)}{3} \tag{4.11}$$

where, *n* is the total number of sublaminates, *h* is the thickness of the sublaminate, t_k is the thickness of the k^{th} layer (ply), z^{k+1} and z^k the distance of the top and bottom faces of the k^{th} layer, and n_l the total number of layers (plies) in the laminate (Figure 4.4) . The inplane and bending stiffness are normalized by the quantities *nh* and $(nh)^3/12$ to give A_{ij}^* and D_{ij}^*.

If we use the equivalent material properties to calculate bending stiffness, the normalized equivalent bending stiffness is given by the expression

$$D_{ij_{eq}}^* = \frac{12 D_{ij_{eq}}}{(nh)^3} = A_{ij}^*, \tag{4.12}$$

The exact bending stiffness of the laminate is given by the expression

$$D_{ij} = \int_{-nh/2}^{nh/2} (\overline{Q}_{ij}) z^2 dz = \int_{-nh/2}^{-(n-2)h/2} (\overline{Q}_{ij}) z^2 dz + \ldots + \int_{-h/2}^{h/2} (\overline{Q}_{ij}) z^2 dz \ldots + \int_{(n-2)h/2}^{2h/2} (\overline{Q}_{ij}) z^2 dz \quad (4.13)$$

Rewriting the integrals for each sublaminate with same integration limits results in

$$D_{ij} = \sum_{p=1}^{n} \int_{-nh/2+(p-1)h}^{-nh/2+ph} (\overline{Q}_{ij}) z^2 dz = \sum_{p=1}^{n} \int_{-h/2}^{h/2} (\overline{Q}_{ij}) (z - (n+1)\frac{h}{2} + ph)^2 dz \quad (4.14)$$

Expanding and regrouping the integrals gives

$$\begin{aligned} D_{ij} = \left(\sum_{p=1}^{n} 1 \right) \int_{-h/2}^{h/2} (\overline{Q}_{ij}) (z)^2 dz + \left(\sum_{p=1}^{n} \left((n+1)\frac{h}{2} - ph \right)^2 \right) \left(\frac{h}{2} \right)^2 \int_{-h/2}^{h/2} (\overline{Q}_{ij}) dz + \\ -2 \left(\sum_{p=1}^{n} \left((n+1)\frac{h}{2} - ph \right) \right) \left(\frac{h}{2} \right)^2 \int_{-h/2}^{h/2} (\overline{Q}_{ij}) z dz \end{aligned} \quad (4.15)$$

Recognizing the integrals in the above equation as the bending ($D_{ij_{sub}}$), inplane ($A_{ij_{sub}}$), and bending-extension coupling ($B_{ij_{sub}}$) stiffness terms of the sublaminate, respectively, Eq. (4.15) can be rewritten as

$$\begin{aligned} D_{ij} = \left(\sum_{p=1}^{n} 1 \right) D_{ij_{sub}} + \left(\sum_{p=1}^{n} \left((n+1)\frac{h}{2} - ph \right)^2 \right) \left(\frac{h}{2} \right)^2 A_{ij_{sub}} + \\ -2 \left(\sum_{p=1}^{n} \left((n+1)\frac{h}{2} - ph \right) \right) \left(\frac{h}{2} \right)^2 B_{ij_{sub}} \end{aligned} \quad (4.16)$$

For symmetric sublaminates $B_{ij_{sub}}$ is zero. Simplifying the summations in Eq. (4.16), obtains

$$D_{ij} = nD_{ij_{sub}} + \frac{(n-1)(n)(n+1)}{3} \left(\frac{h}{2} \right)^2 A_{ij_{sub}} \quad (4.17)$$

Normalizing D_{ij} in above equation by $(nh)^3/12$, gives

$$D_{ij}^{*} = \frac{1}{n^2} D_{ij_{sub}}^{*} + \frac{(n-1)(n+1)}{n^2} A_{ij_{sub}}^{*} \tag{4.18}$$

The ratio of bending stiffness of laminate calculated using equivalent properties and exact approach is then given by the expression

$$\frac{D_{ij_{eq}}^{*}}{D_{ij}^{*}} == \frac{n^2}{\frac{D_{ij_{sub}}^{*}}{A_{ij_{sub}}^{*}} + (n-1)(n+1)} \tag{4.19}$$

Laminate with Half-Sublaminate Repetitions

Next, a laminate with half-sublaminate repetitions is considered. The laminate with half-sublaminate repetitions has the same inplane stiffness properties as the laminate with full-sublaminate repetitions, but has different bending properties due the difference in the stacking sequence. Since the inplane stiffness does not change, the equivalent bending stiffness is same as before (Eq. 4.12)

Let $(\overline{Q}_{ij})_b$ and $(\overline{Q}_{ij})_t$ be the inplane stiffness of the plies in the bottom and top half of the sublaminate. The bending stiffness of the laminate can be expressed as

$$\begin{aligned} D_{ij} = \int_{-nh/2}^{nh/2} (\overline{Q}_{ij}) z^2 dz = \int_{-nh/2}^{-(n-1)h/2} (\overline{Q}_{ij})_b z^2 dz + \ldots + \int_{-h/2}^{0} (\overline{Q}_{ij})_b z^2 dz \\ + \int_{0}^{h/2} (\overline{Q}_{ij})_t z^2 dz + \ldots + \int_{(n-1)h/2}^{nh/2} (\overline{Q}_{ij}) z^2 dz \end{aligned} \tag{4.20}$$

Rewriting all integrals of the bottom and top sublaminates using the same limits and expressing the above expression as a summation series gives

$$D_{ij} = \sum_{p=1}^{n} \int_{-h/2}^{-0} (\overline{Q}_{ij})_b \left(z - (i-1)h/2\right)^2 dz. + \sum_{p=1}^{n} \int_{0}^{h/2} (\overline{Q}_{ij})_t \left(z + (i-1)h/2\right)^2 dz \tag{4.21}$$

Expanding the integrals and regrouping similar terms gives

$$D_{ij} = \left(\sum_{p=1}^{n} 1\right)\left\{\int_{-h/2}^{0} (\overline{Q}_{ij})_b z^2 dz + \int_{0}^{h/2} (\overline{Q}_{ij})_t z^2 dz\right\}$$
$$+\left(\frac{h}{2}\right)^2\left(\sum_{p=1}^{n} (p-1)^2\right)\left\{\int_{-h/2}^{0} (\overline{Q}_{ij})_b dz + \int_{0}^{h/2} (\overline{Q}_{ij})_t dz\right\} \qquad (4.22)$$
$$-h\left(\sum_{p=1}^{n} (p-1)\right)\left\{\int_{-h/2}^{0} (\overline{Q}_{ij})_b z dz - \sum_{p=1}^{n} \int_{0}^{h/2} (\overline{Q}_{ij})_t z dz\right\}$$

Recognizing the first two terms of Equation 4.22 as the bending and inplane stiffness of the sublaminate gives

$$D_{ij} = nD_{ij_{sub}} + \left(\frac{h}{2}\right)^2 \frac{1}{6} n(n-1)(2n-1) A_{ij_{sub}}$$
$$-\frac{h}{2} n(n-1)\left\{\int_{-h/2}^{-0} (\overline{Q}_{ij})_b z dz - \sum_{p=1}^{n} \int_{-h/2}^{0} (\overline{Q}_{ij})_t z dz\right\} \qquad (4.23)$$

For symmetric sublaminates the last term in Eq. 4.23 can be further simplified, because the two integrals are equal in magnitude but differ in sign. Normalizing the bending stiffness by $(nh)^3/12$ results in

$$D_{ij}^* = \frac{1}{n^2} D_{ij_{sub}}^* + \frac{1}{2} \frac{(n-1)(2n-1)}{n^2} A_{ij_{sub}}^* - \frac{12(n-1)}{n^2 h^2} \int_{-h/2}^{0} (\overline{Q}_{ij})_b z dz \qquad (4.24)$$

The ratio of the bending stiffness obtained from equivalent properties and exact method for laminate $[(t_1/t_2)_n]_s$, with n half-sublaminate repetitions is

$$\frac{D_{ij_{eq}}}{D_{ij}^*} = \frac{n^2}{\dfrac{D_{ij_{sub}}^*}{A_{ij_{sub}}^*} + \dfrac{1}{2}(n-1)(2n-1) - \dfrac{12(n-1)}{h^2 A_{ij_{sub}}^*} \displaystyle\int_{-h/2}^{0} (\overline{Q}_{ij})_b z dz} \qquad (4.25)$$

The evaluation of Eq. (4.25) will require in addition to the terms $A_{ij_{sub}}^*$ and $D_{ij_{sub}}^*$ the following integral:

$$\int_{-h/2}^{0} (\overline{Q}_{ij})_b \, z dz \tag{4.26}$$

Evaluating this integral for the four ply sublaminate (Figure 4.2) results in the expression

$$\int_{-h/2}^{0} (\overline{Q}_{ij})_b \, z dz = \overline{Q}_{ij_2} \left(\frac{t_2^2}{2}\right) + \overline{Q}_{ij_1} \left(\frac{(t_1 + t_2)^2}{2} - \frac{t_2{}^2}{2} \right) \tag{4.27}$$

$$\int_{-h/2}^{0} (\overline{Q}_{ij})_b \, z dz = \frac{h^2}{2} \overline{Q}_{ij_2} \left\{ v_2^2 + k\left(1 - v_2^2\right) \right\} \tag{4.28}$$

$$\frac{\int_{-h/2}^{0} (\overline{Q}_{ij})_b \, z dz}{h^2 A^*_{ij_{sub}}} = \frac{1}{2} \left(\frac{k v_2^2 + \left(1 - v_2^2\right)}{k v_2 + \left(1 - v_2\right)} \right) \tag{4.29}$$

The derived expressions are used to calculate the ratio of bending stiffness from the approximate and exact approach for the $[t_1 / t_2]_s$ sublaminates for the two stacking schemes discussed. The ratios were calculated for values of volume fraction of Layer 2 (v_2), from 0.0 to 1.0 in increments of 0.1.

Table 4.7: Maximal error in D_{ij} terms for *n* full-sublaminate repetitions, as in $[t_1/t_2]_{sn}$ laminate

Stiffness ratio, *k*	Volume ratio of layer-2, v_2	Maximal error in D_{ij} (%) n=1	n=2	n=3	n=4
10.0	0.3	198.0	19.9	8.0	4.3
4.0	0.4	84.6	12.9	5.4	2.9
0.25	0.7	-36.0	-12.4	-5.9	-3.3
0.10	0.8	-48.1	-18.8	-9.3	-5.5

The maximal error in the bending stiffness for laminates with *n* full-sublaminate repetition is presented in Table 4.7. The value of volume fraction resulting in maximal error is independent of the number of sublaminate repetition (*n*). For full-sublaminate

repetitions, the error reduces rapidly as the number of sublaminate increases. The maximal error is strongly dependent on the ratio of the inplane stiffness of the plies.

Table 4.8: Maximal error in D_{ij} terms for n half-sublaminate repetitions, as in $[(t_1/t_2)_n]_s$ laminate

Stiffness ratio, k	Volume ratio of layer-2, v_2	Maximal error in D_{ij} (%) n=1	n=2	n=3	n=4
10.0	0.3	198.0	55.7	32.3	22.7
4.0	0.4	84.6	31.1	19.0	13.7
0.25	0.7	-36.0	-21.0	-14.8	-11.4
0.10	0.8	-48.1	-29.8	-21.5	-16.8

Table 4.8 shows the errors in bending stiffness for laminates with half-sublaminate repetition. For n=1, the laminate is the same as in Table 4.8 and hence exhibits the same maximal error. However, compared to full-sublaminate repetition, the error reduces more slowly when the number of sublaminates is increased. The maximal errors for k=10 are 55.7%, 32.3%, and 22.7%, respectively, for n=2, 3, and 4. The error is higher because the stiffer ply is located closer to the symmetry (reference) plane and thereby contributes less to the bending stiffness. An example of a $[90/0]_s$ sublaminate with two repetitions is considered here. Full-sublaminate repetition results in a laminate with layup of $[90/0_2/90]_s$ while the half-sublaminate repetition results in a layup of $[90/0/90/0]_s$. The D_{11} stiffness of the $[90/0/90/0]_s$ laminate is lower compared to that of the $[90/0_2/90]_s$ laminate because the 0° ply is closer to the symmetry plane, leading to larger errors due to equivalent properties. The volume fraction at maximal error is identical for full-sublaminate and half-sublaminate repetitions.

Anti-Optimization of Sublaminate Lay-up for Maximal Buckling Load Error

In the previous section, maximal errors in bending stiffness were investigated for two-ply sublaminates. This section will investigate errors in buckling loads due to the use of equivalent properties for laminates made from 0˚, ±45˚ and 90˚ plies. In order to estimate the maximal errors in buckling loads, laminates were optimized for maximal error, a process known as anti-optimization [114].

The error in buckling load (λ_c) due to use of equivalent properties was calculated for a simply supported rectangular plate in biaxial compression. The buckling load is

$$\lambda_c = \frac{\pi^2\left[D_{11}\left(\frac{m}{a}\right)^4 + 2\left(D_{12}+2D_{66}\right)\left(\frac{m}{a}\right)^2\left(\frac{n}{b}\right)^2 + D_{22}\left(\frac{n}{b}\right)^4\right]}{\left[N_x\left(\frac{m}{a}\right)^2 + N_y\left(\frac{n}{b}\right)^2\right]} \tag{4.30}$$

where D_{ij} represents bending stiffness terms, N_x and N_y are the loads in the axial and transverse directions, a, b are the dimensions of the plate and m, n are the number of half waves in the axial and transverse directions.

The percent relative error in buckling loads due to equivalent laminate properties is defined as

$$\%Error = 100\frac{\left(\lambda_c^{approx} - \lambda_c^{exact}\right)}{\lambda_c^{exact}} \tag{4.31}$$

where λ_c^{approx} is the buckling load factor calculated using equivalent laminate properties and λ_c^{exact} is the buckling load factor calculated using exact ply representation.

The anti-optimization of the laminate lay-ups was performed using a genetic algorithm to maximize the absolute relative error in buckling load (Eq. 4.31) for 16-ply

symmetric and balanced laminates. The design variables of the genetic algorithm were ply-orientations that were restricted to, $\pm$45°, 0°, and 90°.

Table 4.9: Maximal buckling load errors (percent) of a single sublaminate (The coding A-P refers to the stacking sequences in Table 4.10)

Load	Aspect Ratio (a/b)								
N_x/N_y	0.0625	0.125	0.250	0.500	1.000	2.000	4.000	8.000	16.00
0.0625	58	58	65	51	94	154	175	180	59
	(P)	(P)	(P)	(P)	(A)	(E)	(B)	(B)	(B)
0.125	67	65	66	81	51	94	154	175	180
	(N)	(N)	(N)	(O)	(A)	(E)	(B)	(B)	(B)
0.250	101	101	104	90	41	94	154	175	180
	(M)	(M)	(M)	(M)	(A)	(E)	(B)	(B)	(B)
0.500	162	160	149	94	24	94	154	175	180
	(M)	(M)	(M	(L)	(A)	(E)	(B)	(B)	(B)
1.000	179	175	154	94	22	94	154	175	179
	(O)	(O)	(O)	(L)	(N)	(E)	(B)	(B)	(B)
2.000	180	175	154	94	24	94	149	160	162
	(O)	(O)	(O)	(L)	(P)	(E)	(D)	(D)	(D)
4.000	180	175	154	94	41	91	104	101	101
	(O)	(O)	(O)	(L)	(P)	(D)	(D)	(D)	(D)
8.000	180	175	154	94	51	81	65	65	67
	(O)	(O)	(O)	(L)	(P)	(B)	(C)	(C)	(C)
16.00	180	175	154	94	51	65	59	58	58
	(O)	(O)	(O)	(L)	(P)	(C)	(C)	(C)	(C)

Table 4.10: Stacking sequence of sublaminates optimized for maximal error in buckling load for 1 sublaminate in total laminate

CODE	Sublaminate layup	CODE	Sublaminate layup
A	$[0_2/0_2/0_2/\pm45]_s$	I	$[\pm45/90_2/90_2/90_2]_s$
B	$[0_2/0_2/0_2/90_2]_s$	J	$[90_2/0_2/0_2/0_2]_s$
C	$[0_2/0_2/\pm45/\pm45]_s$	K	$[90_2/0_2/\pm45/\pm45]_s$
D	$[0_2/0_2/\pm45/90_2]_s$	L	$[90_2/90_2/0_2/0_2]_s$
E	$[0_2/0_2/90_2/90_2]_s$	M	$[90_2/90_2/\pm45/0_2]_s$
F	$[0_2/90_2/\pm45/\pm45]_s$	N	$[90_2/90_2/\pm45/\pm45]_s$
G	$[0_2/90_2/90_2/90_2]_s$	O	$[90_2/90_2/90_2/0_2]_s$
H	$[\pm45/0_2/0_2/0_2]_s$	P	$[90_2/90_2/90_2/\pm45]_s$

A genetic algorithm uses operators that mimic biological evolutionary processes such as mutation and crossover to obtain improved designs. The operators work on a population of designs, each represented by a chromosome. The selection of the

chromosome for reproduction depends on the fitness value assigned to the chromosome. The fitness value here is the magnitude of the error. The genes of the chromosome (that determine the characteristics of the design) are the encoded optimization variables. For laminate stacking sequence design, the discrete ply orientation angles are coded using integer variables. In this work, the basic unit of coding represented a stack of two plies: 0_2, 90_2 or ± 45. This was used for convenience to ensure that all laminates obtained were balanced. With the two-ply stack coding, the 16-ply symmetric laminate is represented using a chromosome with 4 genes. The errors were obtained for a laminate made of graphite-epoxy plies with properties E_1=18.5 Mpsi, E_2=1.89 Mpsi, G_{12}=0.93 Mpsi and ν_{12}=0.3.

The stacking sequence optimization is performed for plates with varying aspect (a/b) and load (N_y/N_x) ratios. The aspect ratio and loading ratio were varied from one sixteenth to sixteen, with steps of factors of 2.0 giving 81 cases in all. The maximal value of the errors in buckling load factor and the resulting laminate for a range of aspect ratios and load ratios are shown in Table 4.9, with laminates having maximal errors given in Table 4.10.

For the optimized 16-ply laminate, the largest maximal error (180%) occurs when there is a combination of high aspect ratio and high load ratio. The smallest maximal error (22%) is obtained for a plate with unit aspect and load ratios. Of all possible 81 sublaminates, only a small set of 10 (A-E, L-P) were found in the anti-optimization for the case of one sublaminate through the thickness. The large errors shown in Table 4.9 are for the extreme case where the laminate has a single sublaminate.

A select number of cases from Table 4.9 were chosen for further investigation of the effect of the number of sublaminates on buckling load error. This is shown in Table 4.11 for a laminate with half-sublaminate repetition and in Table 4.12 for full-sublaminate repetition.

Table 4.11: Effect of number of sublaminates in half sublaminate repetition on error in buckling load calculated using equivalent properties

Case No.	N_x/N_y	a/b	Worst case sublaminate	% Error in buckling load for multiple sublaminates				
				n=1	n=2	n=3	n=4	n=5
1	0.5	1/16	$[(90_4 / \pm 45 / 0_2)_n]_s$	162.1	45.85	26.09	18.20	13.90
2	0.5	0.5	$[(90_4 / 0_4)_n]_s$	94.22	32.02	19.29	13.40	10.75
3	1.0	1.0	$[(90_4 / \pm 45_2)_n]_s$	21.50	9.71	6.27	4.63	3.67

Table 4.12: Effect of number of sublaminates in full sublaminate repetition on error in buckling load calculated using equivalent properties

Case No.	N_x/N_y	a/b	Worst case sublaminate	% Error in buckling load for multiple sublaminates				
				n=1	n=2	n=3	n=4	n=5
1	0.5	1/16	$[90_4 / \pm 45 / 0_2]_{sn}$	162.1	16.54	6.57	3.55	2.24
2	0.5	0.5	$[90_4 / 0_4]_{sn}$	94.22	13.80	5.70	3.21	1.98
3	1.0	1.0	$[90_4 / \pm 45_2]_{sn}$	21.50	4.63	2.00	1.11	0.71

The errors decay more slowly for half-sublaminate repetition. The decay in errors is consistent with that observed for the bending stiffness errors (Tables 4.7 and 4.8).

Large errors in buckling loads are observed for plates with large aspect and load ratios (Table 4.9). Smaller buckling load errors (21.5%) were found for the $[90_4 / \pm 45_2]_S$ laminate (Table 4.12) obtained from anti-optimization of a plate with unit aspect ratio and load ratio. At unit aspect ratio, the dominant term in the buckling equation (Eq. 13) is the D_{66} term. The maximal error occurs when the stiffer layer (±45° layers) is closer to the symmetry plane. The reduced errors at unit aspect and load ratios

are also due to the compensating errors in the different bending stiffness terms (Eq. 4.30). For plates with high (or low) aspect and load ratios, the buckling loads are more dependent on individual bending stiffness terms (D_{11}, D_{22}). For $[90_4/\pm 45/0_2]_S$ laminate in Table 4.12, equivalent properties underestimate the D_{11} stiffness term and overestimate the D_{22} stiffness term, resulting in large errors in buckling loads.

Facesheet Wrinkling of Sandwich Panels

Homogenization approximations analogous to those discussed for composite laminates are used in the design of sandwich panels. Often sandwich panels are analyzed using models developed for composite laminates when they can correctly account for transverse shear deformation. However, sandwich laminates exhibit some unique local failure modes that are different from those of laminated composites. Simple physical models that have closed form solutions are used to capture such local failure modes. One such local failure mode is facesheet wrinkling failure.

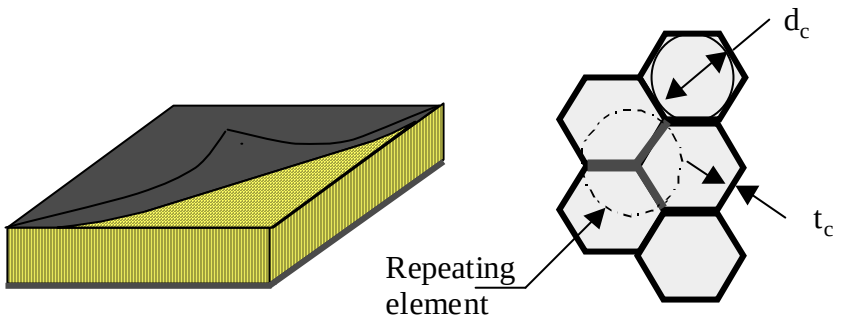

Figure 4.5: Honeycomb sandwich laminate showing core (cell) dimensions

The facesheet wrinkling loads are calculated from a beam on elastic foundation analogy. For this model, the foundation stiffness is calculated from the properties of the sandwich core material (Figure 4.5). In the case of sandwich panels with hexagonal cells, the core is approximated as a continuum to calculate the facesheet wrinkling load. The

approximation is accurate when the facesheet wrinkling (buckling) half-wavelength spans the width of many hexagonal cells. For design optimization, PANDA2 imposes a constraint on the wavelength so that the ratio of wrinkling half-wavelength to sandwich core diameter ratio (w_0/s) is greater than 2.0 (Figure 4.6). This ensures that the continuum approximation is valid.

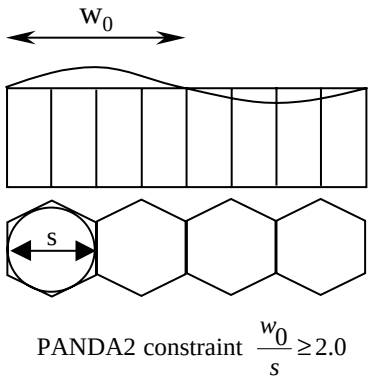

Figure 4.6: Wrinkling of face sheet on sandwich core

The wrinkling wavelength constraint is imposed even when the wrinkling load margin is very high. Enforcing that constraint increases the facesheet thickness leading to a design with a longer wrinkling wavelength. In this section, the error margin for the wrinkling load factor prediction when the wavelength constraint is not satisfied is discussed and a correction is proposed to account for wrinkling at short wavelengths. In order to demonstrate that this is indeed a true design problem, a sandwich cylinder is optimized with selected loads used in the design of liquid hydrogen tanks from Chapter 3.

Sandwich Facesheet Thickness Optimization

Typical sandwich panels were obtained for core densities of 1.0 to 12.0 lb/ft^3 or pcf (pound per cubic feet). The facesheet thickness of a 60 inch long cylindrical panel

clamped at ends and loaded with a uniform axial compression load of 1000 lb/in was calculated with and without the face sheet wrinkling wavelength constraint.

Table 4.13: Effect of wrinkling wavelength constraint on optimal facesheet thickness

Core density (pcf)	2.0	4.0	8.0	12.0
Face sheet thickness without constraint (inch)	0.0231	0.0155	0.0133	0.0131
Percentage weight of face sheet in total laminate	34.735	15.151	7.116	4.789
Wrinkling wavelength to cell diameter ratio	0.382	0.408	0.556	0.719
Wrinkling load factor	5.04	3.54	3.86	4.56
Face sheet thickness with constraint (inch)	0.1207	0.0761	0.0478	0.0365
Percentage weight of face sheet in total laminate	97.09	91.32	76.77	62.71
Wrinkling load factor	28.72	31.96	33.70	31.79

Table 4.13 shows the facesheet thickness required to satisfy overall buckling, stress, dimpling, and wrinkling failure constraints. When the wrinkling wavelength constraint is not imposed, the wrinkling wavelength is smaller than the cell size. Hence, the wrinkling load factors predicted for such cases are not valid and may be much smaller than those indicated on the fifth row of Table 4.13. In contrast, it is to be observed that imposing the constraint results in designs with very thick facesheets. The thick facesheet satisfies the geometrical constraint of wrinkling wavelength. The wrinkling load factor was found to be very large as shown in the last row of Table 4.10. Consequently, there is substantial weight penalty due to wrinkling even when wrinkling is not even close to being citical.

Beam on Elastic Foundation Model

A simple study was performed using a beam on elastic foundation model (Figure 4.7) to determine the magnitude of the errors when facesheet wrinkling wavelength is

comparable to the cell size. The beam was modeled with discrete springs. Facesheet wrinkling (buckling for the beam model case) was calculated using the discrete springs and by smearing the discrete springs to get the equivalent foundation modulus.

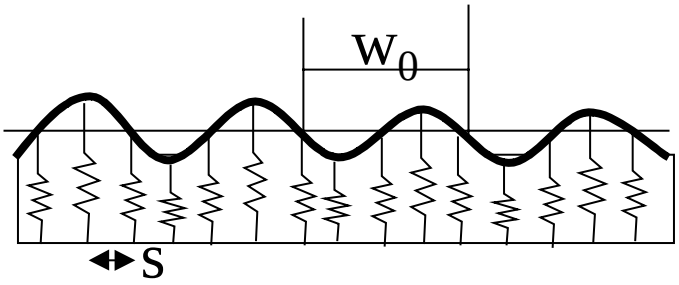

Figure 4.7: Schematic of beam on an elastic (discrete spring) foundation.

The beam on elastic foundation is analyzed using minimum energy principles. A beam of length *l*, with simple supports is considered. The beam and elastic spring foundation are analogous of facesheet and sandwich core in the case of a sandwich laminate wrinkling failure. The number of springs in this length can be varied and is determined by the cell size.

The total strain energy of this system is the sum of the strain energy due to the beam bending (U_b) and the extensional strain energy in the springs (U_s). A displacement shape function that satisfies the kinematic (natural) boundary conditions is given by

$$w = \sum_{n=1}^{\infty} a_n \sin\left(\frac{n\pi\pi}{l}\right) \tag{4.30}$$

Discrete Spring Model

The bending strain energy of the beam, U_b and the strain energy in the springs, U_s are expressed as follows:

$$U_b = \int_0^l \frac{1}{2} EI \left(\frac{\partial^2 w}{\partial x^2} \right)^2 dx \tag{4.31}$$

$$U_s = \sum_{i=1}^{Ns} \frac{1}{2} k \left(w(x_i) \right)^2 \tag{4.32}$$

The potential due to the axial load P acting on the beam (or virtual work, V) is given by

$$V = -\int_0^l \frac{1}{2} P \left(\frac{\partial w}{\partial x} \right)^2 dx \tag{4.33}$$

The variation of the total potential energy (Π) is zero at equilibrium position.

$$\delta \Pi = \delta U + \delta V = 0 \tag{4.34}$$

Substitution of the expressions for U, V and w in the above expression lead to

$$\begin{aligned} \frac{\partial \Pi}{\partial a_m} = \int_0^l EI \sum_{n=1}^{\infty} a_n \left(\frac{n\pi}{l} \right)^2 \left(\frac{m\pi}{l} \right)^2 \sin\left(\frac{n\pi x}{l} \right) \sin\left(\frac{m\pi x}{l} \right) dx \\ + \sum_{i=1}^{Ns} k \sum_{n=1}^{\infty} a_n \sin\left(\frac{n\pi x_i}{l} \right) \sin\left(\frac{m\pi x_i}{l} \right) \\ - \int_o^l P \sum_{n=1}^{\infty} \sum_{n=1}^{\infty} a_n \left(\frac{n\pi}{l} \right) \left(\frac{m\pi}{l} \right) \cos\left(\frac{n\pi x}{l} \right) \cos\left(\frac{m\pi x}{l} \right) \end{aligned} \tag{4.35}$$

The orthogonality of the cosine and sine functions simplifies Eq. (4.35) to the following eigenvalue problem for the buckling load P:

$$\begin{aligned} &[\mathbf{C}]\{\mathbf{a}\} = 0, \\ &C_{pq} = k \sum_{i=1}^{Ns} \sin\left(\frac{p\pi x_i}{l} \right) \sin\left(\frac{q\pi x_i}{l} \right), \text{ for } p \neq q \\ &\quad = k \sum_{i=1}^{Ns} \sin\left(\frac{p\pi x_i}{l} \right)^2 + EI \left(\frac{p\pi}{l} \right)^4 \left(\frac{l}{2} \right) - P \left(\frac{p\pi}{l} \right)^2 \left(\frac{l}{2} \right), \quad \text{for } p = q \end{aligned} \tag{4.36}$$

The critical buckling load P_{cr}^{d} is the smallest eigenvalue obtained by solving the equation, $\det(\mathrm{C})=0$. Normalization of the critical wrinkling load by the Euler buckling load results in the a non-dimensional load factor, λ_{cr}^{d} given by

$$\lambda_{cr}^{d}=\frac{P_{cr}^{d}}{\left(\pi^{2}EI/l^{2}\right)} \tag{4.37}$$

The non-dimensionalization results in a parameter β that determines the ratio of the stiffness of the foundation to the bending stiffness of the facesheet (beam).

$$\beta=\frac{k_f l^{4}}{\pi^{4}EI} \tag{4.38}$$

Continuum (or Smeared) Foundation Model

The discrete springs are replaced by a smeared continuum foundation with modulus k_f,

$$k_f=\left(Ns+1\right)k/l \tag{4.39}$$

where N_s is the total number of springs, k is the spring stiffness, and l the length of the beam. Substituting k_f in the expression for strain energy in foundation (U_f) gives

$$U_f=\int\frac{1}{2}k_f\,w(x)^{2}\,dx \tag{4.40}$$

Substituting for w from Eq. (4.30) and integrating gives

$$U_f=\sum_{n=1}^{\infty}\frac{k_f l}{4}a_n^{2} \tag{4.41}$$

The critical value for facesheet (beam) buckling (P_{cr}^{s}) under a uniform foundation is expressed as follows:

$$P_{cr}^{s} = \min\left(\frac{n^2\pi^2}{l^2} EI + k_f \frac{l^2}{n^2\pi^2} \right) \tag{4.42}$$

Non-dimensionalizing the above equation results in

$$\lambda_{cr}^{s} = \frac{P_{cr}^{d}}{\left(\pi^2 EI / l^2\right)} = \min\left(n^2 + \frac{\beta}{n^2} \right) \tag{4.43}$$

Errors in Using Beam Model for Wrinkling

Critical load factors were calculated for different values of β, the foundation stiffness parameter, using the smeared foundation model.

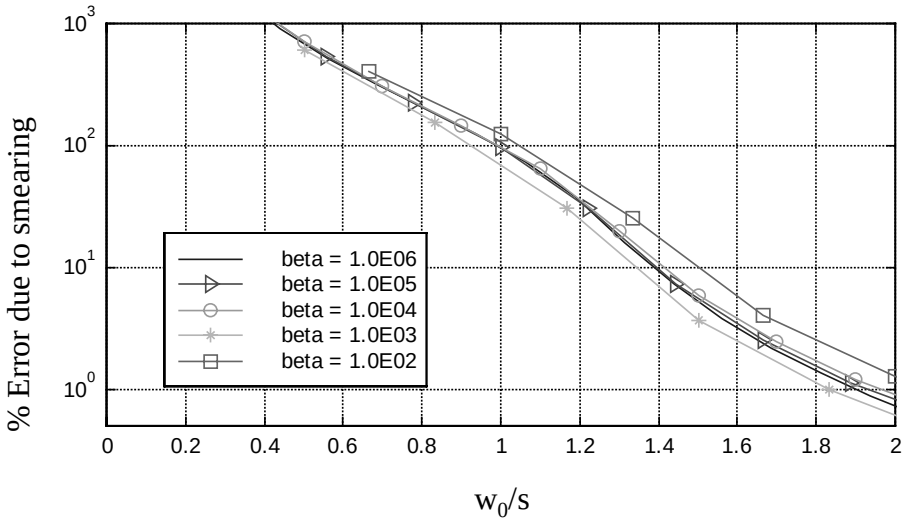

Figure 4.8: Percentage error in wrinkling load factor due to using smeared properties for beam on elastic foundation

For given values of β, the number of springs was varied to obtain critical load factors predicted from the discrete spring model. The error due to smearing the springs is plotted (Fig. 4.8) as a function of the ratio of the wrinkling half wavelength to spring spacing (for sandwich, the equivalent is cell size).

The error is smaller than 1% when the ratio of half wavelength to cell diameter is 2.0 as enforced in PANDA2. However, the error at w_0/s=1.5 soon reaches values of 5 to 10%, and at w_0/s =1.0 the error is as high as 100%.

The continuum model is not valid for cases where the beam wrinkling half wavelength is smaller than the spring spacing. It can be seen that the error is 100% (Fig. 4.8) when half wavelength of wrinkling is equal to the spring spacing.

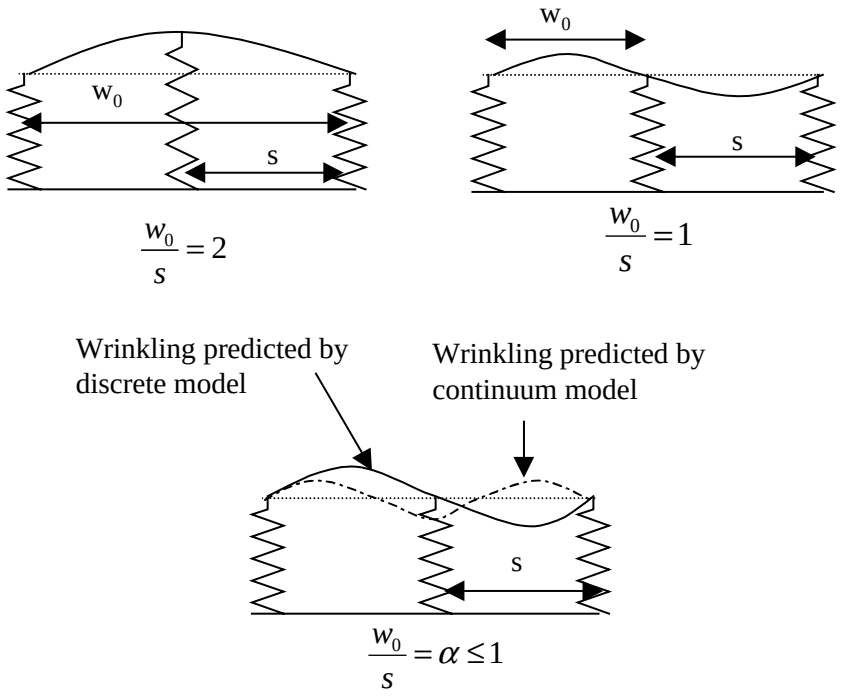

Figure 4.9: Facesheet wrinkling from discrete and continuum models at different wavelengths

When a continuum model is used, at buckling, the energy in the beam is equal to the energy in the foundation. If the same were modeled using discrete springs for foundation, for a w_0/s ratio of 1.0, the springs will be at the nodal points (Fig. 4.9) and thus will not deform. The strain energy is zero in springs. Hence, the discrete model will only have half the strain energy as that of the continuum model. This explains the 100%

error at $w_0/s = 1.0$. For ratios of w_0/s less than 1.0 (predicted from continuum model), the discrete model exhibits buckling such that the half wavelength is equal to the spring spacing (Fig. 4.9).

Correction Factor for Wrinkling Load Calculation

If the ratio of the half wavelength to cell size (spring spacing) w_0/s (α) is less than 1.0 (Fig. 4.9), the ratio of wrinkling load of beam from continuum model to discrete model is a factor of $\left(2/\alpha^2\right)$. The ratios of wrinkling loads from continuum models and discrete models are plotted in Figure 4.10 for different vales of the non-dimensional parameter β along with the $\left(2/\alpha^2\right)$ curve.

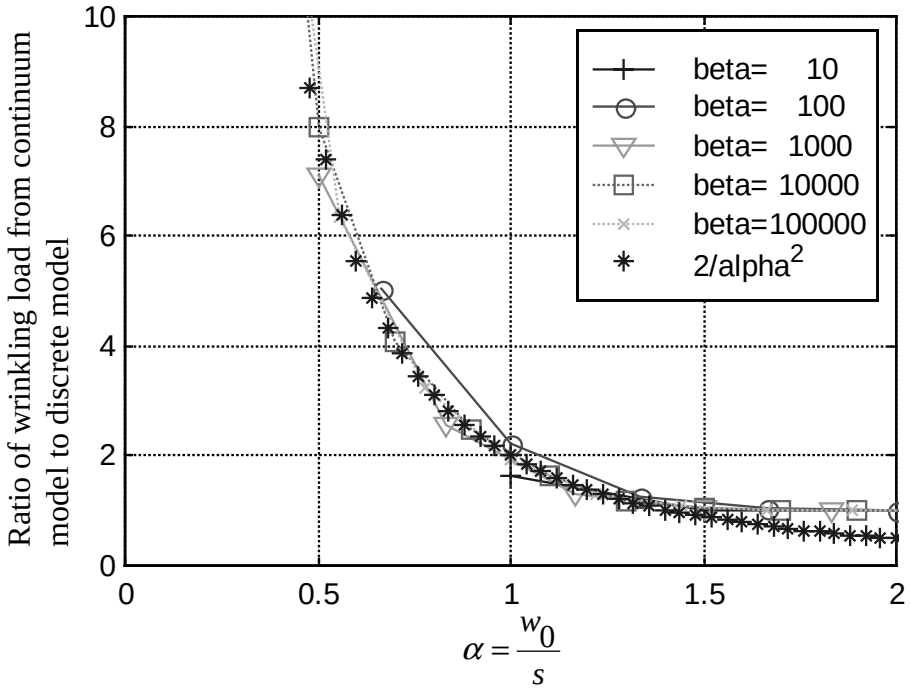

Figure 4.10: Ratio of wrinkling loads from continuum and discrete models for a < 2.0

From Figure 4.10 it appears that for values of $\alpha < 1.5$, a correction factor of $\left(\alpha^2/2\right)$ must be applied to the wrinkling loads obtained from the model with continuum foundation. This indicates that the wrinkling wavelength constraint can be relaxed if the proposed correction factor is used. The proposed correction factor can be applied to continuum models to adjust for the wrinkling half wavelengths that are smaller than the spring spacing.

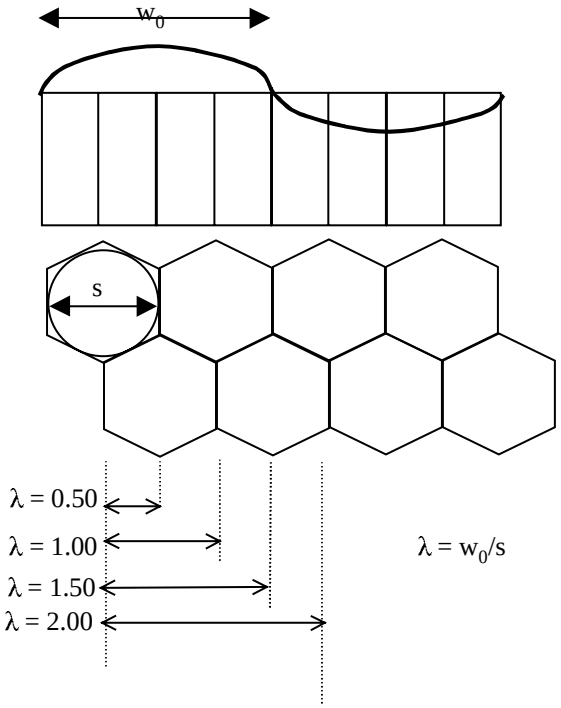

Figure 4.11: Possible half wavelengths for wrinkling us facesheet at lower wavelengths

In the case of a beam on discrete spring foundation, there is no support between the springs. In the case of sandwich, there is support under the wrinkled face sheet. When the wrinkling half wavelength equals the cell diameter (or distance between the flat faces of the hexagon), the four sides not parallel to the flat faces will contribute to the foundation stiffness. A correction based on reduced foundation stiffness might be more

appropriate for the sandwich facesheet on hexagonal core. Possibly this should be used for correcting the wrinkling load when the wavelength becomes small. The foundation modulus will need to be reduced accordingly.

The expression for calculating wrinkling load factor used in PANDA2 is as follows:

$$N_x = 0.5 t_{face} \left(\frac{A_{11}}{t_{face}} E_z G_{xz} \right)^{\frac{1}{3}} \qquad (4.23)$$

The expression above indicates that if the foundation stiffness (E_z) is reduced by a factor *n*, the wrinkling load factor will only decrease by $\sqrt[3]{n}$. This suggests that if the foundation stiffness were reduced by a factor of eight, the wrinkling load will decrease by half (50%).

The way the facesheet will wrinkle at such small wavelengths, when w_0/s is less than 2 should be investigated. It may be that the wrinkling does not exhibit a continuous behavior. Wrinkling could occur at some discrete values of half wavelengths such that the flat faces of the hexagonal core do not deform (Fig. 4.11). An appropriate reduced stiffness for foundation should be calculated and used for correction for such discrete wavelengths of wrinkling. This will require verification using a more detailed model.

This work has resulted in modification of the PANDA2 wrinkling failure analysis model (see item 477 in the file …panda2/doc/panda2.news [25]). For the wrinkling failure analysis, the core foundation stiffness has been modified as follows. The full value of the core modulus is used in the wrinkling load factor calculation if the half wavelength of the wrinkling mode is long enough that "smearing" is valid ($w_0/s. \geq 2$). If wrinkling half wavelengths is smaller than the cell diameter ($w_0/s < 1$), then the value of the core

modulus is reduced by half for calculating the wrinkling load factor. For intermediate values of wrinkling half wavelength ($1.0 < w_0/s < 2$), some interpolated value of the core modulus between 0.5 and 1.0 times the actual value is used for wrinkling load calculation.

There are local stresses in the face sheets associated with amplification of the initial face sheet waviness. This initial waviness is assumed to be in the wavelength of the wrinkling mode. The shorter the wrinkling wavelength, the higher the bending stresses in the face sheets associated with amplification under load of the initial face sheet waviness. Therefore, the wrinkling wavelength obtained from the assumption that the core modulus for thickness-wise stretching has the full value (not half the value) is used in PANDA2 for calculating bending stresses in the facesheet.

CHAPTER 5
RESPONSE SURFACE APPROXIMATION

Response surface methodology is a collection of statistical tools and techniques used for constructing an approximate functional relationship between response (calculated or measured phenomenon) and design variables (a number of independent factors or variables that affect the response). The approximate functional relation, typically in the form of a low order polynomial, is referred to as the response surface. Response surface approximations were originally developed for fitting data from physical experiments. The response surfaces served the purpose of filtering noise and providing the designer with a simple surrogate model to describe the response.

The relationship between the response (y) and the independent variables (x) can be expressed using a mathematical model of general form,

$$y = f(x_1, x_2, \ldots, x_k) + \varepsilon \tag{5.1}$$

where ε represents the *'total error'* (that is the difference between the actual values and the predicted values) and k is the number of predictor variables in the model.

The function $f(x)$, is normally chosen to be a low order polynomial, typically linear or quadratic. A quadratic model may be represented mathematically as follows:

$$y = \beta_0 + \sum_i \beta_i x_i + \sum_{i \le j} \beta_{ij} x_i x_j \tag{5.2}$$

where the β's are the true coefficients that describe the response function. The estimated coefficients of a fitted model will be denoted by *b*. For *k* variables, the quadratic model, Eq. (5.2) has a total of $p = (k+1)(k+2)/2$ coefficients.

Response Surface Approximation Construction

If *f(x)* accurately describes the process being modeled, ε may be considered as a random error, often assumed to have a normal distribution with zero mean. In this case *f(x)* is an unbiased estimate of *y* and ε accounts for sources of variation not accounted for by *f*(x), but which are still inherent to the process such as noise and measurement errors.

Once the model to characterize the response is selected, then the coefficients b_0, $b_1,...,b_k$ will have to be estimated. Typically, a least squares method that minimizes the error residual is utilized for estimating the coefficients of the model equation.

If we have *n* observations (or measurements), then the values of the observed response can be written as follows using the model equation.

$$\begin{Bmatrix} y_1 \\ y_2 \\ \vdots \\ y_n \end{Bmatrix} = \begin{bmatrix} 1 & x_{12} & x_{13} & \cdots & x_{1p} \\ 1 & x_{22} & x_{23} & \cdots & x_{2p} \\ \vdots & \vdots & \vdots & \vdots & \vdots \\ 1 & x_{1n} & x_{2n} & \cdots & x_{np} \end{bmatrix} \begin{Bmatrix} \beta_0 \\ \beta_1 \\ \vdots \\ \beta_p \end{Bmatrix} + \begin{Bmatrix} \varepsilon_1 \\ \varepsilon_2 \\ \vdots \\ \varepsilon_n \end{Bmatrix} \tag{5.3}$$

or using matrix form as,

$$\mathbf{y} = \mathbf{[X]b} + \boldsymbol{\varepsilon} \tag{5.4}$$

where [**X**] is the matrix of response surface approximation terms (usually monomials) evaluated at the fitting points, and the vector ***b*** contains estimates of the unkown coefficients β_i of the response surface approximation.

The values of the unknown linear regression coefficients, β_i are found by using a least squares procedure that minimizes the sum of the squares of the residuals, L, which is defined as

$$L = \sum_{i=1}^{n} \varepsilon_i^2 \tag{5.5}$$

Minimizing L with respect to β_t we obtain

$$\frac{\partial L}{\partial \beta_i} = -2\boldsymbol{X}^{\boldsymbol{T}}\boldsymbol{b} + 2\boldsymbol{X}^{\boldsymbol{T}}\boldsymbol{X}\boldsymbol{b} \tag{5.6}$$

The regression coefficients may then be solved from Eq. 5.7 which is a direct result of Eqns. (5.6) and (5.7).

$$\mathbf{X}^{\mathbf{T}}\mathbf{X}\mathbf{b} = \mathbf{X}^{\mathbf{T}}\mathbf{y} \tag{5.7}$$

$$\mathbf{b} = \left(\mathbf{X}^{\mathbf{T}}\mathbf{X}\right)^{-1}\mathbf{X}^{\mathbf{T}}\mathbf{y} \tag{5.8}$$

The above equations are referred to as the normal equations.

Design of Experiments

Response surface methodology has methods for selecting data points at which the response function should be evaluated. The procedure of choosing a small set of optimal points in the design space to fit the approximation is termed “design of experiments”. The design points are chosen to maximize the predictive capabilities of the approximating function. In cases where there is significant noise (variance) errors, the points are chosen such that they minimize the variance error in the fitted coefficients. For problems with small numbers of design variables in regularly shaped domains, selection schemes, called standard designs, are available. Examples of such standard designs are the central composite and Box-Behnken [20] designs.

For irregularly shaped design space, several computer generated designs that are usually based on an optimality criterion are available. The best known among them is the D-optimal design. The D-optimal criterion minimizes the value of the variance error in the fitted coefficients. Under the D-optimal criterion, the design points are chosen such that the determinant of the moment-matrix [M], ($|\mathbf{M}| = |\mathbf{X}^T\mathbf{X}|$) is minimized. There are also other criteria available for selecting minimum variance design points (e.g., A-optimality, G-optimality) that derived from minimizing other measures of the moment matrix M, such as trace or maximum value on the diagonal.

Another error that can occur in response surface approximations is the bias error. Bias error results from choosing a lower order model to approximate the response. In cases where bias error is dominant, it is necessary to choose points that minimize bias errors. Gauss integration points are example of minimum bias design points. Some schemes that provide minimum bias design points exist for low dimensional and regularly shaped design space (Myers and Montgomery, 1995 [80], pp. 406-421). For irregularly shaped design spaces, one has to resort to numerical procedures.

Orthogonal designs or orthogonal arrays also provide minimum variance designs. The first order orthogonal design is one in which the points diagonalize the moment matrix $\mathbf{X}^T\mathbf{X}$. This implies that the columns of the $\mathbf{X}$ matrix are orthogonal. Thus the elements on the diagonal of the $(\mathbf{X}^T\mathbf{X})^{-1}$ matrix are minimized by making the off diagonal terms of $\mathbf{X}^T\mathbf{X}$ as large as possible thereby forcing $\mathbf{X}^T\mathbf{X}$ to be as large as possible. The orthogonal arrays are minimum variance designs that minimize variance of the fitted coefficient on a per observation basis. However, unlike D-optimal points that are selected predominantly on the boundary, the orthogonal design points are more uniformly

distributed through the design space. This can possibly result in improved design point bias error protection.

Error Estimation

The response surface approximations are constructed for prediction of the response at other design points. Hence, it is necessary to know how well the model predicts the response at the points of interest. The root mean square (rms) error is a useful measure of model accuracy. If the estimate of the response surface model is denoted as $\hat{y}$, where $\hat{\mathbf{y}} = \mathbf{Xb}$, then the error (**e**, vector of residuals) is as follows:

$$\mathbf{e} = \hat{\mathbf{y}} - \mathbf{y} \tag{5.9}$$

The sum of square of errors SS_e are expressed as

$$SS_e = \sum_{i=1}^{n} e_i^2 = (\mathbf{y} - \mathbf{Xb})^{\mathrm{T}} (\mathbf{y} - \mathbf{Xb}) \tag{5.10}$$

The root mean square (*RMS*) error, e_{rms}, at the data points is then calculated as

$$e_{rms}^2 = \frac{SS_e}{n} \tag{5.11}$$

The *RMS* error given by Eq. (5.11) decreases as the order of the polynomial used for the model equation is increased; however, this does not guarantee better accuracy in predicting the response at other points. In other words, increasing the number of degrees of freedom of the model will enable it to pass closer to all the given design points and hence will have a very small *RMS* error. A better and unbiased estimate for the *RMS* error at points not used in the construction is

$$\hat{e}_{rms}^2 = \frac{SS_e}{n - p} \tag{5.12}$$

In order to assess prediction accuracy it is also possible to use a set of points to generate the response surface (estimation data set) and another set of points to perform the error analysis (prediction data set). However, this would require additional analyses that will not be used for the regression fitting. In order to economize on the analyses and use all points for the regression, another measure of the error (residual), known as PRESS (prediction error sum of squares) is used. To calculate PRESS, the error residual at each design point is obtained from a regression model fitted using *n-1* points, which excludes that point. Then the PRESS statistic is defined as the sum of squares of the *n* PRESS residuals as in

$$PRESS = \sum e_{(i)}^2 = \sum (\hat{y}_i - y_i)^2 \tag{5.13}$$

where $e_{(i)}$ is the PRESS residual at the i^{th} point, $\hat{y}_i$ is the prediction value of regression obtained excluding the i^{th} design, and y_i is the observed value.

The PRESS estimate uses all possible subsets of *n*-1 observations as the estimation data set, and every observation in turn forms the prediction data set. It would seem that calculating PRESS requires fitting *n* different regressions. However, it is possible to calculate PRESS from results of a single least squares fit to all *n* observations, as shown in Myers and Montgomery [80].

$$PRESS = \sum_{i=1}^{n} \left(\frac{e_i}{1 - h_{ii}} \right)^2 \tag{5.14}$$

where, e_i are the residuals at the fitted points and h_{ii} are the diagonal terms of the matrix **H**.

$$\boldsymbol{H} = \boldsymbol{X}\left(\boldsymbol{X}^T \boldsymbol{X}\right)^{-1} \boldsymbol{X}^T \tag{5.15}$$

Because the matrix **X'X** is often ill-conditioned, for large problems the PRESS estimation using Eq. (5.14) is not recommended.

Confidence Measures for Approximation Model

The coefficient of determination statistic R^2 or the adjusted-R^2 (R^2_{adj}) statistic are commonly reported for approximation models. The coefficient of determination statistic R^2 characterizes the proportion of variability in the response data that is captured by the response surface approximation and is defined as

$$R^2 = 1 - \frac{SS_e}{S_{yy}} \tag{5.16}$$

where $SS_e = \sum_{i=1}^{n} (y_i - \hat{y}_i)^2$ and $SS_{yy} = \sum_{i=1}^{n} y_i^2 - \frac{\left(\sum_{i=1}^{n} y_i\right)^2}{n}$ (5.17)

The R^2 statistic has a value between 0 and 1. Higher values of R^2 are desired for a fitted response surface approximation. Unfortunately, R^2=1 does not imply a good response surface approximation because the value of R^2 can be increased by adding more (higher order) terms. However, adding more terms does not increase the prediction accuracy of the approximation. The adjusted-R^2 provides a more reasonable estimate for the variability captured by the approximation and is defined as

$$R^2_{adj} = 1 - \frac{SS_e/(n-p)}{S_{yy}/(n-1)} = 1 - \frac{(n-1)}{(n-p)}(1-R^2) \tag{5.18}$$

The R^2_{adj} has the desired property that its value does not necessarily increase when additional terms are included in the response surface approximation. When a large difference exists between R^2 and R^2_{adj} values, there is a good chance that the chosen approximation contains insignificant terms.

In a response surface model some coefficients are sensitive to small differences in the data. These coefficients can be identified by estimating the standard deviations of the coefficients. The estimate of the standard deviation of a component of $\boldsymbol{b}$ is called the standard error (se). A useful measure of accuracy of a component of $\boldsymbol{b}$ is the estimate of the coefficient of variation c, defined as the ratio of the standard deviation or standard error of a coefficient to its estimated value.

$$c_i = \frac{se(b_i)}{b_i} \tag{5.19}$$

In most response surface procedures, the quantity used to assess the need for a coefficient is the inverse of c_i, which is called the test statistic, or t-statistic. The t-statistic is used for removing or adding coefficients for improving model prediction accuracy. The t-statistic is usually available from most statistical regression software, such as JMP software available from the SAS Institute [7]. One scheme for removing redundant coefficients is the "Stepwise regression."

Stepwise Regression

Since the exact form of the response is rarely known, it is general practice to assume a polynomial as a response model, Eq. (5.2). Due to the general nature of such a polynomial, the response model will usually include redundant parameters. Unnecessary parameters in the response model may increase the error of the model and thus decrease its predictive capabilities (Myers and Montgomery, pp. 641 [80], and Kaufman *et al.*[67]). Elimination of these redundant terms from the response model is an important step in constructing a high accuracy response surface approximation.

Stepwise regression represents a family of procedures that investigates only a small number of partial models, by either adding or deleting one parameter at a time. The present research used a mixed stepwise regression procedure implemented in the JMP software package, from SAS Institute [7]. This procedure starts with an initial model. At each step of the procedure, the least significant parameter is removed from the model and more significant parameters from the set of previously removed parameters are investigated for possible re-inclusion in the model. The procedure may be summarized as follows:

1. Start with the full model as an initial model.

2. Delete the least significant parameter from the model being considered.

3. Check to see if any of the previously deleted terms have a significant influence on the predictive capability of the model being considered.

4. Go to step 2 and repeat until some stopping criteria is met.

In the above procedure, the criterion used to determine whether or not a parameter will be re-included in the model is more stringent than the criterion used to remove a parameter. The criterion used for determining the best model is Mallow's C_p statistic, defined as

$$C_p = \frac{SSe_p}{s_\varepsilon^2} - (n - 2p) \tag{5.20}$$

where SSe_p is the sum of the squares of the error terms for a model with p parameters and s_ε^2 is the mean sum of squares of the error terms obtained from the response model with all parameters included. As before, n is the number of data points.

The C_p statistic addresses the prediction capability of the model by trying to estimate a "total error". This "total error" consists of two parts, one that results from modeling errors (bias) and the other from noise (variance error). An under-specified model (insufficient number of parameters) increases that part of the total error resulting from bias, while an over-specified model (too many parameters) increases that part of the total error resulting from variance. Based on the C_p statistic, the best model in a set of candidate models is the model with the lowest C_p value. A good model should at least have a C_p value close to p. The C_p statistic favors a good fit obtained from a simple model.

CHAPTER 6
ANALYSIS INTEGRATION USING APPROXIMATIONS

The design optimization of a vehicle or tank structure needs to include a variety of failure modes and their associated design constraints. The different modes often require different analysis models and very often different analysis programs. Hence, integrating them into a design optimization may be expensive and cumbersome. In this chapter, the use of approximation methods discussed in *Chapter 5* in developing surrogate models is demonstrated. The surrogate models are used to integrate analysis models or replace the analysis models or programs in the design optimization cycle, leading to higher computational efficiency and easy software integration.

Two examples of reusable launch vehicle (RLV) liquid hydrogen tank designs were chosen for demonstration of the integration of different analysis models (and computer programs) by using approximations. The first example is the integration of vehicle and panel analysis models in the design of the RLV tank wall laminate. A vehicle finite element (NASTRAN) model was used to calculate global buckling and out of plane displacements, while a panel (PANDA2) model was used to calculate buckling loads and stresses in individual panels. The second example is the integration of an expensive and detailed analysis model into the optimization with use of a correction response surface fitted to a small number of expensive STAGS analyses. The correction response surface obtained is then applied to the approximate ring local buckling load factor calculated by

PANDA2 (version prior to the addition of discrete analysis model for ring-skin segment [33]) which requires less computational effort and also is less accurate.

Integration of Overall and Panel level Analyses for a RLV Tank Optimization

Design Problem

The tank is a pressurized ring stiffened cylindrical tank. The finite element model of the single stage to orbit (SSTO) launch vehicle structure is shown in Figure 6.1. The vehicle has a conical (droop-nose) liquid oxygen tank and a cylindrical hydrogen tank as part of the vehicle structure. Since the liquid oxygen and liquid hydrogen tanks are an integral part of the vehicle structure, they have to carry loads in addition to serving as cryogenic fuel storage tanks. The load case arising from the vehicle on the launch pad with only liquid oxygen tank filled was used. The weight of the liquid oxygen tank (1.6 million pounds) introduces a compressive load on the liquid hydrogen tank structure. This load case was chosen because it is the most critical case for buckling. Also, the eccentricity between the center of mass of the liquid oxygen and the hydrogen tank (cylinder) axis introduces an overall bending moment on the liquid hydrogen tank.

The goal was to design the tank wall laminate to resist buckling and stress failures. Design constraints are local buckling and stress failure of the cylinders (obtained using a PANDA2 analysis model), overall or global buckling of the tank structure and the out-of-plane deflection (overall buckling and tank out-of-plane displacements are obtained using a finite element analysis model of the overall vehicle structure). The design requirement for the optimization was to satisfy the following safety factors: global buckling load factor of 1.4, local buckling load factor of 1.1, ring buckling load factor of

1.1, stress safety factor of 1.1 and maximum allowable out of plane deflection on tank wall of 0.5 inch.

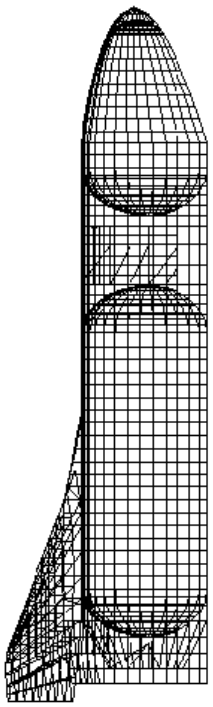

Figure 6.1: Finite element analysis model of the RLV

A composite material (Graphite-Epoxy) was used for the tank wall laminate design. The ply properties of the composite material are as follows: elastic modulus in fiber direction E_1=0.25x10^8 psi, elastic modulus of ply transverse to fiber direction E_2=1.2 x10^6 psi, in-plane shear modulus G_{12}=0.62 x10^6 psi, Poisson's ratio ν_{12}=0.3 and density ρ=0.057 lb/in^3. The maximum allowable stresses in the composite material ply are maximum stress along fibers (F_1) of 2.22x10^5 psi, maximum stress transverse to fibers (F_2) of 7.2x10^3 psi, and maximum allowable shear stress (F_{12}) of 1.12x10^4 psi. The ring stiffeners were made of an isotropic material (aluminum) with properties of elastic modulus E= 10^7 psi, Poisson's ratio ν = 0.3 and maximum allowable stress of 70,000 psi.

Finite element analysis was necessary to capture the non-uniform load on the liquid hydrogen tank and to model the wing attachment to the tank. The global finite element model was also necessary to capture buckling under overall bending of the tank. The finite element model used for the global analysis (NASTRAN) of the tank had the minimal details and refinement required to capture the overall or general buckling of the tank structure. The NASTRAN global model was also used to obtain loads used for the local panel design.

Local details such as stiffener buckling and skin local buckling were modeled separately using the PANDA2 analysis program. The PANDA2 analysis models were circular ring stiffened panels loaded with uniform in-plane and pressure loads. The panel models were used to calculate the buckling of local panels, the buckling failure of stiffeners, and the stresses in the panels.

Options for Overall and Panel Level Analysis Integration

A preliminary analysis of the liquid hydrogen tank was performed using NASTRAN to extract the loads for panels that were then optimized using the PANDA2 program. The ply thicknesses of the wall laminate were used as design variables. The optimized wall laminate was used in the NASTRAN finite element analysis program. It was found that the designs obtained from PANDA2 violated the global buckling and overall displacement constraints. The optimization cycle was iterated with new loads obtained at the end of each PANDA optimization from the global model. The iteration procedure failed to converge to a feasible design since the PANDA2 optimization did not have any information about the constraints from the global failure modes. This

demonstrated the need to include the overall buckling and deflecction constraints (vehicle level analysis) in the local optimization of panels.

Using the NASTRAN analysis directly for calculation of the vehicle-level constraints was not considered for two reasons. First, having PANDA2 call NASTRAN required substantial code modification. Second, using a detailed finite element analysis for constraint evaluation directly in the optimization would be too expensive. In order to integrate the global and local responses into the optimization at a minimal cost, the use of approximations was explored.

Both NASTRAN and PANDA2 analysis programs have optimization capabilities. The two programs also allow the use of algebraic constraint equations. Hence, a sequential constraint approximation strategy was chosen for the optimization. Unlike finite element analysis that uses a single model to calculate the desired responses, PANDA2 uses a suite of approximate models to capture the different possible failure modes. Therefore, approximating PANDA2 responses was impractical. For this reason, the vehicle level responses obtained from the NASTRAN analyses (namely global buckling and out-of-plane deflection) were approximated and used as algebraic constraints in the PANDA2 optimizer. Both linear (derivative based) local approximations and quadratic response surface approximations for the global responses from the vehicle model were created and used in the panel design code.

Linear Local Approximation Constraints

In addition to the panel buckling and stress failure constraints calculated by PANDA2, the overall buckling and bowing constraints (from NASTRAN) were introduced as constraints in the panel design using approximations. The NASTRAN finite

element analysis of the LH2 tank structure provided the overall buckling load factor, maximum displacement and their derivatives with respect to the decision variables. A local linear approximation of the responses from the vehicle model was used as inequality constraints in the PANDA2 optimization of local panels.

The inequality constraint equation for the overall buckling load factor introduced in the PANDA2 optimization, is of the form

$$\lambda_{cr} \le \lambda_0 + \sum_{i=1}^{n} \frac{\partial \lambda}{\partial x_i}\left(x_i - x_{i0}\right) \qquad (6a)$$

where λ_{cr} is the critical load factor and x_{i0} is a nominal design point. Similarly, the constraint equation for the bowing displacement (δ) is

$$\delta_a \ge \delta + \sum_{i=1}^{n} \frac{\partial \delta}{\partial x_i}\left(x_i - x_{i0}\right) \qquad (6b)$$

where, δ_a is the maximum allowable bowing displacement for the LH2 tank.

This local approximation is used in a sequential approximate optimization. In this process, optimization is carried in a region near the nominal design point x_{i0} bounded by move limits. When an optimum is found, a new approximation is created about the optimum and the process is restarted. Each approximate optimization is called a cycle.

Optimization of the tank wall laminate was performed using two laminates that were modeled with three and six design variables respectively. All laminates were balanced and symmetric.

Local linear approximation for the case with three design variables

The laminate $[\pm 45/0/90]_{2s}$ was modeled with three variables: the ply thickness of the 0, 45, and 90 degree plies. Table 6.1 shows the designs obtained at each cycle.

Table 6.1: Optimization of tank wall laminate using local linear approximations for the case with three design variables(ply thicknesses of a $[\pm 45/0/90]_{2s}$ laminate, ply thickness in mils).

No.	Starting design ply thickness, total thickness, buckling load factors and bowing displacement	Optimum design ply thickness total thickness, Buckling load factors and, bowing displacement
1	$[5.0 / 5.0 / 5.0 / 5.0]_{2S}$	$[10.0 / 10.0 / 10.0 / 10.0]_{2S}$
	t_{wall} = 0.080 inch	t_{wall} = 0.160 inch
	λ_{panel} = 0.073, λ_{global} = 2.238 (exact)	λ_{panel} = 0.268, λ_{global}= 6.412, (exact 3.570)
	δ_{bowing} = 1.888 in (exact)	δ_{bowing} = 1.1694 in (predicted), 1.007 in (exact)
2	$[10.0 / 10.0 / 10.0 / 10.0]_{2S}$	$[15.0 / 15.0 / 15.0 / 15.0]_{2S}$
	t_{wall} = 0.160 inch	t_{wall} = 0.240 inch
	λ_{panel} = 0.268, λ_{global} = 3.570 (exact)	λ_{panel} = 0.6417, λ_{global} = 4.645, (exact 4.646)
	δ_{bowing} = 1.007 in (exact)	δ_{bowing} = 0.9755 in (predicted), 0.7066 in (exact)
3	$[15.0 / 15.0 / 15.0 / 15.0]_{2S}$	$[18.8 / 18.8 / 18.8 / 18.8]_{2S}$
	t_{wall} = 0.240 inch	t_{wall} = 0.300 inch
	λ_{panel} = 0.6417, λ_{global} = 4.646 (exact)	λ_{panel} = 1.015, λ_{global} = 5.4582 , (exact 5.4638)
	δ_{bowing} = 0.7066 in (exact)	δ_{bowing} =0.5611 in (predicted), 0.5827 in (exact)
4	$[18.8 / 18.8 / 18.8 / 18.8]_{2S}$	$[23.4 / 23.4 / 23.4 / 23.4]_{2S}$
	t_{wall} = 0.300 inch	t_{wall} = 0.375 inch
	λ_{panel}= 1.015, λ_{global} = 2.238 (exact)	λ_{panel} = 1.45, λ_{global} = 4.1343, (exact 6.504)
	λ_{global} = 1.888 in (exact)	δ_{bowing} = 0.5229 in (predicted), 0.4811 in (exact)
5	$[23.4 / 23.4 / 23.4 / 23.4]_{2S}$	$[20.9 / 20.9 / 21.1 / 20.6]_{2S}$
	t_{wall} = 0.375 inch	t_{wall} = 0.334 inch
	λ_{panel} = 1.45, λ_{global} = 6.504 (exact)	λ_{panel} = 1.0944, λ_{global} = 4.166, (exact 5.902)
	δ_{bowing} = 0.4811 in (exact)	δ_{bowing} = 0.4863 in (predicted), 0.5284 in (exact)
6	$[20.9 / 20.9 / 21.1 / 20.6]_{2S}$	$[19.4 / 19.4 / 23.2 / 22.7]_{2S}$
	t_{wall} = 0.334 inch	t_{wall} = 0.338 inch
	λ_{panel} = 1.0944, λ_{global} = 5.902 (exact)	λ_{panel} = 1.1315, λ_{global} = 6.0873, (exact 6.57216)
	λ_{global} = 0.5284 in (exact)	λ_{global} = 0.5020 in (predicted), 0.4959 in (exact)

The ply thicknesses are indicated using a notation similar to the ply lay-up angle notation commonly used. The ply thickness of a $[\pm 45/0/90]_{2s}$ laminate when all plies are at a uniform ply thickness of 5.0 mils (1 mil = 1.0×10^{-3} inch) is indicated as $[5.0/5.0/5.0/5.0]_{2S}$. The table also shows the total wall laminate thickness (t_{wall}) in units of inches at the end of each cycle. The values of the buckling load factor and bowing displacement obtained using the approximation and exact analysis are compared for designs at each cycle.

A starting design with uniform ply thickness of 0.005 inch was used. For this laminate (Design 1), the local buckling factor (0.073) was much below the required load factor of 1.1, and bowing deflection of tank (1.888 inch) was approximately four times the allowable deflection (0.5 inch). Hence, the first two cycles were allowed to have very large move limits (100% and 50% respectively) to allow the design to quickly move into the feasible design space. The overall buckling load factor was not critical for the design in this case because the deflection constraint was more critical in increasing the bending stiffness of the wall laminate.

The predicted values of the responses from the local linear approximation have large errors for the first two cycles due to the large move limits (Table 6.1). The approximation employs the gradient information at a given design point, and the accuracy is poor far away from that point. This necessitated a reduction in the move limits. The move limits used for design cycles three to five were reduced to 25%. It was found that the accuracy of the predicted value of the vehicle responses for the resulting designs was better. However, to get a final convergence, a smaller move limit of 10% was chosen for iteration six. This resulted in the final design with a total thickness of 0.338 inch. The

design cycle iteration was stopped because the change in total thickness of the wall laminate was sufficiently small (1.2%) and all design requirements were met.

It is to be noted that the error in overall buckling prediction was still substantial (7.3%) in the last iteration that resulted in only 1.2% change (from 0.334 to 0.338 inch) in total laminate thickness. The design cycle was still terminated because the load factor of 6.087 was several times the required 1.4 safety factor for global buckling. However, this illustrates the problem of using linear local approximations for buckling load factors in terms of thickness variables. Since buckling loads are often cubic functions of the laminate thickness, the error in using linear approximations is significant even for small move limits. It was found that as the design progressed with each optimization cycle, it was important to use smaller move limits to ensure convergence. However, this strategy could also result in the design being trapped in a local optimum.

Local linear approximation for the case with six design variables

The procedure detailed above was repeated for a similar laminate $[\pm 45/0/90/\pm 45/0/90]s$, modeled using six design variables. As before, a starting design with all plies at 5.0 mils (1.0 mil = 0.001 inch) was chosen. In this case, the first two cycles used a move limit of 100% each, so as to move the design into the feasible design space. The experience from the designs in the three variable case was used here in allowing such large move limits. Thereafter, the move limits were restricted to 25%.

The optimization was stopped after four cycles as the weight change was 0.3% and no constraints were violated. In moving from Design Cycle 3 (0.6% violation of local buckling margin) to Design Cycle 4, the total laminate thickness changes very little (0.3%), from 0.333 inch to 0.332 inch. The optimizer simply redistributes the material

between the different ply orientations. For most practical applications, the design obtained at the end of design cycle 3 would have been just as useful.

Table 6.2: Optimization of tank wall laminate using local linear approximations for the case with six design variables (ply thicknesses of a $[\pm 45/0/90/\pm 45/0/90]_S$ laminate, ply thickness in mils).

No.	Starting design ply thickness total thickness buckling load factors bowing displacement	Optimum design ply thickness, total thickness, buckling load factors and, bowing displacement
1	$[5.0/5.0/5.0/5.0/5.0/5.0/5.0/5.0]_S$ t_{wall} = 0.080 inch λ_{panel} = 0.073 $\lambda_{overall}$ = 2.238 (exact), δ_{bowing} = 1.888 in (exact)	$[10/10/10/10/10/10.0/10.0/10.0]_S$ t_{wall}= 0.160 inch λ_{panel}= 0.289 $\lambda_{overall}$ = 6.192 (predicted), 3.570(exact) δ_{bowing} = 0.685 in (predicted), 1.007 in (exact)
2	$[10.0/10.0/10.0/10.0/10.0/10.0/10.0/10.0]_S$ t_{wall} = 0.160 inch λ_{panel} = 0.289 $\lambda_{overall}$ = 3.570(exact) δ_{bowing} = 1.007 in (exact)	$[20.0/20.0/20.0/20.0/20.0/20.0/20.0/20.0]_S$ t_{wall}= 0.320 inch λ_{panel}= 1.147 $\lambda_{overall}$ = 6.3987 (predicted), 5.7402(exact), δ_{bowing} = 0.551 in (predicted), 0.427 in (exact)
3	$[20.0/20.0/20.0/20.0/20.0/20.0/20.0/20.0]_S$ t_{wall} = 0.320 inch λ_{panel}= 1.147 $\lambda_{overall}$ = 5.7402(exact) δ_{bowing} = 0.427 in (exact)	$[25.0/25.0/21.2/18.7/15.2/15.2/25.0/21.0]_S$ t_{wall}= 0.333 inch λ_{panel}= 1.094 $\lambda_{overall}$ = 5.746 (predicted),5.7267(exact) δ_{bowing} = 0.502 in (predicted), 0.508 in (exact)
4	$[25.0/25.0/21.2/18.7/15.2/15.2/25.0/21.0]_S$ t_{wall} = 0.333 inch λ_{panel}= 1.094 $\lambda_{overall}$ = 5.7267(exact) δ_{bowing} = 0.508 in (exact)	$[26.6/26.6/16.0/18.2/12.2/12.2/31.2/22.9]_S$ t_{wall}= 0.332 inch λ_{panel}= 1.1 $\lambda_{overall}$ = 5.925 (predicted),5.740(exact) δ_{bowing} = 0.496 in (predicted), 0.5028 in (exact)

As was discussed for the previous case of three design variables, the error in the predicted global buckling load factor was relatively high (3.2%) for a small (0.3%) change in total thickness of the laminate. In comparing the cases with three and six

design variables, it was found that the final total thickness of the wall laminate was lower by 2% for the case with six variables, from 0.338 inch to 0.332 inch.

The sequential approximate optimization approach reduced the computational analysis time in comparison to an optimization using the detailed finite element analysis. However, the approximation is limited in its capability for the following reasons. Optimization using local approximation requires move limits to ensure convergence to an optimum design. The convergence depends on good selection of move limits. In addition, the PANDA2 program uses a gradient-based local optimizer. In order to ensure a global optimum, it is necessary to restart the optimization from different starting points. Using a local approximation would require recalculating the approximation every time a new starting point is chosen.

Response Surface Approximations

In order to overcome the problem with linear local approximation, a higher order global approximation using response surface methodology was used for approximating the global buckling and bowing displacement obtained from the NASTRAN analyses.

RS approximation for the case with three design variables

The lay-up of $[(\pm 45/0/90)_2]_S$ was used for the wall laminate with ply thickness of 0, 45, and 90 degree plies as design variables. The overall buckling and out of plane deflection were approximated with quadratic polynomials estimated from least square regression. A nominal design with all plies at uniform ply thickness of 0.005 inch was chosen. A quadratic polynomial in three design variables has 10 coefficients to be fitted. For this, a standard central composite design with 15 design points, along with 8 extra

points from inside the box, was chosen to give a total of 23 design points. Central composite designs with center point replication improves the prediction accuracy of the model and minimizes variance error. Since center point replications for computer experiments have identical response function values, extra points were chosen with small perturbations from the center points for this case. The 15 points of the central composite design were obtained by a ±50% perturbation of the nominal design. The eight additional points were the vertices of the box obtained by a ±10% perturbation to the nominal value.

Table 6.3: Error analysis for the response surface approximations used in PANDA2 design optimizations.

No. of Design Variables	cycle #	Response	Number of coeff. in full model	Number of coeff. retained	No. of fitting points n	R^2_{adj}	*RMS* error based on *PRESS*	Least t-statistic
3	1	Buckling	10	9	23	0.972	0.078	1.58
3	2	Buckling	10	7	23	0.996	0.026	2.29
3	2	Displacement	10	8	23	0.985	0.055	2.39
5	1	Buckling	21	14	43	0.999	0.003	2.38
5	1	Displacement	21	17	43	0.996	0.014	3.60

The accuracy of the response surface models fitted to the buckling and bowing responses is presented in Table 6.3. The adjusted R^2 of the model, the normalized mean square root value of the Prediction Error Sum of Squares (or PRESS statistic), and the values of the least t-statistic of the coefficient of the model are presented in Table 6.3. A discussion of the different error and confidence measures is provided in *Chapter 5*. To quickly recapitulate, the PRESS statistic gives a measure of the prediction accuracy of the model, while the R^2 and t-statistic are confidence measures in the model and individual coefficients respectively. For each selected set of points after the initial regression,

coefficients that are not very relevant to the model are eliminated using a *Stepwise Regression* procedure (see *Chapter 5*). This strategy eliminates insignificant terms or coefficients, resulting in a model with higher prediction accuracy.

Table 6.3 gives the details of the number or points retained in the approximation model after such a stepwise regression procedure. The first three rows of Table 6.3 correspond to the three design variable case and the last two rows correspond to the five design variable case. The adjusted R^2 values of the regression are close to 1.0 (the optimum value) indicating that the model captured the variation in the responses well. The normalized RMS error based on PRESS statistic (Eq. 5. 14) is used to characterize the prediction error of the approximation model and is defined as

$$\text{RMS error based on PRESS} = \frac{\sqrt{PRESS/n}}{\bar{y}} \tag{6.1}$$

where, PRESS is the prediction error sum of squares, n is the number of fitting points, and $\bar{y}$ is the root mean square value of the fitted response. As can be seen from Table 6.3, the prediction error of the response surface used to approximate the overall buckling load factor for the three design variable case in Design Cycle-1 was 7.8% of the mean value of the response function. In the next iteration, this was reduced to 2.6% for buckling load prediction and 5.5% for bowing displacement prediction. The least value of the t-statistic of fitted the coefficients was less than 3.0. A value of 3.0 for the t-statistic indicates that the coefficient has 90% probability of being significant in the approximation model. Smaller values of t-statistic indicate a low level of confidence in the fitted coefficients and result in lower prediction accuracy of the model.

Table 6.4: Optimization of tank wall laminate using response surface approximations for case with three design variables(ply thickness of a $[\pm 45 / 0 / 90]_{2S}$, lay-up, ply thickness in mils)

No.	Starting design: ply thickness, total thickness, buckling load factor and, bowing displacement	Optimum design: ply thickness, total thickness, buckling load factor and, bowing displacement
1	$[5.0 / 5.0 / 5.0 / 5.0]_{2S}$	$[10.0 / 10.0 / 10.0 / 10.0]_{2S}$
	t_{wall} = 0.080 inch	t_{wall} = 0.160 inch
	λ_{panel} = 0.073	λ_{panel} = 0.289
	$\lambda_{overall}$ = 2.206 (predicted), 2.238(exact)	λ_{global} = 3.495 (predicted), 3.570(exact)
	δ_{bowing} = 1.888 in (exact)	δ_{bowing} = 1.007 in (exact)
2	$[20.0 / 20.0 / 20.0 / 20.0]_{2S}$	$[18.9 / 18.9 / 24.0 / 16.9]_{2S}$
	t_{wall} = 0.320	t_{wall}= 0.315
	λ_{panel} =1.147	λ_{panel} = 1.4
	$\lambda_{overall}$ = 5.738 (predicted), 5.740 (exact)	$\lambda_{overall}$ = 5.207 (predicted), 5.252 (exact)
	δ_{bowing} = 0.552 in (predicted), 0.551 in (exact)	δ_{bowing} = 0.499 in (predicted), 0.508 in (exact)

The results of the optimization are presented in Table 6.4 and discussed in the following paragraphs. The move limit of 100% chosen for the first iteration resulted in a design with all plies at 0.01 inch. The design was infeasible because the buckling load factor for the panel was only 0.289. It is to be observed that the move limit allowed for this case is 100%, whereas the design space used for selecting points for response surface fitting was obtained by a ±50% perturbation of the nominal design. It is not common to use response surface approximation for such large 50% extrapolations. However, since it was desired to get to a feasible design space quickly and since the prediction errors were not significant, this was allowed. A short cut was used in order to reduce the number of design analyses and find a design in the feasible design space quickly. As the panel

buckling at the end of the first design cycle was 0.289, it was decided to double the thickness of all plies in order to get a feasible design. Thickness was therefore doubled to 0.020 inch for all ply thicknesses to obtain an almost feasible design. This design was then used as the nominal design for the next design cycle. The response surface approximation was built around this design point for a domain size of 50% change. The optimization of the panel with bowing constraint resulted in a new design. The predicted values for the global buckling and displacement for the new optimal design were found to be in good agreement with the exact values and satisfied all design requirements.

The final design obtained from PANDA2 using the quadratic response surface constraint approximation, had a total thickness of 0.315 inch. This design is about 7% lighter than that obtained using linearized constraints (t_{wall} = 0.338 inch) in three design variables. While the number of cycles required for the response surface method is fewer, the number of designs analyzed is quite high. Even with the shortcut, the response surface method process used 48 analyses (24 analyses per cycle) as compared to the 42 analyses used (7 analyses per cycle) in the example with linearized constraints in three-design variables. If the ply thicknesses were not doubled, it is estimated that it would have required at least one extra cycle, increasing the number of analyses to 72 for response surface based optimization. The extra cost of the approximation provides higher prediction accuracy away from the initial or nominal design. This can be seen from the design at the end of the first cycle in Table 6.4. Despite a 100% move limit and 50% extrapolation using response surface, the prediction error in the global buckling load factor is only 2.0%. This is in stark contrast to case with linearized constraints where

even a small perturbation away from the nominal design point caused big errors in buckling load predictions.

RS approximation for the case with five design variables

At the time tis work was done, PANDA2 allowed only twenty terms in its constraint equations, ten of which were of the form $a_i x_i^n$ and the other ten restricted to the cross product terms, $a_{ij} x_i x_j$. Due to the limitation in the number of coefficients allowed in the constraint equations, it was not possible to model the laminate [$\pm$45/0/90/$\pm$45/0/90]s with six design variables. In order to reduce the number of coefficients, the thickness of the 90-degree plies were linked in the laminate description such that they had the same thickness. This reduced the number of terms in the full quadratic polynomial used in PANDA2.

Response surface approximations of the buckling and bowing displacement using the design variables were constructed from a central composite design. No additional points were used with the central composite design because the number of points in this case was already twice the number of coefficients. The fitted approximation function was introduced into PANDA2 as inequality constraints. The accuracy of the fitted function is shown in the last two rows of Table 6.3. The prediction errors for the overall buckling and bowing displacement were 0.3% and 1.4 % respectively. This high accuracy is a result of the large number of points used in the fitting. The quadratic polynomial used to approximate buckling retained only 14 terms after stepwise regression elimination and was fitted with thrice that number of design points (n=43). Similarly, the bowing displacement approximation fitted 17 coefficient with 43 analyses.

Information available from previous response surface design showed that a starting design with all plies at 0.02 inches was an almost feasible design and hence it was chosen as the point at which to construct the response surface. For the case of five design variables, the domain size was limited to 40% change from nominal value of the design variables. This is because as dimension of the design space increases, the distance between the center (nominal design) and designs at the vertices of the hyper-cube increases.

Table 6.5: Optimization of tank wall laminate using response surface approximations for the case with five variables (ply thicknesses for a $[\pm 45/0/90/\pm 45/0/90]_S$ lay-up, ply thickness in mils).

	Starting design: ply thickness, total thickness, buckling load factor and, bowing displacement.	Optimum design: ply thickness, total thickness, buckling load factor and, bowing displacement.
1	$[20.0/20.0/20.0/20.0/20.0/20.0/20.0/20.0]_S$ t_{wall} = 0.320 inch λ_{panel} = 1.147, $\lambda_{overall}$ = 5.701, (exact5.740) δ_{bowing} = 0.550 in, (exact 0.551 in)	$[20.0/20.0/16.6/19.6/14.4/14.4/32.6/19.6]_S$ t_{wall} = 0.3144 inch λ_{panel} = 1.4, $\lambda_{overall}$ = 5.402, (exact5.408) δ_{bowing} = 0.501 in (exact 0.503 in)

The optimization of the panel using PANDA2 (Table 6.5) resulted in a laminate with total thickness of 0.3144 inch, which is marginally lower than that obtained using three design variables, and about five percent lower than that obtained by using linearized constraints for a similar case with six design variables. There was not a significant difference in the total weight for the three- and five-design variable cases approximated using response surfaces.

The above example integrated the NASTRAN and PANDA2 analysis programs for optimization of the tank wall laminate using linearized (local) approximation and response surface approximations. The thicknesses of the tank wall laminate plies were the design variables. The overall buckling and bowing displacements were approximated and used as constraint equations in the panel optimization. It was shown that the constraint equations based on approximations allowed easy integration of the overall buckling and bowing response from the global finite element model into the panel (local) design. The linear approximations, while cheaper to use, required careful selection of move limits and furthermore, when used with a gradient based local optimizer, were more likely to get stuck in a local optimum. Response surfaces overcame the problems encountered in using linear local approximations, however, the advantage came at an increased computational expense.

Integration of Low and High Fidelity Models with the Use of Correction Response Surface Approximations

Structural analysis programs used for shell analysis can generate different results due to differences in the physical models used to capture the failure. Analyses using detailed finite element models can be used to model shell structures as close to reality as possible. These models are very expensive for use in design optimization or conceptual design studies. Using approximation allows the easy integration of multiple models or analysis programs in the optimization. This also allows the analyst to work separately from the designer. Response surface approximations have been used in the previous section for the integration of vehicle and panel analyses. The RS approximation has good accuracy and provides a global approximation. However, this method suffers from the

curse of dimensionality and becomes expensive to fit in large design domains or for highly non-linear responses.

Correction response surface approximations provide an alternative method of approximating responses when a less accurate (low-fidelity) but cheaper analysis program or model is available that can capture the desired failure modes. It is desirable in such cases to keep the cheaper and efficient analysis program and apply corrections to its solutions. The analysis of vehicle structures must account for a variety of failure modes. Often analysis programs cannot capture all the failure modes and may have inaccuracies in some models. Limitations or deficiencies in such models or analysis programs mean that they have to be supplemented by other more accurate analysis models or programs. The increased accuracy often comes at an increased price or substantial effort. The present section demonstrates the use of a correction applied to the less expensive analysis using a few accurate and expensive analyses to obtain a less expensive and more accurate approximation model.

The example studied here makes use of a detailed STAGS [4, 90] finite element model to correct an inaccurate approximation of inter-ring buckling obtained from an earlier version of PANDA2 (the only version available to us at the time this work was done). It is emphasized that a later version of PANDA2 now exists [33] which can predict inter-ring buckling with the same fidelity as BOSOR4 [24] or as the STAGS model used for the particular configuration studied in this section. However, this does not diminish the importance of the demonstration of the technique of using correction response surface approximations, because designers will always be faced with the need for more accurate and less expensive analysis programs.

Ring Stiffened Cylinder Design

The design of a ring-stiffened cylindrical shell for the reusable launch vehicle liquid hydrogen tank, with use of correction response surface approximations is presented in this section. The shell was optimized for minimum weight with buckling, displacement (bowing) and stress constraints. A simply supported ring-stiffened cylinder under uniform axial load was analyzed to calculate the buckling failure margin. A balanced symmetric 16 ply quasi-isotropic laminate with a layup of $[(-45/0/45/90)_2]_s$ was chosen for the tank wall laminate. The material properties of the composite are E_1=2.1 Mpsi, E_2=1.2 Mpsi, ν_{12}=0.3, G_{12}=0.62 Mpsi and ρ=0.057 lb/in^3. The ring stiffeners are isotropic T shaped stiffeners made of Titanium (E=16.5 Mpsi, ν=0.32 and ρ=0.16 lb/in^3).

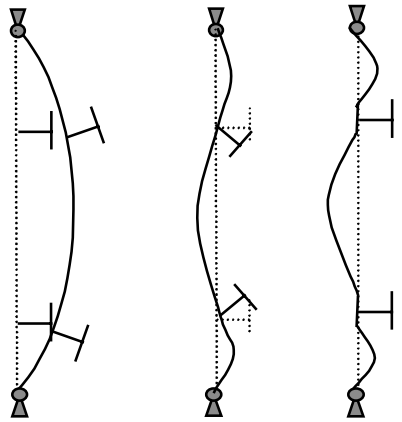

General buckling Local buckling

Figure 6.2: Schematic of local and general buckling of a ring stiffened cylinder under compression loads and simple support (pinned) boundary conditions

PANDA2 was used for analysis and design. PANDA2 first performs a prebuckling analysis, and calculates load factors for general and local buckling failures. The schematic representation of general buckling and local buckling (with and without stiffener rolling) is shown in Fig. 6.2

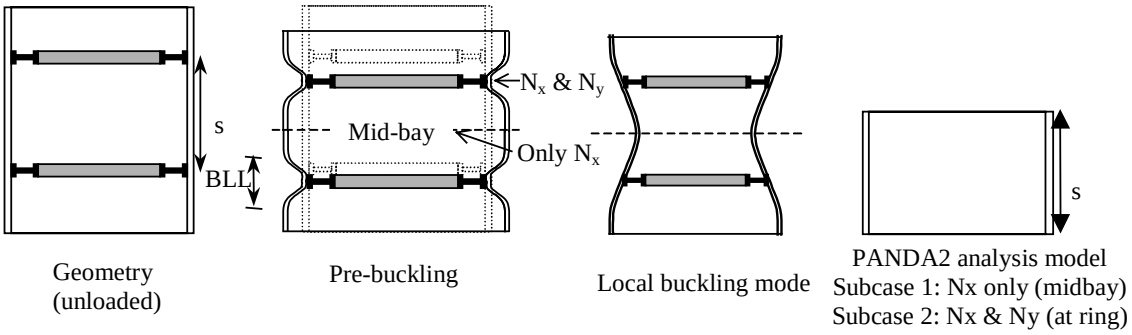

Figure 6.3: PANDA2 analysis model for local buckling load factor

General buckling occurs when the skin and ring stiffener deform and buckle together; local buckling is the buckling mode where the ring cross-section does not undergo deformations. For general buckling, the program smears the ring stiffeners and calculates an equivalent stiffness for the wall laminate. This equivalent stiffness is used for the general buckling analysis of the cylinder.

For local buckling analysis, PANDA2 used two different physical models (referred to as Subcase 1 and Subcase 2 analyses). PANDA2 calculates the stress resultants in the prebuckling analysis at the rings and at midway between the rings (Figure 6.3).

In Subcase 1, the mid-bay stress resultants were used to calculate buckling load of a simply supported cylinder between rings to obtain an estimate for the local buckling failure. This analysis model assumes that the ring stiffener does not participate in the buckling and only provides hoop stiffness in the prebuckling phase of the analysis.

Subcase 2 accounts for the conditions at the rings. At the rings, the stiffeners do not permit the full Poisson radial expansion of the cylinder loaded in axial compression that would occur if they were absent. This creates local compressive hoop stress in the cylinder in the neighborhood of the ring. Hence, in Subcase 2 the buckling load for the

inter-ring cylindrical portion is calculated using stress resultants calculated at the ring sections. This is to capture the local effects of the ring stiffener on local buckling. The optimization uses the load factors from both Subcase 1 and Subcase 2.

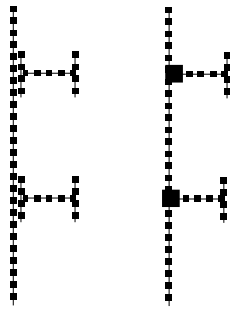

Figure 6.4: BOSOR4 1-D model

The ring-stiffened cylinder was also analyzed using the BOSOR4 and STAGS programs. An example of the one-dimensional discretization of the BOSOR4 analysis is shown in Fig. 6.4.

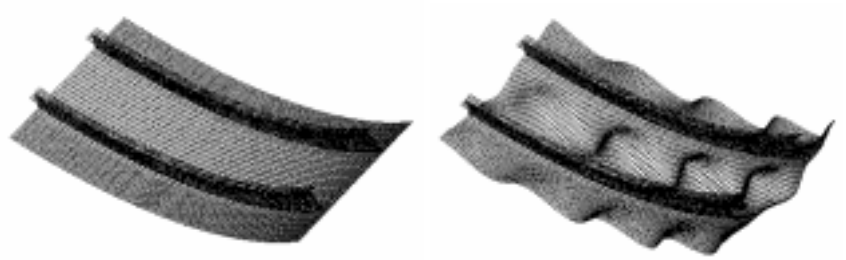

Figure 6.5: Finite element mesh used for STAGS model and the first critical mode from a linear buckling analysis.

The ring-stiffened cylindrical panel is modeled as a branched shell assembly, discretized with 2-D shell elements (4-node isoparametric, 410 elements), in the STAGS finite element analysis model. A model with two ring bays and symmetry boundary conditions along the curved edges is used to capture the local buckling failure. To decrease computation time, only a 45^{o} segment of the cylinder was modeled with

symmetry conditions. An example of the STAGS finite element analysis model (FE mesh) used for the ring local buckling analysis is shown in Fig. 6.5.

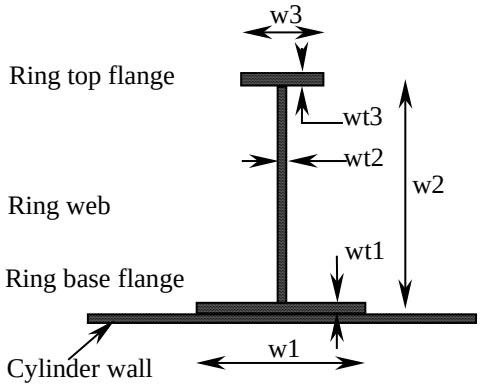

Figure 6.6: Schematic of a T-ring stiffener showing design variables and terminology

Table 6.6: Design variables

DESIGN VARIABLES
Ply thickness for laminate$[-45 / 0 / +45 / 90]_{2s}$
Thickness of ±45º ply, (t45)
Thickness of 0º ply, (t0)
Thickness of 90º ply, (t90)
Ring spacing, (b)
Ring geometry
Bottom flange width (w_1)
Web Height (w_2)
Top Flange width ($w_3=w_1$)
Thickness of bottom flange (wt_1)
Thickness of web (wt_2)
Thickness of top flange (wt_3)

The design variables used to characterize the ring cylinder geometry and the ring stiffener (Fig. 6.6) are listed in Table 6.6. Local buckling load factors obtained from linear bifurcation buckling analyses from the three programs (PANDA2, BOSOR4 and STAGS) are presented in Table 6.7 for six designs. The results show varying levels of agreement.

Table 6.7: Comparison of local buckling load calculated from different programs

	PLY THICKNESS			RING SPACING & DIMENSIONS					PANDA2 Subcase		STAGS	BOSOR4	BLL
	±45º	0º	90º	s	w_1	w_2	wt_1	wt_2	1	2			
1	0.02	0.02	0.02	30	1.0	1.0	0.1	0.1	2312	2229	2463	2431	22.8
2	0.01	0.02	0.02	30	5.0	1.0	0.2	0.2	1154	968	1617	1634	20.0
3	0.01	0.01	0.01	30	5.0	9.0	0.2	0.1	578	365	664	655	16.1
4	0.01	0.02	0.02	90	1.0	9.0	0.2	0.2	1109	633	1125	1208	20.0
5	0.01	0.01	0.02	90	1.0	1.0	0.1	0.1	827	480	833	854	16.5
6	0.01	0.01	0.01	90	1.0	9.0	0.2	0.2	544	167	550	567	16.1

When the ratio of ring spacing to flange width is high ($w_1/s = 1/90$, for Designs 4, 5 and 6), the ring acts like a line contact. Hence, the PANDA2 Subcase 1 approximation of replacing rings with simple support boundary conditions was fairly accurate. However, in Subcase 2, PANDA2 calculates the stress resultants in the cylinder wall at the ring section and applies them to the cylinder between rings with simple support boundary conditions to calculate local buckling failure. The ring stiffeners prevent Poisson expansion of the cylinder wall and thereby introduce hoop compression and bending in the cylinder at the rings. The length of the region from the rings where these bending effects exist in the cylinder wall is referred to as the boundary layer length (BLL). BLL is a function of the bending stiffness and the in-plane stiffness of the cylinder wall. When BLL is comparable to the ring spacing, the Subcase 2 approximation works well (Design 1, PANDA2 Subcase 2 results, Table 6.7). However, when BLL is small compared to ring spacing (as is shown for Designs 4, 5 and 6), applying the local stress conditions at the ring over the entire portion between rings makes Subcase 2 analysis very

conservative. This explains why local buckling results for Subcase2 for Designs 4, 5 and 6 are lower by a factor of 2 to 3.

The agreement between STAGS and BOSOR4 results is good because the ring-stiffened cylinder is a shell of revolution. This may not be the case for axially stiffened cylinders with ring stiffeners. In such cases BOSOR4 smears the axial stiffeners.

Correction Response Surface Approximation for Local Buckling Response

In this section a correction response surface is fitted using a small number of STAGS analyses to correct PANDA2 estimates of local buckling load factor. Since it was not easy to incorporate a correction response surface directly in the PANDA2 code, the local buckling load factor λ_P, Subcase 1, obtained from PANDA2 was first approximated as λ_{PRS} using a response surface approximation. This response surface model was then used as a low-fidelity model. The design variables were ply thicknesses of the cylinder wall laminate, the ring spacing, and ring size parameters.

In order to reduce the number of variables used in fitting the approximation the geometrical variables (length, width and thickness of ring frame segments) were replaced with intervening variables that describe the size, shape and stiffness of the ring stiffeners (such as ring frame cross-section area (A_r), bending moment of inertia (I_x) and polar moment of inertia (J)) For the present example, intervening variables reduce the number of variables used to describe the ring from six to three. The intervening variables were

---

[1] PANDA2 has now been modified to so that inter-ring buckling of an axially compressed ring-stiffened cylindrical panel corresponding to conditions in the panel skin in the neighborhoods of the rings (Subcase 2) is not as conservative as before (see Items 434 and 475 in the file panda2/doc/panda2.news [25]). Also a discretized BOSOR4 model of the skin-ring module is now used in PANDA2 [33] to calculate inter-ring buckling.

chosen as they influence the behavior of the shell for local buckling failure. The area of the ring cross-section influences the amount of Poisson radial expansion in the cylinder wall at the ring section, while the bending and twisting moment of inertia are responsible for bending and ring rolling in local buckling. Intervening variables used in constructing approximations increase the accuracy of the approximations.

A quadratic polynomial was used to approximate the local buckling load factor calculated by PANDA2. The polynomial was fitted using seven design variables, namely three ply thickness (t_0, t_{45}, t_{90}), ring spacing (r), ring cross-section area (A_r), bending moment of inertia (I_x), and polar moment of inertia (J). A set of 72 points (twice the number of 36 coefficients in the quadratic polynomial) was chosen from a set of 2,169 (3^7) equally spaced discretized design points using the D-optimal criterion.

Table 6.8: Regression statistics for response surface fitted to PANDA2 buckling load factor

Response Surface model fitted to PANDA2 local buckling load prediction (λ_{PRS}) $\lambda_{PRS} = 0.373 - 0.684r - 6598.0t_{45} + 4750.2\,t_0 + 4108.5t_{90} + 970821.4\,t_{45}^2 - +2053186.9t_0t_{45} + 2675741.1t_{90}t_{45}$ (units of length in inch)	
STATISTIC	*VALUE*
R^2	0.997
R^2 adjusted	0.997
Mean value of response	1277.7
RMS error	30.31 (2.3%)
Error based on PRESS statistic $\sqrt{PRESS/n}\,/\,\bar{y}$	32.10 (2.5%)

Table 6.8 shows the response surface approximation (λ_{PRS}) that describes the local buckling prediction from PANDA2 and its regression statistics. The insignificant terms of the fitted polynomial (response surface model) were eliminated using a stepwise

regression. The resulting model has all coefficients with t-statistic value above 3.0. The final response surface models only have nine coefficients. It is observed that the PANDA2 response surface model does not include any of the ring stiffener variables. This is because the model used for calculating inter-ring buckling in the Subcase-1 of the PANDA2 analysis ignores the presence of the ring stiffener. Subcase-1 model analyzes a simply supported cylinder between the rings with prebuckling stress resultants from mid-bay. The prediction error was found to be 2.5% and the error at the fitted points was 2.3% (Table 6.8). The adjusted R^2 value indicates that the model captures the behavior of the response fairly well.

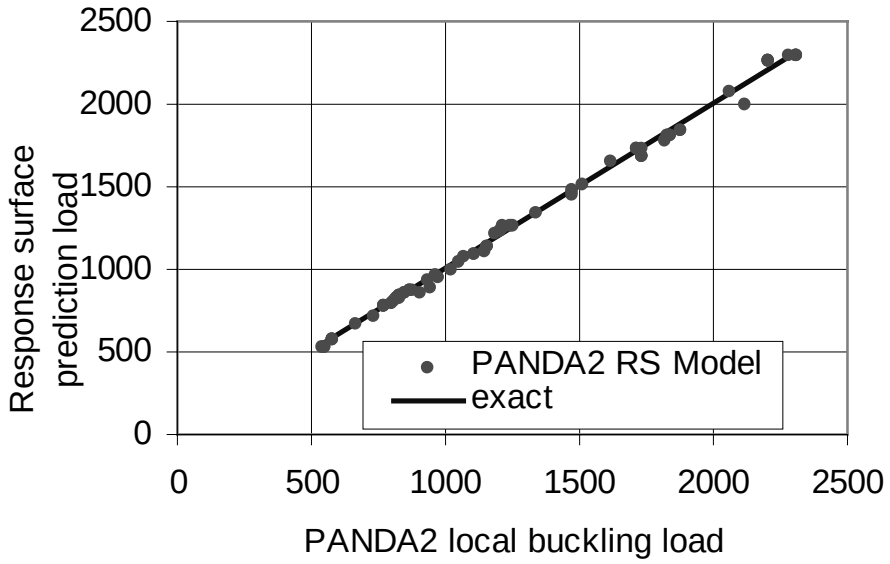

Figure 6.7: Response surface approximation prediction compared with PANDA2 prediction.

Figure 6.7 shows the response surface prediction plotted against the actual PANDA2 analysis values. If the response surface approximation is exact, then all points lie on the diagonal line. The points are fairly close to this line indicating good model accuracy.

The PANDA2 local buckling load was corrected using STAGS analyses performed for local buckling of a ring-skin module. Detailed STAGS analyses of ring-skin module local buckling are performed for a small number of design points to obtain a more accurate estimate for the local buckling load factor (λ_S). A response surface model r_{CRS} was fitted to the ratio (r_C),

$$r_c = \frac{\lambda_P}{\lambda_S} \tag{6.2}$$

which is the ratio of STAGS local buckling (λ_S) to the PANDA2 local buckling estimate (λ_P). The quantity r_c characterizes the required correction to the low fidelity model over the entire design space. This correction function was used with the PANDA2 analysis to correct the response surface function fitted to the PANDA2 local buckling load as

$$\lambda_C = \frac{\lambda_{PRS}}{r_{CRS}} \tag{6.3}$$

Table 6.9: Correction response surface model

Correction response surface approximation model, (r_{CRS}) $r_{CRS} = 0.832 - 7.963t_{45} - 5.442t_0 - 0.272t_{90} - 0.016I_x + 0.002r - 0.0273A_r + 0.0144J$ (units of length in inch)	
STATISTIC	*VALUE*
R^2	0.952
R^2 adjusted	0.910
Mean value of response	0.931
Predicted RMS error	0.028 (3.0%)
Error based on PRESS $\sqrt{PRESS/n}\,/\,\bar{y}$	0.040 (4.3%)

A linear polynomial in the design variables was assumed for the correction response surface function. A set of 16 design points was chosen using the D-optimal

criterion for the linear correction function. The ratio of the STAGS prediction for local buckling factor to the PANDA2 response surface model was fitted with the linear correction response surface model. This correction response surface and its regression statistics are shown in Table 6.9.

The adjusted R^2 is only 0.910. Typically, a value closer to 1.0 is desired. This indicates that the model needs more terms to capture the behavior or the response. It is possible that including some quadratic terms would have been helpful. However, the prediction error of the response surface and PRESS errors are small (3.0 and 4.3%, respectively). The correction model includes the parameters that describe the ring cross-section and the ring spacing.

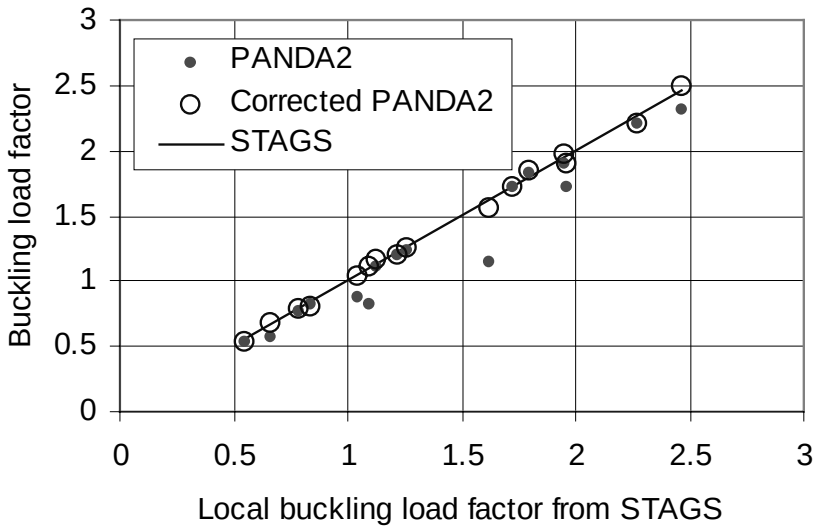

Figure 6.8: Comparison of PANDA2 and corrected PANDA2 local buckling load prediction with STAGS local buckling prediction.

The response surface model developed using the low-fidelity and correction response surface approximation was used to evaluate the buckling loads for a set of 21 designs (16 points used to fit correction response surface and an additional five randomly

chosen designs). Figure 6.8 shows the comparison of the response surface model and STAGS analysis.

The PANDA2 buckling load prediction for the skin-ring local buckling was significantly lower than STAGS for some designs (maximum error of 28.7%). The correction response surface applied to the PANDA2 estimate yielded results that agree well with the STAGS analysis (maximum error of 4%).

Table 6.10: Optimized designs for ring-stiffened cylinder (Units of thickness and length are in inch)

Design variables (units of length in inch)	Lower Bound	Upper bound	Optimum design from PANDA2	Optimal design using RS model
Thickness of 45 plies, t_{45}	0.01	0.025	0.010	0.014
Thickness of 0 plies, t_0	0.01	0.025	0.017	0.010
Thickness of 90 plies, t_{90}	0.01	0.025	0.023	0.018
Ring spacing, s	30	90	63.0	53.64
Ring flange width, w_1,w_3	1.0	5.0	1.0	1.0
Ring web height, w_2	1.0	9.0	1.0	1.0
Ring flange thickness, wt_1,wt_3	0.1	0.25	0.1	0.1
Ring web thickness, wt_2	0.1	0.25	0.1	0.1
Optimum weight/unit length (lb/in.)			18.90	17.13
PANDA2 buckling load factor			1.10	1.03
STAGS buckling load factor			1.36	1.11
Predicted buckling load from correction response surface model			1.40	1.10

The correction model was used to compute buckling load factors at five random points inside the design domain in which the approximation was developed and at five random points outside the domain (extrapolation). It was found that that the average root mean square errors of the corrected model were 4.0% and 4.8%, respectively, at the interpolation and at the extrapolation points. The contributions of the PANDA2 response

surface model error and the correction response surface model error were 2.4% and 1.8%, respectively. The small extrapolation error (4.8%) indicates that the correction response surface provides an accurate and robust approximation. Low-fidelity analyses that employ physical models for the failure predictions have smaller extrapolation errors when compared to empirical models (or response surface approximation models). A correction applied to low-fidelity analysis from physical models therefore provides a robust and more accurate model.

The correction response surface approximation model was used as a constraint equation to minimize the weight of a ring stiffened cylinder loaded in uniform axial compression (N_x = -1000 lb/in). The designs obtained by PANDA2 with and without the response surface are compared in Table 6.10. The results obtained were evaluated using the BOSOR4 program. The PANDA2 optimization produces a heavier design (10%) but there is a 24% margin on local buckling.

CHAPTER 7
CONCLUDING REMARKS

The use of approximate models and analysis methods for the design of stiffened panels was investigated in this dissertation. Optimization of a reusable launch vehicle propellant tank was used as an example of stiffened panel design. The dissertation addresses three topics.

1. Investigation of the effect of homogenization approximations used for composite laminates and sandwich cores in optimization models.
2. Investigation of PANDA2 analysis models and the effect of modeling choices on optimum design of stiffened panels of a reusable launch vehicle propellant tank, and
3. Demonstration of the use of response surface and correction response surface approximations for integrating analysis models or computer programs used in stiffened panel design.

Homogenization Approximation in Composites

Investigation of errors due to the use of equivalent or effective material properties for laminates showed that large errors can occur when approximating the entire laminate. The maximal errors are function of ratio of inplane stiffness of the plies and their

respective volume fractions. Bending stresses obtained from models using equivalent properties can result in large errors.

For multiple sublaminates, the severity of the errors is reduced when the entire sublaminate is repeated. The error decays more slowly for laminates with half-sublaminate repetition. Anti-optimization of laminates for maximal buckling load errors results in large errors for plates with high aspect and load ratios. The compensating errors in the different bending stiffness terms result in smaller errors in the buckling loads.

Assuming that errors of up to 20% are acceptable in the design stage, the designer should avoid using equivalent properties;

1. for approximating entire laminates
2. for laminates have less than three full-sublaminate repetitions
3. for laminates have less than four half-sublaminate repetitions
4. for calculating bending stresses
5. for calculating buckling loads of plates with high aspect ratio and load ratios.

Using equivalent properties in optimization models of composite structures can lead to sub-optimal designs because optimization programs are notorious for exploiting model errors.

In sandwich laminates, honeycomb cores were approximated as continuum foundations to obtain the facesheet wrinkling loads. For wrinkling failures with short wavelength, using smeared properties to approximate hexagonal (honeycomb) core resulted in large errors. It was found that the foundation stiffness of the core reduced to one-half of the smeared stiffness when the wrinkling half wavelength was smaller than

the cell size. A possible correction was proposed for the approximate facesheet-wrinkling model.

Stiffened Panel Optimization using PANDA2

Preliminary optimization of stiffened panels demonstrated the accuracy and efficiency of simple models implemented in PANDA2. Investigation of the different modeling options revealed that closed form analysis of PANDA2 program was sufficiently accurate for linear analysis. The discrete model can to capture the postbuckling response of stringer stiffened panels after local buckling has occurred and calculate its effect on general instability. Stiffened panel optimization problems have several local optima. The multi-start gradient search strategy implemented in PANDA2 was effective in obtaining a practical global optimum. The accurate and inexpensive analysis of PANDA2 makes it an ideal choice for performing preliminary optimizations and design trade studies in the conceptual design phase.

The main findings of the stiffened panel design comparisons can be summarized as follows:

1. The sandwich concept was most efficient for metallic designs, due to the material used, the high bending stiffness of sandwich constructions, and the presence of fewer local failure modes.
2. Composite panel designs are much lighter than the corresponding metallic designs for the stringer ring concept. The weight savings depends on the laminate design chosen or the degree of freedom allowed in tailoring the stacking sequence. Composite stringer-ring stiffened panel was the most efficient concept overall. Sandwich panels

had weights close to those obtained for stringer ring panels when the core weight was not included but instead was considered as insulation.

3. For metallic construction, sandwich panels were least sensitive to initial geometric imperfections. Isogrid and orthogrid panels exhibited the largest weight increase when imperfections were introduced. The blade stiffeners were more critical in buckling failure when imperfections were present, resulting in higher weight penalty. The stringer-ring stiffened panel showed moderate weight increase when imperfections were introduced.
4. Composite stringer-ring stiffened panels were less sensitive to imperfections than their metallic counter parts, resulting in lower weights for optimized panels. The design freedom available to tailor the properties by changing ply thicknesses helped to reduce weight of optimized composite panels. However, optimizing ply thicknesses made composite panels more sensitive to imperfections and load changes.
5. Truss core panels were the most inefficient concept for metallic and composite constructions. This is attributed partially to some unique failure local failure modes exhibited by truss core panels, the restriction of corrugation angle to 45 due to manufacturing constraints and the modeling limitation of PANDA2 in not being able to include ring stiffeners. PANDA2 should be used with caution for truss-core constructions that need ring stiffeners, and other more accurate models and analysis must be used to verify PANDA2 optimum designs.

Response Surface Approximations for Model or Analysis Integration

Complex structures require finite element models to capture details. Often, different analysis models are used for the global and local analyses. Integrating different analysis models and computer programs for optimization is cumbersome and expensive.

The present dissertation demonstrated the use of response surface approximations for introducing buckling and displacement constraints obtained a finite element analysis (NASTRAN) of the overall vehicle model into local panel optimization (PANDA2). The methodology is relatively easy to implement and provides significant savings in computational effort. However, because response surface approximations have large errors when used for interpolation, they do not work well for design space with high dimensions.

Designers often encounter limitations in the analysis or design programs they use. Simple design codes often have some failure modes that are not modeled with adequate accuracy. Replacing such programs with more expensive finite element analyses is not a viable option for optimization due to cost constraints. Correction response surface approximations provide a method to correct the less accurate analysis model using a small number of accurate analyses. In this dissertation, a less accurate PANDA2 model for inter-ring buckling was corrected using a correction response surface approximation obtained from a small number of STAGS finite element analyses. The procedure was applied to the design of a cylindrical shell with ring stiffeners. Correction response surface approximations provide robust models with high accuracy for use in optimizations.

REFERENCES

1. Agarwal, B., and Davis, R. C., "Minimum Weight Designs for Hat Stiffened Composite Panels under Axial Compression," *NASA-TN D-7779*, National Aeronautics and Space Administration, Washington, D.C., Nov. 1974.

2. Agarwal, B., and Sobel, L. H., "Weight Comparisons of Optimized Stiffened, Unstiffened, and Sandwich Cylindrical Shells," *Journal of Aircraft*, Vol. 14, No. 10, 1977, pp. 1000-1008.

3. Almroth, B. O., Brogan, F. A., Miller, E., Zele, F., and Peterson, H. T., "Collapse Analysis for Shells of General shape; II. User's Manual for the STAGS-A Computer Code," *Technical report AFFDL-TR-71-8, Air Force Flight Dynamics Laboratory*, Wright Patterson Air Force Base, Ohio, March 1973.

4. Almroth, B. O., and Brogan F.A., "The STAGS Computer Code," *NASA CR-2950*, NASA Langley Research Center, Hampton, Virginia, 1978.

5. Almroth, B. O., Brogan, F. A., and Stanley, G. M., " Structural Analysis of General Shells," *Report LMSC D633873, Lockheed Missiles and Space Co.*, Palo Alto, California, Vol. 2, Users Instructions for the STAGSC-1, 1983.

6. Anderson, M. S., and Stroud, W. J., "General Panel Sizing Computer Code and Its Application to Composite Structural Panels," *AIAA Journal*, Vol. 17, No. 8, 1979, pp. 892-897.

7. Anon, *JMP Statistics and Graphics Guide Version 3.1*, SAS Institute, Inc., Cary, North Carolina, 1995.

8. Anon, *MSC/NASTRAN Quick Reference Guide, Version 68*, The MacNeal-Schwendler Corporation. 1994.

9. Arbocz, J., "The Effect of Initial Imperfections on Shell Stability – An updated Review," *Report LR-695, Delft University of Technology, Faculty of Aerospace Engineering*, The Netherlands, September 1992.

10. Arbocz, J., and Hol, J. M. A. M., "ANILISA – Computational Module for Koiter's Imperfection Sensitivity Theory," *Report LR-82, Delft University of Technology, Faculty of Aerospace Engineering*, The Netherlands, January 1989.

11. Arbocz, J., and Hol, J. M. A. M., "Koiter's Stability Theory in a Computer Aided Engineering (CAE) Environment," *International Journal of Solids and Structures*, Vol. 26, No. 9/10, 1990, pp. 945-973.

12. Arbocz, J., and Hol, J. M. A. M., "Shell Stability Analysis in a computer Aided Engineering (CAE) Environment," *AIAA Paper 93-1333-CP, Proceedings of the 34th AIAA/ ASME/ ASCE/ AHS/ ASC Structures, Structural Dynamics and Materials Conference*, La Jolla, California, April 1993, pp. 300-314.

13. Arbocz, J., Notenboom, R. P., and van der Wekken, A. J. P., "Collapse – Buckling of Imperfect Anisotropic Shells Under combined Loading," *Report LR-702, Delft University of Technology, Faculty of Aerospace Engineering*, The Netherlands, April 1993.

14. Arbocz, J., Starnes, J. H., and Nemeth, M. P., "A Hierarchial Approach to Buckling Load Calculations," *Proceedings of the 40th AIAA/ ASME / ASCE/ AHS/ ASC Strcutures, Structural Dynamics and Materials Conference*, St. Louis, MO, April 1999.

15. Arendsen, P., "Postbuckling Analysis Using the Finite Strip Method, Derivation of 2nd, 3rd, and 4th Order Energy Terms," *NLR CR 89386L*, 1989.

16. Arendsen, P., Thuis, H. G. S. J., and Wiggenraad, J. F. M., "Optimization of Composite Stiffened Panels with Postbuckling Analysis," *Proceedings of the 4th International Conference on Computer Aided Design in Composite Material Technology*, Southampton, UK, June 1994, pp 109.

17. Baburaj, V., Kalyanaraman, V., "STIPSY – A Program for Stiffened Plate Synthesis," *Computers and Structures*, Vol. 48, No. 2, 1993, pp. 347-355.

18. Baruch, M., and Singer, J., "Effect of Eccentricity of Stiffeners on the General Instability of Stiffened Cylindrical Shells under Hydrostatic Pressure," *Journal of Mechanical Engineering Science*, Vol. 5, 1963, pp. 23-27.

19. Bolukbasi, A. O., and Laanen, D. H., "Energy Absorption in Composite Stiffeners," *Composites*, Vol. 26, 1995, pp. 291-301.

20. Box, G.E. P., and Behnken, D.W., "Some New Three-Level Designs for the Study of Quantitative Variables," *Technometrics* 30, 1960, pp. 1-40.

21. Burden, R. L., and Faires, J.D., *Numerical Analysis, Fourth Edition*. Boston: PWS-Kent Publishing Company, 1989.

22. Bushnell, D., "Evaluation of Various Analytical Models for Buckling and Vibration of Stiffened Shells," *AIAA Journal*, Vol. 11, No. 9. September 1973, pp. 1283-1291.

23. Bushnell, D., “Finite Difference Energy Models versus Finite Element Models: Two Variational Approaches in One Computer Program,” *Numerical and Computer Methods in Structural Mechanics,* Academic Press, 1973, pp. 291-336.

24. Bushnell, D., “BOSOR4: program for stress, buckling, and vibration of complex shells of revolution,” *Structural Mechanics Software Series*, Vol. 1 (edited by N. Perrone and W. Pilkey) University Press of Virginia, Charlottesville, Virginia, 1977. See also *Computers and Structures*, vol. 4, 1974, pp. 399-435; *AIAA Journal*, Vol. 9, 1974, pp. 2004-2013; *Structural Analysis Systems*, Vol. 2 (Edited by Nikulari), Pergamon Press, Oxford 1986, pp. 25-54; *Computers and Structures*, Vol. 18, 1986, pp. 471-536.

25. Bushnell, D., "PANDA2 - Program for Minimum Weight Design of Stiffened, Composite, Locally Buckled Panels," *Computers and Structures*, Vol. 25, No. 4, 1987, pp. 469-605. (See also the PANDA2 update log file, …/panda2/doc/panda2.news, distributed with the PANDA2 program, which contains a complete log of changes made in PANDA2 since 1987.)

26. Bushnell, D., "Theoretical Basis of the PANDA Computer Program for Preliminary Design of Stiffened Panels Under Combined In-plane Loads," *Computers and Structures*, Vol. 27, No. 4., 1987, pp. 541-563,.

27. Bushnell, D., "Nonlinear Equilibrium of Imperfect, Locally Deformed Stringer-Stiffened Panels Under Combined Loads," *Computers and Structures*, Vol. 27, No. 4, 1987, pp. 519-539.

28. Bushnell, D., "Truss Core Sandwich Design Via PANDA2," *Computers and Structures*, Vol. 44, No. 5, 1992, pp. 1091-1119. See also *Proceedings of the 31st AIAA/ ASME/ ASCE/ AHS/ ASC Structures, Structural Dynamics and Materials Conference, AIAA Paper 90-1070,* Long Beach, CA, April 2-4, 1990, pp. 1313-1332.

29. Bushnell, D., "Optimization of Composite, Stiffened, Imperfect Panels Under Combined Loads for Service in the Postbuckling Regime," *Computer Methods in Applied Mechanics and Engineering*, Vol. 103, 1993, pp. 43-114.

30. Bushnell, D., "Recent Enhancements to PANDA2 (A Program for Minimum Weight Structural Design)," *Proceedings of the AIAA/ ASME/ ASCE/ AHS/ ASC 37th Structures, Structural Dynamics and Materials Conference, AIAA paper 96-1337,* Salt Lake City, Utah, April 1996.

31. Bushnell, D., "Optimum Design Via PANDA2 of Composite Stiffened Sandwich Panels with Honeycomb or Foam Cores" *Proceedings of the 38th AIAA/ ASME/ ASCE/ AHS/ ASC Structures, Structural Dynamics and Materials Conference, AIAA Paper 97-1142,* Kissimmee, Florida, April 1997, pp. 2163-2202.

32. Bushnell, D., “Optimization of Panels with Riveted Z-shaped Stiffeners via PANDA2,” *Proceedings of the 39th AIAA/ ASME/ ASCE/ AHS/ASC Structures,*

Structural Dynamics & Materials Conference, AIAA Paper 98-1990, April 1998, pp. 2357-2388.

33. Bushnell, D., "Additional Buckling Solutions in PANDA2" *Proceedings of the 40th AIAA/ ASME/ ASCE/ AHS/ ASC Structures, Structural Dynamics and Materials Conference, AIAA Paper 99-1233,* St. Louis, Missouri, April 1999, pp. 302-345.

34. Bushnell, D., and Bushnell, W. D., "Minimum Weight Design of a Stiffened Panel via PANDA2 and Evaluation of the Optimized Panel via STAGS," *Computers and Structures*, Vol. 50, No. 4, 1994, pp. 569-602.

35. Bushnell, D., and Bushnell, W. D., "Approximate Method for the Optimum Design of Ring and Stringer Stiffened Cylindrical Panels and Shells with Local, Inter-Ring, and General Buckling Modal Imperfections," *Proceedings of the AIAA/ ASME/ ASCE/ AHS/ ASC 35th Structures, Structural Dynamics and Materials Conference, AIAA paper 94-1576,* Hilton Head, South Carolina, April 1994, pp. 2028-2060.

36. Bushnell, D., and Bushnell, W. D., "Optimum design of Composite Stiffened Panels under combined loads," *Computers and Structures*, Vol. 55, No. 5, 1995, pp. 819-856.

37. Bushnell, D., and Bushnell, W. D., "Approximate Method for the Optimum Design of Ring and Stringer Stiffened Cylindrical Panels and Shells with Local, Inter-Ring, and General Buckling Modal Imperfections," *Computers and Structures*, Vol. 59, No. 3, 1996, pp. 489-527.

38. Bushnell, D., Holmes, A. M. C., Flaggs, D. L., and McCormick, P.J., "Optimum Design, Fabrication and Test of Graphite-Epoxy, Curved Stiffened, Locally Buckled Panels Loaded in Axial Compression," in *Buckling of Structures,* Elishakoff, I. *et al.*, eds., Elsevier, Amsterdam, 1988, pp. 61-131.

39. Bushnell, D., Rankin, C. C., and Riks, E., "Optimization of Stiffened Panels in which Mode Jumping is Accounted For", *Proceedings of the 38th AIAA/ ASME/ ASCE/ AHS/ ASC Structures, Structural Dynamics and Materials Conference, AIAA Paper 97-1141,* Kissimmee, Florida, April 1997, pp. 2123-2162.

40. Butler, R., "Optimum Design and Evaluation of Stiffened Panels with Practical Loading," *Computers and Structures*, Vol. 52, No. 6, 1994, pp. 1107-1118.

41. Butler, R., "Optimum Design of Composite Stiffened Wing Panels- a Parametric Study," *Aeronautical Journal*, Vol. 99, No. 985, May 1995, pp. 169-177.

42. Butler, R. and Williams, F. W., "Optimum Design Features of VICONOPT, an Exact Buckling and Vibration Program for Prismatic Assemblies of Anisotropic Plates," *AIAA Paper 90-1068, Proceedings of the 31st AIAA / ASME / ASCE/ AHS/ ASC Structures, Structural Dynamics and Materials Conference,* Long Beach, California, 1990, pp. 1289-1299.

43. Butler, R., and Williams, F. W., "Optimum Design Using VICONOPT, a Buckling and Strength Constraint Program for Prismatic Assemblies of Anisotropic Plates," *Computers and Structures*, Vol. 43, No. 4, 1992, pp. 699-708.

44. Cohen, G.A., "FASOR A – A Program for Stress, Buckling and Vibration of Shells of Revolution," *Advanced Engineering Software*, Vol. 3, No. 4, October 1981, pp. 155-162.

45. Crossley, W. A., Laananen, D. H., "Genetic Algorithm-Based Optimal Design of Stiffened Composite Panels for Energy Absorption," *In Proceedings of the American Helicopter Society 52nd Annual Forum, Washington*, D. C., June 1996, pp. 1367-1376.

46. Chryssanthopoulos, M. K., Baker, M. J., and Dowling, P.J., "Imperfection Modeling for Buckling Analysis of Stiffened Cylinders," *Journal of Structural Engineering*, Vol. 117, No. 7, July 1991, pp. 1998-2017.

47. Dawe, D. J., "Finite Strip Buckling Analysis of Curved Plate Assemblies under Biaxial Loading," *International Journal of Solids and Structures*, Vol. 13, No. 11, 1977, pp. 1141-1155.

48. Dawe, D. J., "Finite Strip Post-Local-Buckling Analysis of Composite Prismatic Plate Structures," *Computers and Structures*, Vol. 48, No. 6, 1993, pp. 1011-1023.

49. Dawe, D. J., and Peshkam, V., "Buckling and Vibration of Finite Length Composite Prismatic Plate Structures with Diaphragm Ends: 1. Finite Strip Formulation," *Computer Methods in Applied Mechanics*, Vol. 77, No. 1-2, 1989, pp. 1-30.

50. Dawe, D. J., and Wang, S., "Buckling of Composite Plates and Plate Structures Using the Spline Finite Strip Method," *Composite Engineering*, Vol. 4, No. 11, 1994, pp. 1099-1117.

51. Dawe, D. J., Wang, S., "Postbuckling Analysis of Thin Rectangular Laminated Plates by Spline FSM," *Thin Walled Structures*, Vol. 30, No. 1-4, 1998, pp. 159-179.

52. Dudley, J., Huang, X., MacMillin, P.E., Grossman, B., Haftka, R.T., and Mason, W. H., "Multidisciplinary Optimization of the High Speed Civil Transport," *34th Aerospace Sciences Meeting and Exhibit*, Reno, Nevada, Jan. 1995, Paper No. 95-0125.

53. Edwards, D. A., Williams, F. W., and Kennedy, D., "Cost Optimization of Stiffened Panels using VICONOPT," *AIAA Journal*, Vol. 36, No. 2, Feb. 1998, pp. 267-272.

54. Elseifi, M. A., Gürdal, Z., and Nikolaidis, E., "Convex/Probabilistic Models of Uncertainties in Geometric Imperfections of Stiffened Composite Panels," *AIAA Journal*, Vol. 37, No. 4, April 1999, pp. 468-474.

55. Elseifi, M. A., Gürdal, Z., and Nikolaidis, E., "A New Scheme for the Optimum Design of Stiffened Composite panels with Geometric Imperfections," *Proceedings of the 40th AIAA/ ASME/ ASCE/ AHS/ ASC Structures, Structural Dynamics and Materials Conferenc,e, AIAA-99-1257*, St. Louis, Missouri, April 1999,pp. 588-600.

56. Eschenauer, H. A., Hans, A., and Weber, C., "Stiffened CRFP-Panels under Buckling Loads - Modeling, Analysis, Optimization," *ASME Design Engineering Division Publication*, Vol. 82, No. 1, 1995, pp. 233-239.

57. Giunta, A. A., Dudley, J. M., Narducci, R., Grossman, B., Haftka, R.T., and Watson, L.T., "Noisy Aerodynamic Response and Smooth Approximations in HSCT Design," *Proceedings of the 5th AIAA / USAF/ NASA/ ISSMO Symposium on Multidisciplinary Analysis and Optimization*, Panama City, Florida, Sep. 1994, pp. 1117-1128.

58. Graesser, D. L., and Tuttle, M. E., "Damage Tolerance of Composite Structures," *Proceedings of the 35th AIAA/ ASME/ ASCE/ AHS/ASC Structures, Structural Dynamics and Materials Conference, AIAA Paper 94-1497*, April 1994, Hilton Head, South Carolina, pp. 1434-1444

59. Graesser, D. L., Zabinsky, Z.B., Tuttle, M. E., and Kim, G. I., "Optimal Design of a Composite Structure," *Composite Structures*, Vol. 24, No. 4, 1993, pp. 273-281.

60. Gürdal, Z., Haftka, R. T., and Hajela, P., (1999), *Design and Optimization of Laminated Composite Materials*, John Wiley and Sons, Inc., New York.

61. Harrison, P.N., Le Riche, R., and Haftka, R.T., "Design of Stiffened Composite Panels by Genetic Algorithm and Response Surface Approximations," *Proceedings of the 36th AIAA/ ASME/ ASCE/ AHS/ ASC Structures, Structural Dynamics and Materials Conference, AIAA Paper 96-1163-CP*, New Orleans, Louisiana, April 1995, pp. 58-68.

62. Hutchinson, J. W., and Amazagio, J. C., "Imperfection-Sensitivity of Eccentrically Stiffened Cylindrical Shells," *AIAA Journal*, Vol. 5, No. 3, 1967, pp. 392-401.

63. Jaunky, N., Knight, N. F., Jr., and Ambur, A. R., "Optimal Design of Grid Stiffened Composite Panels Using Global and Local Buckling Analyses," *Journal of Aircraft*, Vol. 35, No. 3, 1998, pp. 478-486.

64. Jaunky, N., Knight, N. F. Jr., and Ambur, D. R., "Optimal Design of General Stiffened Composite Circular Cylinders for Global Buckling with Strength Constraints," *Composite Structures*, Vol. 41, 1998, pp. 243-252. See also *Proceedings of the 39th AIAA / ASME/ ASCE/ AHS/ ASC Structures, Structural*

Dynamics and Materials Conference, *AIAA Paper 97-1402,* Kissimmee, Florida, April 1997, pp. 2521-2531.

65. Jiang, H., "Analysis and Design of Composite Sandwich panels using PANDA2," *M. S. Thesis*, Aerospace Engineering, Old Dominion University, Norfolk, Virginia, 1998.

66. Kassapoglou, C., "Simultaneous Cost and Weight Minimization of Composite-Stiffened Panels under Compression and Shear," *Composites, Part A*, Vol. 28 A, 1997, pp. 419-435.

67. Kaufman, M., Balabanov, V., Grossman, B., Mason, W.H., Watson, L.T., and Haftka, R.T., "Multidisciplinary Optimization via Response Surface Techniques," *Proceedings of the 36th Israel Conference on Aerospace Sciences*, Israel, Feb. 1996, pp. A-57 – A-67.

68. Kim, G. I., and Tuttle, M. E., "Buckling Analysis for a Stiffened Panel," *Proceedings of the 35th AIAA/ ASME/ ASCE/ AHS/ASC Structures, Structural Dynamics and Materials Conference, AIAA Paper 94-1496,* April 1994, Hilton Head, South Carolina, pp. 1423-1433.

69. Knill, D.L., Giunta, A.A., Baker, C.A., Grossman, B., Mason, W.H., Haftka, R.T., and Watson, L.T., ``HSCT Configuration Design Using Response Surface Approximations of Supersonic Euler Aerodynamics," *Proceedings of the 36th Aerospace Sciences Meeting & Exhibit, AIAA Paper 98-0905,* Reno, NV, January 1998.

70. Koiter, W. T., "On the Stability of Elastic Continuum.*" Ph.D. Thesis (in Dutch), TH-Delft,* The Netherlands, H.J. Paris, Amsterdam, 1945. English Translation *NASA TTF-10,* 1967, pp. 1-833.

71. Koiter, W.T., "Het Schuifplooiveld by Grote Overshrijdingen van de Knikspanning, *Report X295, Nationaal Luchtvaart Laboratorium*, The Netherlands, November 1946 (in Dutch). English translation, *AFFDL-TR-70-25*, February 1970.

72. Lamberti, L., Venkataraman, S., and Haftka, R. T., "Comparison of Preliminary Designs of Reusable Launch Vehicle Propellant Tank Stiffened Panels Optimized using PANDA2," *Technical Report AeMES-TR-99-3-01,* Department of Aerospace Engineering, Mechanics and Engineering Science, University of Florida, Gainesville, Florida, 1999.

73. Le Riche, R., Haftka, R. T., "Improved Genetic Algorithm for Minimum Thickness Composite Laminate Design," *Composites Engineering,* Vol. 5, No. 2, 1995, pp. 143-161.

74. Li, Y-W., Elishakoff, I., Starnes, J. H., Jr., and Bushnell, D., "Effect of Thickness Variation and Initial Imperfection on Buckling of Composite Cylindrical Shells: Asymptotic Analysis and Numerical Results by BOSOR4 and PANDA2,"

International Journal of Solid and Structures, Vol. 34, No. 28, 1997, pp. 3755-3767.

75. Liu, B., Haftka, R. T., Akgun, M., "Permutation Genetic Algorithm for Stacking Sequence Optimization," *Proceedings of the 39th AIAA / ASME/ ASCE/ AHS/ ASC Structures, Structural Dynamics and Materials Conference, AIAA-98-1830,* Long Beach, California, April 1998, pp. 641-652.

76. Mabson, G. E., Flynn, B. W., Ilcewicz, L. B., and Graesser, D. L., "The Use of COSTADE in Developing Composite Commercial Aircraft Fuselage Structures," *Proceedings of the 35th AIAA/ ASME/ ASCE/ AHS/ASC Structures, Structural Dynamics and Materials Conference, AIAA Paper 94-1492,* Hilton Head, South Carolina, April 1994, pp. 1384-1393.

77. Manne, P. M., and Tsai, S. W., (1998) "Practical Considerations For the Design of Composite Structures," *Mechanics of Composite Materials and Structures,* Vol. 5, 1998, pp. 227-255.

78. Mason, B., Haftka, R.T., and Johnson, E.R., "Analysis and Design of Composite Channel Frames," *Proceedings of the AIAA/ NASA/ USAF/ ISSMO 5th Symposium on Multidisciplinary Analysis and Optimization, Vol. 2, AIAA Paper 94-4346-CP,* Panama City, Florida, September 1994, pp. 1023-1040.

79. McGowan, D. M., and Anderson, M. S., "Development of Curved Plate Elements for the Exact Buckling Analysis of Composite Plate Assemblies Including Transverse Shear Effects," *Proceedings of the 38th AIAA/ ASME/ ASCE/ AHS/ ASC Structure, Structural Dynamics and Materials Conference, AIAA Paper 97-1305,* Kissimmee, Florida, USA, April 1997, pp. 2678-2692.

80. Myers, R.H., and Montgomery, D.C., *Response Surface Methodology: Process and Product Optimization Using Designed Experiments.* John Wiley & Sons Inc., New York, 1995.

81. Nagendra, S., Haftka, R.T., and Gürdal, Z., "Design of a Blade Stiffened Composite Panel by a Genetic Algorithm," *Proceedings of the 34th AIAA/ ASME/ ASCE/ AHS/ ASC Structures, Structural Dynamics and Materials Conference,* La Jolla, California, April 19-22, 1993, pp. 2418-2436.

82. Nagendra, S., Haftka, R.T., and Gürdal, Z., "PASCO-GA: A Genetic Algorithm Based Design Procedure for Stiffened Composite Panels Under Stability and Strain Constraints," *Proceedings of the Tenth DOD/ NASA/ FAA Conference on Fibrous Composites in Structural Design,* Hilton Head, South Carolina, Nov. 1993.

83. Nagendra, S., Jestin, D., Gürdal, Z., Haftka, R.T., and Watson, L.T., "Improved Genetic Algorithm for the Design of Stiffened Composite Panels," *Computers and Structures,* Vol. 58, No. 3, 1996, pp. 543-555.

84. Park, O., Haftka, R.T., Sankar, B.V. and Nagendra, S., "Analytical and Experimental Study of a Blade Stiffened Panel in Axial Compression," *Proceedings of the 39th AIAA/ ASME/ ASCE/ AHS/ ASC Structures, Structural Dynamics and Materials Conference, AIAA paper 98-1993,* Long Beach California. April 1998.

85. Perry, C., Gürdal, Z, "Design Trends of Minimum Weight Blade Stiffened Composite Panels for Postbuckling Response," *Proceedings of the First World Congress of Structural and Multidisciplinary Optimization*," Goslar, Germany, May 28-June 2, 1995, pp. 733-740.

86. Perry, C., Gürdal, Z, and Starnes, J. H. Jr., "Minimum Weight Design of Compressively loaded Stiffened Panels for Postbuckling Response," *Engineering Optimization*, Vol. 28, 1997, pp. 175-197.

87. Peshkam, V., and Dawe, D. J., "Buckling and Vibration of Finite Length Composite Prismatic Plate Structures with Diaphragm Ends. 1. Computer Programs and Buckling Applications," *Computer Methods in Applied Mechanics*, Vol. 77, No. 3, 1989, pp. 227-252.

88. Ragon, S.A., Gürdal, Z, Haftka, R.T., and Tzong, T.J., "Global/Local Structural Wing Design Using Response Surface Techniques," *Proceedings of the 37th AIAA/ASME/ASCE/AHS/ASC Structures, Structural Dynamics and Materials Conference, Vol. 2, AIAA Paper 97-1051,* Kissimmee, Florida, April 1997, pp. 1204-1214.

89. Rankin, C. C., and Brogan, F. A., " An Element Independent Corotational Procedure for Treatment of Large Rotations," *Journal of Pressure Vessel Technology*, Vol. 108, 1986, pp. 165-174.

90. Rankin, C.C., Stehlin, P., and Brogan, F. A., "Enhancements to the STAGS computer code," *NASA CR 4000*, NASA Langley Research Center, Hampton, Virginia, 1986.

91. Rebel, G., "ANOVSI – Computational Module for the Solution of Nonlinear Compound Eigenvalue Problems via Subspace Iteration," *Doctoral Thesis, Delft University of Technology, Faculty of Aerospace Engineering*, The Netherlands, March 1992.

92. Rhodes, J., and Marshall, I. H., "On the Use of Effective Width Concepts for Composite Plates," *Proceedings of the 2nd International Conference on Composite Structures* (Edited by Marshall, I. H.), Applied Science, 1982, pp. 335-351.

93. Riks, E., "An Incremental Approach to the Solution of Snapping and Buckling Problems," *International Journal of Solid and Structures*, Vol. 15, 1979, pp. 529-551.

94. Riks, E., “A Finite Strip Method for the Buckling and Postbuckling Analysis of Stiffened Panels in Wing Box Structures,” *NLR CR 89383L*, 1989.

95. Schmit, L.A. and Farshi, B., "Optimum Design of Laminated Fibre Composite Plates," *International Journal for Numerical Methods in Engineering*, Vol. 11, 1977, pp. 623-640.

96. Stoll, F., and Gürdal, Z., “Nonlinear Analysis of Compressively Loaded Linked-Plate Structures,” AIAA Paper 90-0968-CP, *Proceedings of the AIAA/ ASME/ ASCE/ AHS/ ASC 31st Structures, Structural Dynamic and Materials Conference*, Long Beach California, April 1990, pp. 903-913.

97. Stoll, F., “Geometrically Nonlinear Analysis of Stiffened Composite Panels with Various End-Support Conditions,” *Proceedings of the 34th AIAA/ ASME/ ASCE/ AHS/ ASC Structures, Structural Dynamics and Materials Conference, AIAA Paper 93-1615-CP*, La Jolla, California, April 1993, pp. 2699-2709.

98. Stoll, F., Gürdal, Z, and Starnes, J. H. Jr., “A Method for Geometrically Nonlinear Analysis of Compressively Loaded Prismatic Composite Structures,” *CCM-91-03 (VPI-E-91-01)*, Center for Composite Materials and Structures, Virginia Polytechnic Institute and State University, Blacksburg, Virginia, 1991.

99. Stroud, W. J., and Agranoff, N., “Minimum-Mass Design of Filamentary Composite Panels Under Combined Loads: Design Procedure Based on Simplified Buckling Equations,” *NASA-TN D-8257*, Oct. 1976.

100. Stroud, W. J., and Agranoff, N., “Minimum-Mass Design of Filamentary Composite Panels Under Combined Loads: Design Procedure based on a Rigorous Buckling Analysis,” *NASA-TN D-8417*, July 1977.

101. Stroud, W.J., and Anderson, M. S., “PASCO: Structural Panel Analysis and Sizing Code, Capability and Analytical Foundations,” *NASA TM-80181*, 1981.

102. Stroud, W. J., Greene, W. H., and Anderson, M. S., “Buckling Loads of Stiffened panels subjected to combined longitudinal compression and shear: results obtained with PASCO, EAL and STAGS computer programs,” *NASA TP-2215*, 1984.

103 Sun, C. T., and Li, S., “Three-Dimensional Effective Elastic Constants for Thick Laminates,” *Journal of Composite Materials*, Vol. 22, July 1988, pp. 629-639.

104. Sun, G., and Mao, R., “Optimization of Stiffened Laminated Composite Circular Cylindrical Shells for Buckling,” *Composite Structures*, Vol. 23, 1993, pp. 53-60.

105. Swanson, G. D., Gürdal, Z., and Starnes, J.H., “Structural Efficiency Study of Graphite-Epoxy Aircraft Rib Structures,” *Journal of Aircraft*, Vol. 27, No. 12, Dec. 1990, pp. 1011-1020.

106. Thurston, G. A., Brogan, F. A., and Stehlin, P., "Postbuckling Analysis Using a General Purpose Code," *AIAA Journal*, Vol. 24, 1986, pp. 1013-1020.

107. Tomashevskii, V. T., Anufriev, A. P., Shalygin, V. N., Yakolev, V. S., and Kalimulin, R. I., "Optimization of Reinforced Cylindrical Shells Made of Composites," *Mechanics of Composite Materials*, Vol. 23, No. 5, 1987, pp. 603-607.

108. Tomashevskii, V. T., Kalimulin, R. I., and Yakolev, V. S., "Optimization of Composite Shells of Revolution with a Mixed System of Reinforcing Elements," *Mechanics of Composite Materials*, Vol. 25, No. 6, 1989, pp. 767-772.

109. Toropov, V.V. and Markine, V.L. "Use of Simplified Numerical Models as Approximations: Application to a Dynamic Optimal Design Problem". *Proceedings of the First ISSMO/NASA Internet Conference on Approximation and Fast Reanalysis Techniques in Engineering Optimization*, June 1998.

110. Tripathy, B., and Rao, K. P., "Stiffened Composite Axisymmetric Shells-Optimum Lay-up for Buckling by Ranking," *Computers and Structures*, Vol. 46, No. 2, 1993, pp. 299-309.

111. Tripp, T. L., Tamekuni, M., and Viswanathan, A. V., "Users's Manual – BUCLASP2: A Computer Program for Instability Analysis of Biaxially Loaded Composite Stiffened Panels and Other Structures," *NASA-CR-112226*, 1973.

112. Tuttle, M. E., and Zabinsky, Z.B., "Methodologies for Optimal Design of Composite Fuselage Crown Panels," *Proceedings of the 35th AIAA/ ASME/ ASCE/ AHS/ASC Structures, Structural Dynamics and Materials Conference, AIAA Paper 94-1493*, April 1994, Hilton Head, South Carolina, pp. 1394-1405.

113. Van der Neut, A, "The Interaction of Local Buckling and Column Failure of Thin-Walled Compression Members," *Proceedings of XII International Congress on Applied Mechanics*, Stanford, 1968, pp. 389-399.

114. van Wamelen, A., Haftka R.T. and Johnson, E. R., "Optimum Lay-ups of Composite Specimens to Accentuate the Differences between Competing Failure Criteria," *Proceedings of the 8th American Society of Composites Technical Conference on Composite Materials*, Cleveland, Ohio. October 1993, pp. 1045-1055.

115. Vanderplaats, G.N., CONMIN – A FORTRAN Program for Constrained Function Minimization. User's Manual," *NASA-TM X-62*, 1973.

116. Vanderplaats, G.N., "ADS – A FORTRAN Program for Automated Design Synthesis-Version 1.10," NASA *CR-177985*, 1985.

117. Venkataraman, S., and Haftka, R. T., "Integration of Finite Element Analysis Program and Panel Design Program," *Proceedings of the 37th*

AIAA/ASME/ASCE/AHS/ASC Structures, Structural Dynamics and Materials Conference, AIAA Paper 97-1052, Kissimmee, Florida, April 1997, pp. 1215-1224.

118. Venkataraman, S., Haftka, R.T., and Johnson, T. F., "Use of Effective Engineering Constants for Composite Laminates Optimized for Buckling loads," *Proceedings of the American Society of Composites 12th Technical Conference*, Dearborn, Michigan, Oct. 1997, pp. 12-22.

119. Venter, G., and Haftka, R.T., "Using Response Surface Methodology in Fuzzy Set Based Design Optimization," *Proceeding of the 39th AIAA/ASME/ASCE/AHS/ASC Structures, Structural Dynamics and Materials Conference, Vol. 1, AIAA paper 98-1776,* Long Beach, California, April 1998, pp. 641-652.

120. Venter G, Haftka R. T., and Starnes J. H. Jr., "Construction of Response Surface Approximations for Design Optimization," *AIAA Journal*, Vol. 36, No. 12, Dec. 1998, pp. 2242-2249.

121. Viswanathan, A. V., and Tamekuni, M., "Elastic Buckling Analysis of Composite Stiffened Panels and Other Structures Subjected to Biaxial Loads," *NASA-CR-2216*, 1973.

122. Vitali, R., Park, O., Haftka, RT., and Sankar, B. V., "Optimization of a Hat Stiffened Panel by Response Surface Techniques," *Proceedings of the 38th Structures, Structural Dynamics, and Materials Conference, AIAA 97-1151*, Kisssimmee, Florida, April 7-10, 1997, pp. 2983-2993.

123. Vitali, R., Haftka, R.T., and Sankar, B. V., "Correction Response Surface Approximations for Stress Intensity Factors of a Composite Stiffened Plate," *Proceedings of the 39th AIAA/ ASME/ ASCE/ AHS/ ASC Structures, Structural Dynamics and Materials Conference, AIAA-98-2047,* Long Beach California, April 1998, pp. 2917-2922.

124. Vitali, R., Haftka, R. T., and Sankar, B. V., "Correction Response Surface Design of Stiffened Composite Panel with a Crack," *Proceedings of the AIAA/ ASME/ ASCE/ AHS/ ASC Structures, Structural Dynamics and Materials Conference, AIAA-99-1313,* St. Louis, Missouri, 1999.

125. Wiggenraad, I.F.M., Arendsen, P., and da Silva Pereira, J.M, "Design Optimization of Stiffened Composite Panels With Buckling And Damage Tolerance Constraints," *Proceedings of the 39th AIAA/ ASME/ ASCE/ AHS/ ASC Structures, Structural Dynamics, and Materials Conference, Part 1 (of 4), AIAA-98-1750,* April 1998, Long Beach, California, pp. 420-429.

126. Williams, F. W., and Kennedy, D., *Users Guide to VICON, VIPASA with Constraints,* Dept of Civil Engineering and Building Technology, Univ. of Wales, Inst. of Science and Technology, Aug. 1984.

127. Williams, F. W., and Anderson, M. S., "Incorporation of Lagrange Multipliers into an Algorithm for Finding Exact natural Frequencies or Critical Buckling Loads," *International Journal of Mechanical Sciences*, Vol. 25, No. 8, 1993, pp. 579-584.

128. Williams, F. W., Kennedy, D., and Anderson, M. S., "Analysis Features of VICONOPT, an Exact Buckling and Vibration Program for Prismatic Assemblies of Anisotropic Plates," *AIAA Paper 90-0970, Proceedings of the 31st AIAA / ASME/ ASCE/ AHS/ ASC Structures, Structural Dynamics and Materials Conference*, Long Beach, California, 1990, pp. 920-929.

129. Williams, F. W., and Jianqiao, Y., "Optimum Mass Design of Prismatic Assemblies of Plates with Longitudinal Voids," *Computers and Structures*, Vol. 44, No. 3, 1992, pp. 557-565.

130. Wittrick, W. H., and Williams, F. W., Buckling and Vibration of Anisotropic or Isotropic Plate Assemblies Under Combined Loading," *International. Journal of Mechanical Sciences*, Vol. 16, No. 4, April 1974, pp. 209-239.

131. York, C. B., and Williams, F. W., "Buckling Analysis of Skew Plate Assemblies: Classical Plate Theory Results Incorporating Lagrange Multipliers," *Computers and Structures*, Vol. 56, No. 4, 1995, pp. 625-635.

132. York, C. B., and Williams, F. W., "Aircraft Wing Panel Buckling Analysis: Efficiency by Approximations," *Computers and Structures*, Vol. 68, 1998, pp. 665-676.

133. Zabinsky, Z.B., "Global Optimization for Composite Structural Design," AIAA Paper 94-1494, *Proceedings of the 35th AIAA/ ASME/ ASCE/ AHS/ASC Structures, Structural Dynamics and Materials Conference*, Hilton Head, South Carolina, April 1994, pp. 1406-1412.

134. Zabinsky, Z.B., Graesser, D. L., Tuttle, M. E., and Kim, G. I., "Global Optimization of Composite Laminates Using Improving Hit and Run," *Recent Advances in Global Optimization* (editors Floudas, C., and Pardalos, P.), Princeton University Press, Princeton, 1992, pp. 343-368.

APPENDIX A
MATERIAL PROPERTIES

The properties of the different materials used for stiffened panel in the design optimizations performed for comparing stiffened panel concepts are presented here.

Metallic Alloys

Two metallic alloys were used for this trade study performed to compare weight efficiencies of stiffened panel concepts. The selection was based on structural requirements and the performance of the material at cryogenic temperatures. The structural properties of the materials are provided in Table A.1.

Table A.1: Material properties for metallic panels (at 50° F)

Property	Al 2219-T87	Ti-6Al-4V
Density (lb/in^3)	0.1	0.16
Elastic modulus (Mpsi)	10.7	16.5
Shear modulus (Mpsi)	4	6.3
Poisson's ratio	0.34	0.32
Yield Stress (psi)	58000	135000

Laminated Composite

The two materials chosen, namely the aluminum alloy Al 2219-T 87 and titanium alloy Ti-6Al-4V have almost identical specific modulus, whereas the titanium alloy has a

45% higher specific strength based on yield stress. The Von Mises stress criterion was used for stress failure of the material with safety factor of 1.2.

Composite stiffened panel constructions were designed using the IM7/977-2 graphite-epoxy system. The properties of the material are provided in Table A.2.

Table A.2: Material properties for IM7/977-2 composite panels (at 190° F)

Density (lbs/in3)	0.057
Elastic modulus in the fiber direction (Mpsi)	21.5
Elastic modulus in the transverse fiber direction (Mpsi)	1.08
In plane shear modulus G12 (Mpsi)	0.6
Out of plane shear moduli G13, G23 (Mpsi)	0.51
Small Poisson's ratio	0.1507
Allowable stress in the fiber direction (Kpsi)	129 (tension) 176.3 (compression)
Allowable stress in the transverse fiber direction (Kpsi)	21.6 (tension) 36.0 (compression)
Allowable shear stress (Kpsi)	10.9
Thermal expansion coefficient along fibers ($x10^{-6}$ /°F)	-0.11
Thermal expansion coefficient transverse to fibers ($x10^{-6}$ /°F)	17.0

Honeycomb Sandwich

The properties of the honeycomb core, namely, transverse modulus (E_c) and shear moduli (G_{xz}, G_{yz}) are calculated in PANDA2 using simple geometrical relations. The core failure strength of the core are calculated using empirical relations, provided by manufacturers. The following relations were used for this study

$$F_{cc} = k_1 \left(\frac{\rho_c'}{\rho_c} \right)^{k_2} \left(\frac{F_{tu}}{c^{k_{sc}}} \right) \qquad \text{(B.1)}$$

$$F_{csL} = k_3 \left(\frac{\rho_c^{'}}{\rho_c} \right)^{k_4} \left(\frac{F_{su}}{c k_{ss}} \right) \quad \text{(B.2)}$$

$$F_{csW} = 0.8 F_{csL} \quad \text{(B.3)}$$

In the above expressions F_{cc} is the core crushing strength, F_{csL} and F_{csW} are respectively the longitudinal and transverse core shear strengths, c is the core height (thickness), $\rho_c^{'}$ and ρ_c are the densities of the core and of the core material, where

$$\rho_c^{'} = \frac{8}{3} \frac{t_c}{d_c} \quad \text{(B.4)}$$

In the above expression, t_c and d_c, are the thickness and diameter of the honeycomb core cell. The values of empirical constants used for k_1, k_2, k_3, k_4, k_{sc} and k_{ss} for the equations were 2.31, 1.464, 1.307, 1.34, 0.16 & 0.44, respectively. Core crushing and shear strengths decrease with thicker cores. Core crushing and shear strengths are respectively reduced by 10% and 35% if core thickness is doubled to 2 inches. PANDA2 knocks down core shear strength values by means of factors depending on the ratio of the core thickness to a reference value (1 inch for this study).

APPENDIX B
OPTIMUM DESIGNS OF METALLIC STIFFENED PANELS

This section presents details of optimum values of design variables and critical margins of optimum designs of metallic stiffened panels optimized with and without initial geometric imperfections.

Stringer-ring stiffened Panel

The optimum designs of stringer-ring stiffened panels optimized with and without imperfections are shown in Table B.1. Imperfections increase the weight of panels. The eccentricity introduced by imperfections result in lower buckling loads and higher stresses. The optimized designs reflect this with taller and more closely spaced stringers. The critical failure margins that drive the design are stress constraints in the cylinder wall arising from the internal (hoop) pressure. For panels with imperfections, in addition to the hoop stress from pressure, there are bending stresses induced by the axial load causing amplification of the initial imperfections. Local skin buckling and stringer buckling are critical for the panel with imperfections. When imperfections are introduced the wide column buckling load becomes less critical at the optimum design.

Table B.1: Optimum designs of metallic stringer-ring stiffened panels

Design variables (inch)	Without Imperfections	With Imperfections
Skin thickness	0.0964	0.0971
Stringer spacing	10.430	7.764
Stringer height	1.000	1.927
Stringer web thickness	0.050	0.050
Stringer flange width	0.4 (bottom), 0.3 (top)	0.4 (bottom), 1.065 (top)
Stringer flange thickness	0.05	0.05(bottom), 0.071 (top)
Ring spacing	21.360	30.00
Ring height	2.000	2.000
Ring web thickness	0.05	0.05
Ring flange width	0.4 (bottom), 0.304 (top)	0.436 (bottom), 0.584 (top)
Ring flange thickness	0.05	0.05(bottom), 0.104 (top)
Panel weight (lb/ft2)	1.600	1.840

Grid-Stiffened Panels

Two forms of grid stiffened panels were optimized. An isogrid panel with stiffeners that form a triangular grid pattern and an orthogrid panel that forms rectangular grids. PANDA2 has special analysis modules implemented for the isogrid panels. However the orthogrid panel is simply a stringer-ring stiffned panel with closely spaced blade stiffeners. Comparison of optimized design of isogrid panels optimized with and without imperfections are shown in Table B.2. Isogrid panels modeled in PANDA2 can have ring stiffeners in addition to the isogrid web stiffening.

Isogrid panels exhibit high sensitivity to imperfections. The panel weight increases by 51% when imperfections are included in the analysis model. The increased weight is due the increased loads acting on stiffeners and the bending stresses. This is

reflected in the designs as the optimum with imperfections has thicker and more closely spaced isogrid stiffeners.

Table B.2: Optimum design of isogrid panels optimized with and without imperfections

Design variables (inch)	Without imperfections	With imperfections
Skin thickness	0.098	0.1067
Isogrid stiffener spacing	14.05	10.0
Isogrid web height	1.000	1.509
Isogrid web thickness	0.037	0.1254
Ring spacing	66.92	30.0
Ring height	2.000	2.160
Ring web thickness	0.03	0.03
Ring flange width	0.400 (bottom), 0.300 (top)	0.400 (bottom), 0.330(top)
Ring flange thickness	0.05	0.045(bottom), 0.096 (top)
Ring web thickness	0.03	0.03
Panel weight (lb/ft2)	1.5373	2.409

Table B.3: Optimum design of orthogrid panels optimized with and without imperfections

Design variables (inch)	Without Imperfections	With Imperfections
Skin thickness	0.09613	0.09212
Stringer spacing	9.977	6.544
Ring spacing	9.599	19.70
Orthogrid height	1.050	1.791
Orthogrid web thickness	0.050	0.1563
Panel weight (lb/ft2)	1.5382	2.1468

Optimized designs of orthogrid stiffened panels are presented in Table B.3. Since the orthogrid panels are designed using the PANDA2 models for stringer-ring stiffened

panels it is not possible to add extra rings. However, the optimum weight is comparable to that obtained for isogrid panels. The imperfections in panels results in optimum designs with heavier and more closely spaced stiffeners. The web is three times as thick as that obtained for the optimum without imperfection, while the the stiffener spacing is reduced to one third. The increased stiffening is required to satisfy buckling constraints (skin and stiffener buckling failure modes) experienced by the orthogrid panel.

Active failure mechanisms do not change for optimum designs of both perfect and imperfect orthogrid panels. The larger fraction of axial load is carried by the stiffeners. However, the closely spaced ring stiffener also helps carry some of the hoop loads. It appears that stiffener web buckling causes the high weight increase for panels optimized with imperfections. Table B.4 shows the imperfection sensitivity of grid stiffened panels with two different stiffener profiles, namely blade and T shaped stiffeners.

From table B.4, it appears that the isogrid and orthogrid stiffened panels that use T-shaped stiffeners are much less sensitive to imperfections. Weight penalty reduces by 50% when T-shaped stiffeners replace blade stiffeners in isogrid panels. The outstanding flange increases the bending stiffness of the stiffener, and also helps stabilize the stiffener web. Web thickness for T-shaped stiffeners is one third the thickness of that obtained for isogrid panel designed with blade stiffener.

Orthogrid panels with T shaped stiffeners behave as the stringer-ring stiffened panels analyzed before and imperfections no longer cause stiffener web buckling failure. Stiffener web buckling failure mode is active for the imperfect isogrid but the constraint is much easier to satisfy.

Table B.4: Effect of stiffener profile on optimum weight of grid-stiffened panels optimized with imperfections

Stiffener profile	Isogrid Panel		Orthogrid Panels		% Weight increase due to imperfections	
	Without imperfections	With imperfections	Without imperfections	With imperfections	Isogrid	Orthogrid
Blade	1.5373	2.4090	1.5248	2.156	56.703	41.396
T	1.5803	1.9824	1.5277	1.821	25.445	19.199

Table B5: Grid stiffened panel: web thickness and failure margins for different stiffener profiles

Stiffening concept	Stiffener profile	Stiffener web thickness (inch)	Failure mechanism under axial compression loads
ISOGRID	Blade	0.1254	Local buckling , Isogrid web buckling
	T	0.03185	Local buckling , Isogrid web buckling
ORTHOGRID	Blade	0.1563	Bending stress in stiffener webs, Local buckling, General buckling, Stringer web buckling
	T	0.0500	Stress in ring top flange, Local buckling

Titanium Honeycomb Core Sandwich Panels

Table B.6 presents the optimized designs for symmetric titanium honeycomb core sandwich panels optimized with fixed and varying core thickness. Table B.7 presents the optimal designs of titanium honeycomb core sandwich panels with asymmetric sandwich constructions designed with fixed and varying core thickness.

Optimizations are performed with and without initial geometric imperfections. Imperfections increase the required core thickness for panels optimized with varying core thickness. Also, imperfections reduce the aysmmetry for optimized cores, indicating that the reduction in bending stiffness due to asymmetry affects the design constraints. The

ratio of inner and outer facesheet thickness reduces to 1.26 for panels with imperfections from 3.5 for panels without imperfections. The increased design freedom allowed in having varying core thickness and asymmetric sandwich wall, resulted in reduced weight for the optimal designs. The reduction is almost negligible for panels designed with imperfections.

Table B.6: Symmetric sandwich panel: optimized designs

Design variables	Fixed core thickness		Optimized core thickness	
	Without Imperfections	With Imperfections	Without Imperfections	With Imperfections
Ring spacing	61.22	119.8	78.75	106.3
Ring height	2.102	2.000	2.000	2.000
Ring web thickness	0.012	0.029	0.010	0.031
Ring bottom (and top) flange width	1.577 (1.500)	1.500 (1.501)	1.500 (1.500)	1.500 (1.500)
Ring bottom (and top) flange thickness	0.026 (0.034)	0.029 (0.035)	0.010 (0.030)	0.024 (0.037)
Facesheet thickness	0.021	0.022	0.022	0.022
Core thickness	1.000	1.000	0.250	0.881
Honeycomb cell diameter	0.375	0.375	0.375	0.375
Core density (lb/ft^3)	3.932	3.932	3.932	3.932
Panel weight (lb/ft^2)	1.347	1.358	1.110	1.323

Buckling constraints for perfect panels with thick core are very far from being critical (margins near 200%). In the absence of imperfections, sandwich panels with thin core are more efficient than panels with thick core because the optimizer can choose an adequate value of core thickness to satisfy the critical buckling constraints. However, panels with thin core are more sensitive to imperfections (weight penalty of 21.1%) due to the smaller overall bending stiffness.

Table B.7: Asymmetric sandwich panel: optimized designs

Design variables	Fixed core thickness		Optimized core thickness	
	Without imperfections	With imperfections	Without imperfections	With imperfections
Ring spacing	112.4	120.0	120.0	105.9
Ring height	2.000	2.002	2.128	2.000
Ring web thickness	0.018	0.030	0.011	0.030
Ring bottom (and top) flange width	1.500 (1.500)	1.500 (1.500)	1.596 (1.500)	1.500 (1.500)
Ring bottom (and top) flange thickness	0.019 (0.029)	0.025 (0.044)	0.011 (0.032)	0.021 (0.037)
Internal facesheet thickness	0.024	0.028	0.035	0.024
External facesheet thickness	0.019	0.015	0.010	0.019
Core thickness	1.000	1.000	0.250	0.887
Cell diameter	0.375	0.375	0.375	0.375
Core density (lb/ft^3)	3.932	3.932	3.932	3.932
Panel weight (lb/ft^2)	1.341	1.354	1.095	1.320

Stress constraints due to the internal pressure are active for all the optimized designs. When there are no imperfections present, the panels optimized with freedom to have dissimilar facesheets, result in thicker internal facesheets. The difference is larger for the case of panels with optimized cores. Optimum designs of panels with imperfections have almost identical facesheets.

The final weights of panels with asymmetry are marginally higher than the panels designed with identical facesheets. This indicates that the final designs are not global optima. Extra freedom allowed to optimize the facesheets seperately must have resulted in lower weight or the same weight as the sandwich with identical facesheets.

It can be observed that stress in the facesheet is always critical both for perfect and imperect panels. Global buckling and ring buckling failure modes becomes critical

for the imperfect panel. Buckling failure margins (particularly for ring stiffeners) of imperfect panels have large gradients and this results in objective function oscillations during the optimization process.

Truss-Core Sandwich Panels

Table B.11 presents the optimized designs of truss core panels with and without imperfections. There is a 21% increase in the optimum weight when imperfections are included in the panels. Further weight reduction is possible if the corrugation angle constraint (at present restricted to 45°) is relaxed. Critical failure margins are similar for perfect and imperfect panels. The weight increase from imperfections is primarily from the increase in facesheet thickness of the truss core sandwich construction.

Table B.8: Optimum design of metallic truss-core sandwich panels optimized with and without imperfections

	Without imperfections	With imperfections	
Pitch	1.667	1.800	1.000
Contact segment	0.333	0.360	0.200
Facesheet thickness	0.027	0.033	0.0224
Web thickness	0.018	0.024	0.017
Core height	0.500	0.540	0.572
Corrugation angle	45°	45°	62.3°
Panel weight (lb/ft^3)	1.752	2.126	1.705

APPENDIX C
OPTIMUM DESIGNS OF COMPOSITE PANELS

In this section designs of composite panels are presented and discussed briefly. The optimized lay-up designs and corresponding number of plies that was determined in the rounded optimization are also shown.

Stringer-Ring Stiffened Panels

Table C.1 shows comparison of perfect and imperfect designs for composite stringer-ring stiffened panels. Weight efficiency of composite panels is very dependent on the laminate design chosen for the tank wall. Local buckling and tensile stress fiber failure margins dominate the optimization of composite stringer-ring stiffened panels. Two different lay-up designs are chosen the for shell wall laminate from table 3. No feasible design was found with a 13 ply laminate with stacking sequence of $[45/90_3/-45/0_{3/2}]s$ because the stress constraints were always violated. An angle ply laminate with lay-up of $[\pm 65_3]_S$ is more efficient in carrying hoop tensile loads.

Imperfections result in an 11% weight incrase. The optimized design has taller stiffeners and more closely spaced stringers. The laminate used in the stringer web construction has more plies oriented at 0° to provide higher stiffness and to carry the additional stresses introduced by the initial imperfections.

Table C.1: Optimum designs of composite stringer-ring stiffened panels.

Design variables (inch)	Without Imperfections	With Imperfections
Skin laminate	$[\pm 65_3]_S$	$[\pm 65_3]_S$
Stiffener laminate	$[45/-45/0/-45/45/0_2]s$	$[45/-45/0_3/-45/45/0]s$
Skin thickness	0.060	0.060
Stringer spacing	9.247	8.545
Stringer height	1.000	1.656
Stiffener web thickness	0.070	0.080
Stringer bottom (top) flange width	1.097 (1.000)	1.000 (1.147)
Ring spacing	23.61	34.49
Ring height	2.411	3.221
Ring bottom (top)flange width	1.500 (1.696)	1.500 (1.501)
Panel weight (lb/ft^2)	0.822	0.911

Table C.2: Optimum designs of honeycomb core sandwich panels: fixed core thickness

Design variables	Symmetric composite	Asymmetric composite
Inner facesheet laminate	$[45/90_3/-45/0_{3/2}]_s$	$[45_2/90_2/-45_2/0_{1/2}]_s$
Outer facesheet laminate	$[45/90_3/-45/0_{3/2}]_s$	$[45/90/-45/0_{1/2}]_s$
Inner facesheet thickness	0.065	0.065
Outer facesheet thickness	0.065	0.035
Core thickness	1.000	1.000
Honeycomb cell diameter	0.375	0.375
Core density (lb/ft^3)	3.932	3.932
Ring laminate	$[\pm 45/0/\pm 45/0_{1/2}]_s$	$[\pm 45/0/\pm 45/0_{1/2}]_s$
Ring spacing	59.05	120.0
Ring height	2.000	2.000
Ring bottom and top flange width	1.500	1.500
Panel weight	1.4331	1.167

Honeycomb Core Sandwich Panels

Tables C.2 shows comparison of sandwich panels with symmetric and asymmetric facesheets for a fixed core thickness of 1.0 inch. The increased degree of design freedom results in lower weights. It can be seen that laminate designs do not change for the symmetric sandwich even with imperfections (Table C.3). Imperfections resulted in more closely spaced rings and a thicker core to provide the increased bending stiffness necessary to satisfy the buckling constraints.

Table C.4 shows designs of asymmetric sandwich panels optimized with and without imperfections. For asymmetric sandwich panels, imperfections make local and global buckling modes more critical. Again, imperfect panels have a thicker core in order to make buckling constraints easier to satisfy.

Table C.3: Optimum designs of composite symmetric honeycomb core sandwich panels: optimized core thickness

Design variables	Without imperfections	With Imperfections
Facesheet laminate	$[45/90_3/-45/0_{3/2}]_s$	$[45/90_3/-45/0_{3/2}]_s$
Facesheet thickness	0.065	0.065
Core thickness	0.500	0.726
Honeycomb cell diameter	0.375	0.375
Core density (lb/ft^3)	3.932	3.932
Ring laminate	$[\pm 45/0/\pm 45/\ 0_{1/2}\ ]_s$	$[\pm 45/0/\pm 45/\ 0_{1/2}\ ]_s$
Ring spacing	120.0	43.10
Ring height	2.000	2.000
Ring flange (top and bottom) width	1.500	1.500
Panel weight	1.250	1.358

Table C.4: Optimum design of composite asymmetric honeycomb core sandwich panels

Design variables (inch)	Without Imperfections	With Imperfections
Internal facesheet laminate	$[45_2/90_2/\text{-}45/0]_S$	$[45_2/90_2/\text{-}45_2/0]_S$
External facesheet laminate	$[45/90/\text{-}45/0/\text{-}45/90/+45]_T$	$[45/90/\text{-}45/0/\text{-}45/90/+45]_T$
Ring laminate	$[\pm 45/0/\mp 45/0/\mp 45/0/\pm 45]_T$	$[\pm 45/0/\mp 45/0/\mp 45/0/\pm 45]_T$
Internal facesheet thickness	0.060	0.070
External facesheet thickness	0.035	0.035
Ring spacing	56.63	92.09
Ring height	2.000	2.000
Ring flange width (top and bottom	1.500	1.500
Core thickness	0.500	0.862
Honeycomb cell diameter	0.375	0.375
Core density (lb/ft3)	3.932	3.932
Panel weight	0.975	1.169

Truss-Core Sandwich Panels

Table C.5 shows designs of truss-core sandwich panels optimized with and without imperfections. It was found that lay-up designs do not change and that imperfect panels have a thicker core in order to satisfy the constraint on general buckling. Weight savings from optimizing the corrugation angle are much lesser in the case of composite truss-core designs. Further weight savings could be obtained if facesheets were not required to be symmetric.

Table C.5: Optimum designs of composite truss-core sandwich panels

	Without Imperfections	With Imperfections	
		Fixed corrugation angle	Optimized corrugation angle
Facesheet laminate	$[\pm 65_3]_S$	$[\pm 65_3]_S$	$[\pm 65_3]_S$
Web laminate	$[45/-45/0/-45/45/0]_S$	$[45/-45/0/-45/45/0]_S$	$[45/-45/0/-45/45/0]_S$
Facesheet thickness	0.060	0.060	0.060
Web thickness	0.060	0.060	0.060
Core thickness	0.692	0.769	0.795
Truss core stiffener spacing	3.092	3.163	2.995
Truss core stiffener top flange width	0.854	0.812	0.968
Corrugation angle	45°	45°	56.3°
Panel weight	1.297	1.324	1.299

BIOGRAPHICAL SKETCH

Satchithanandam Venkataraman was born in Coimbatore, India, on September 5, 1969. He received the Bachelor of Engineering degree in mechanical engineering from Anna University in April, 1991, and the Master of Science degree in mechanical engineering from Clemson University in August, 1993. He received the University of Florida College of Engineering Outstanding International Student Academic Achievement Award in 1997. He served as an intern at Ford Research Laboratory in Dearborn, Michigan, during the summer of 1997.